

Institute for Laser Applications in Medicine and Metrology  
at the University of Ulm  
Director: Professor Dr. R. Hibst

***Cell Death Pathways in the Photodynamic Therapy of  
Hepatocellular Carcinoma Cells with  
Tetrasulfonated Aluminum Phthalocyanine***

Dissertation Presented to  
the Faculty of Medicine of the University of Ulm  
for the Obtainment of the Doctorate Degree in Medicine (Dr. med.)

by  
Elke Haseroth  
from Geneva / Switzerland  
2014

Amtierender Dekan

1. Berichterstatter

2. Berichterstatter

Tag der Promotion

Prof. Dr. Thomas Wirth

Prof. Dr. Rudolf Steiner

Prof. Dr. Tatiana Syrovets

16.01.2015

*"Would you tell me, please, which way I ought to go from here?" [asked Alice].*

*"That depends a good deal on where you want to get to," said the Cat.*

*"I don't much care where --" said Alice. "Then it doesn't matter which way you go," said the Cat. "-- so long as I get SOMEWHERE," Alice added as an explanation.*

*"Oh, you're sure to do that," said the Cat, "if you only walk long enough."*

*(‘Alice in Wonderland’ by Lewis Carroll)*

# Contents:

## ABBREVIATIONS

<b>1</b>	<b>INTRODUCTION .....</b>	<b>1</b>
	1.1. Photodynamic Therapy – Principle .....	1
	1.2 Lasers as Light Source for PDT .....	6
	1.3 Modes of Cell Death – Apoptosis and Necrosis.....	7
	1.4 This Work .....	12
	1.5 Cytochrome c and COX 4 in Mitochondria .....	15
	1.6 Caspase Inhibitors – General Considerations .....	16
<b>2</b>	<b>MATERIAL &amp; METHODS.....</b>	<b>18</b>
	2.1 General .....	18
	2.2 Cell Culture .....	20
	2.3 Cell Growth Curve .....	22
	2.4 Viability Assays .....	23
	2.5 Photodynamic Therapy (PDT).....	26
	2.6 Cytochrome c Release from Mitochondria .....	30
	2.7 Western Blotting .....	33
	2.8 L929 Cells and anti-Apo-1 .....	41
	2.9 Caspase Inhibitors (C.I.).....	42
	2.10 Antioxidants and Radical Scavengers .....	44

	2.11 Electron Microscopy .....	45
	2.12 Laser Scanning Microscopy (LSM) .....	46
3	<b>RESULTS.....</b>	<b>53</b>
	3.1 Preliminary Experiments – Cell Growth and Viability Assays .....	53
	3.2 Characterizing AlPc and Comparing AlPc-Cl and AlPc-OH .....	57
	3.3 PDT Effect in Dependence on Time of Incubation after Cell Seeding .....	66
	3.4 PDT Effect in Dependence on Duration of AlPc Incubation.....	67
	3.5 Assaying PDT Effects with Viability Assays .....	69
	3.6 Electron Microscopy .....	75
	3.7 Mitochondrial Cytochrome c Release.....	77
	3.8 AlPc-PDT in the Presence of Caspase Inhibitors.....	81
	3.9 Antioxidants .....	85
	3.10 Laser Scanning Microscopy .....	86
4	<b>DISCUSSION .....</b>	<b>100</b>
5	<b>SUMMARY .....</b>	<b>108</b>
6	<b>LITERATURE.....</b>	<b>110</b>
	<b>ACKNOWLEDGEMENTS</b>	
	<b>CURRICULUM VITAE</b>	

# Abbreviations

[x]	Concentration of x
A	AlPcS <sub>4</sub> , chloride or free
Abs.max.	Maximum of (Light-)Absorption
ACE	Automated Component Extraction (LSM)
ADP	Adenosine Diphosphate
Ala	Alanine
AlPc(S <sub>4</sub> )	(Tetrasulfonated) Aluminum Phthalocyanine
AlPc-Cl	Tetrasulfonated Aluminum Phthalocyanine, chloride
AlPc-OH	Tetrasulfonated Aluminum Phthalocyanine, free form
AM	Acetoxymethyl Ester
A.O.	Amplifier Offset (LSM)
Apaf-1	Apoptotic Protease Activating Factor 1, a cell protein
Asp	Aspartic Acid
ATCC(#)	American Type Culture Collection (Number)
BCA	Bicinchoninic Acid
boc-D-fmk	t-Butoxycarbonyl-Asp-(O-methyl)-fluoromethylketone, a caspase inhibitor
BSA	Bovine Serum Albumin
Cat.#	Catalogue Number
ChMo	Channel Mode (LSM)
CD 95	Cluster of Differentiation 95, a cell surface receptor
C.I.	Caspase Inhibitor
C.I. 1	= z-VAD-fmk
C.I. 3	= boc-D-fmk
conc.	Concentration
COX 4	Cytochrome c Oxydase, subunit 4
ctrl	Control
cyt c	Cytochrome c
D	Aspartic Acid
D <sub>2</sub> R	Rhodamine conjugated to two Asp Residues
ddw	Double Distilled Water
D.G.	Detector Gain (LSM)
DMSO	Dimethylsulfoxide
DNA	Desoxyribonucleic Acid
DTT	Dithiothreitol
EDTA	Ethylenediamine Tetraacetic Acid
Em.	Emission (of Fluorescence)
EM	Electron Microscopy
endconc.	End-/Final Concentration

Ex.	Excitation (of Fluorescence)
ExCh	Extract Channels (LSM)
Fas	Fibroblast Associated Protein, a cell surface receptor
fbm	Fractionation Buffer Mixture (Cytochrome c release kit)
FCS	Fetal Bovine / Calf Serum
fmk	Fluoromethylketone
FW	Formula Weight
<i>g</i>	multiple of earth's gravitational acceleration (unit for centrifugation)
HCC	Hepatocellular Carcinoma
H <sub>e</sub>	Radiant exposure [J/cm <sup>2</sup> ]
Hep3b	Name of a hepatocarcinoma cell line (cf. 'Material')
HEPES	4-(2-Hydroxyethyl)-1-piperazine-ethanesulfonic acid
HepG2	Name of a hepatocarcinoma cell line (cf. 'Material')
HRP	Horse Radish Peroxydase (Western Blotting)
HuH7	Name of a hepatocarcinoma cell line (cf. 'Material')
Irrad	Laser-Irradiation (of cells in PDT)
L	Liter
$\lambda$	Wavelength
LaMo	Lambda Mode (LSM)
lbm	Lysis Buffer Mixture
LiUMx	Linear Unmix (LSM)
LSM	Laser Scanning Microscope/y
M	molar, mol/L
MAD	Median of Absolute Differences
Me	Methyl
MTT	3-(4,5-Dimethylthiazol-2-yl)-2,5-diphenyl-tetrazolium Bromide
MW	Molecular Weight
n.a.	not applicable
NAC	N-Acetyl Cysteine
n.d.	not determined
NR	Neutral Red
O.D.	Optical Density (Photometry)
OM	Optical Microscopy
O.R.	Odds Ratio
PARP	Poly-(ADP-Ribose)-Polymerase
PBS	Phosphate Buffered Saline
PCR	Polymerase Chain Reaction
PDT	Photodynamic Therapy or Treatment
PDTC	Pyrrolidine Dithiocarbamate
PE	Polyethylene
Ph	Phenyl

PP	Polypropylene
PS	Photosensitizer; Polystyrene
P/S	Penicillin/Streptomycin
Rh123	Rhodamine 123
ROI	Region of Interest (LSM)
ROS	Reactive Oxygen Species
RT	Room Temperature
Std	Standard (Solution)
SDS	Sodium Dodecylsulfate
SEM	Scanning Electron Microscopy
TBS	Tris Buffered Saline
T/E	Trypsin/EDTA, 0.125 % each
TCA	Trichloroacetic Acid
TEM	Transmission Electron Microscopy
Tris	Tris(Hydroxymethyl) Aminomethane
Val	Valine
WL	Wavelength
w/o	without
w/v	Weight per Volume
z-	Benzoyloxycarbonyl
z-VAD-fmk	Benzoyloxycarbonyl-Val-Ala-Asp-fluoromethylketone, a caspase inhibitor



# 1 Introduction

## 1.1 Photodynamic Therapy – Principle

Photodynamic therapy (PDT) is used in the treatment of diseases involving abnormal cells as encountered typically in various forms of hyperproliferation issued from cancerous or neo-angiogenic growth. Primarily, organ surfaces are accessible, but interstitial usage is gaining increasing interest (Huang et al. 2008, Wilson et al. 2008).

Other potential applications of PDT include inactivation of microorganisms for example in blood products (Wainwright 2000) or dental caries (Nagata et al. 2012). Bacteria and viruses as well as fungi (Calzavara-Pinton et al. 2005) or eukaryotic parasites (Jori et al. 2006) have been targeted. Moreover, PDT may also be beneficial in the treatment of *acne vulgaris*, chronic wounds (Jori et al. 2006) or atherosclerosis (Waksman et al. 2008).

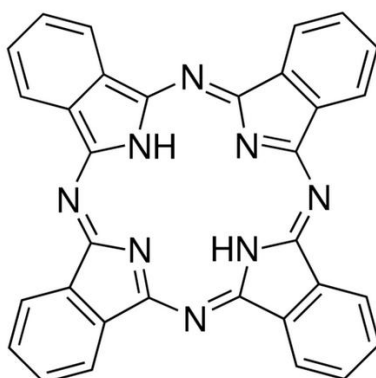


*Figure 1* General formula of phthalocyanines. Substituents on the outer rings and different central metal ions lead to a family of substances that have been used in photodynamic therapy. (From: Phthalocyanines, Sigma-Aldrich Product Directory)

The therapy is based on the administration of a dye, the photosensitizer (PS), which is internalized, ideally in a selective way, by the abnormal cells. Subsequent irradiation with light of a dye-specific wavelength leads to excitation of the photosensitizer molecule. The latter, upon returning to the ground state, transmits

its energy to other intracellular entities (type I reaction) or to oxygen (type II reaction), thus leading to serious deterioration of cell homoeostasis.

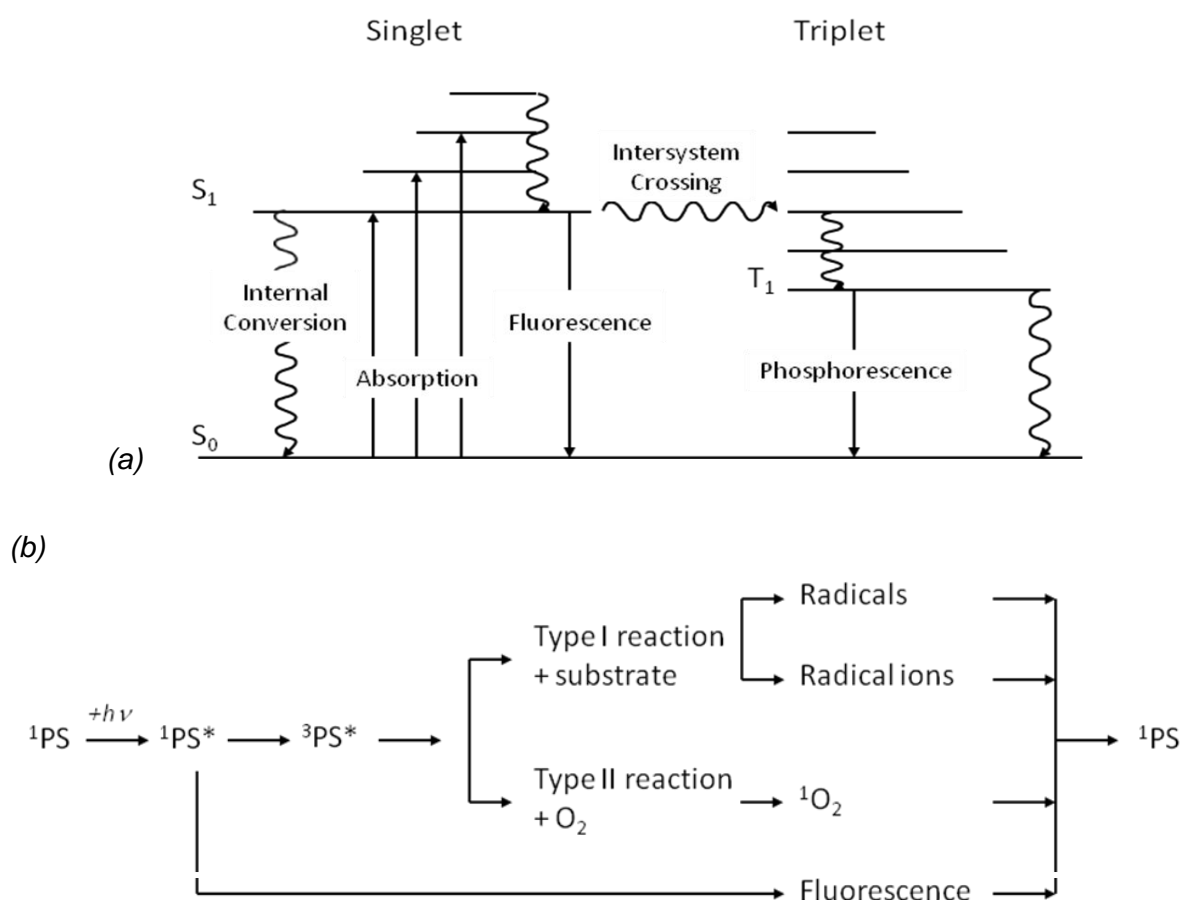


**Figure 2** Representation of reactions a photosensitizer (PS) can undergo:  
 (a) Forms of energy transfer during activation and inactivation (Jablonski diagram), and  
 (b) Possible interactions with other species leading to the formation of radicals or singlet oxygen  $^1\text{O}_2$  (After Triesscheijn et al. 2006 ).

Photosensitizers such as phthalocyanines (*Figure 1*) are typically characterized by a large conjugated ring system with a maximum light absorption in the visible domain. Due to their molecular characteristics, (1) they usually fluoresce and (2) the more common but very unstable singlet excited state ( $^1\text{PS}^*$ ) can convert to the more long-living triplet state ( $^3\text{PS}^*$ ). The (relatively) long life-span of the latter increases the probability that it can interact with other molecules in its surrounding. Besides this, excitation/activation of intracellular species depends on the localization of the photosensitizer and its chemical surrounding. Reactive oxygen

species (ROS), particularly singlet oxygen, have been shown to participate (Almeida et al. 2004).

*Figure 2.a* illustrates schematically the forms of energy-transfer that can be encountered with a typical photosensitizer:

1. Absorption of energy (light).
2. Possible decay with energy-emission in form of fluorescence: This is used in the so-called 'photodynamic diagnostics' (PDD) to detect the cells that have internalized the photosensitizer (and to delimit e.g. a tumor *in vivo*).
3. Transformation to the more long-living triplet form (intersystem crossing): The latter ( $^3\text{PS}^*$ ) transfers its energy to other molecules or to oxygen (*Figure 2.b*), which is the basic reaction in photodynamic therapy.

Internal conversion and phosphorescence, although possible, are of no concern in the context of PDT; the energy released is dissipated and lost.

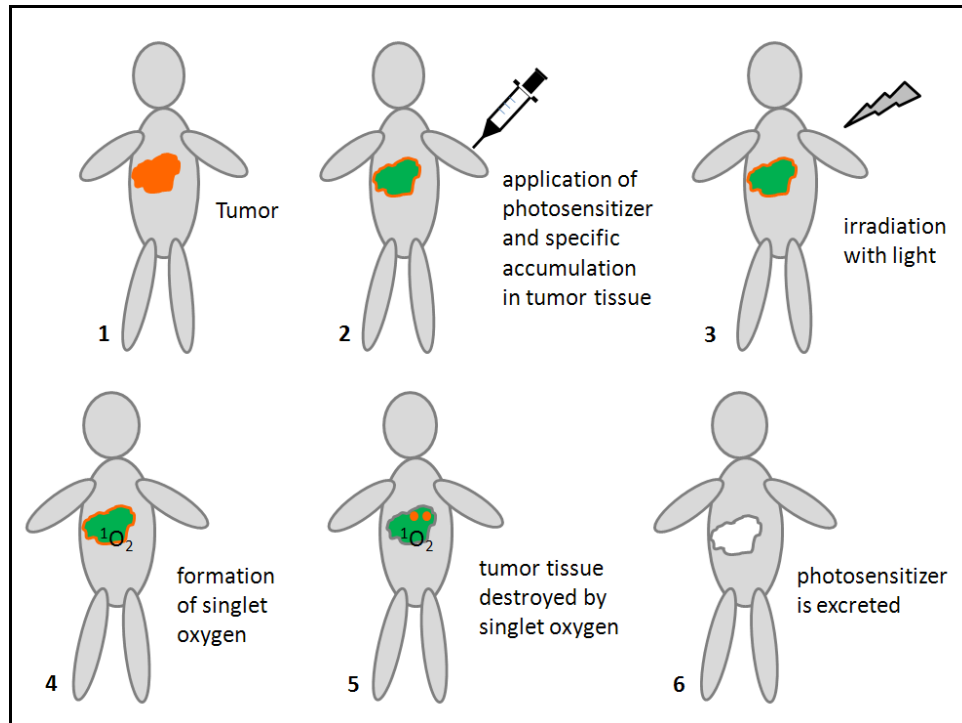


*Figure 3* Schematic representation of the principle of photodynamic therapy.  
( After: Deutsches Medizin-Netz )

The general principle of PDT in medical applications with systemic administration of the photosensitizer and local irradiation is shown in *Figure 3*.

Selectivity, and thus low overall toxicity of the method, is achieved through the selectivity of the photosensitizer's uptake by the abnormal cells, as well as by the dose and wavelength (in the visible range) of the irradiation, usually applied only locally.

Malignant tumors often take up any photosensitizer more readily than normal cells; this selectivity is usually not specific but due to the higher metabolic activity of the tumorous cells or to a defective cell membrane barrier (Brown et al. 2004).

Further selectivity can in some cases be obtained (1) by topical application of the photosensitizer (instead of the more common systemic), for example in the case of skin diseases [Marcus et al. 2002) or internal cavities (e.g. the bladder); and/or (2) by enhancing the selectivity of cellular uptake. To date, coupling the photosensitizer to transferrin (the receptors of which are overexpressed on the surface of tumor cells) (e.g. Derycke et al. 2004), to antibodies (van Dongen et al. 2004) or other peptides (Schmitt et al. 2012) has been performed with some success. Modulating hydrophilicity and/or molecular size of the photosensitizer can be achieved either by modifying the ring substituents (e.g. with sulfonate groups or aliphatic side chains) (Allen et al. 2002) or by binding to macromolecules such as polyethylene glycol or polyvinylalcohol (Brasseur et al. 1999). Besides selective targeting against the tumor cells themselves, attempts have been made to direct PDT *in vivo* against tumor vasculature (Chen et al. 2006). And last but not least, nanoparticles are being used as delivery system for the photosensitizer (Tacelosky et al. 2012, Jia et al. 2012).

Clinical applications of PDT cover a broad spectrum of malignant as well as non-malignant affectations and include:

- In *dermatology*: Cancers (review: Marmur et al. 2004), psoriasis and vitiligo.
- In *internal medicine, otorhinolaryngology, urology and gynecology*:

Various cancers and precancerous affectations (reviews e.g. Simone et al. 2011, Soergel et al. 2008, Upile et al. 2011, Yavari et al. 2011).

- In *ophthalmology*: Age related macula degeneration (AMD) (review: Verteporfin Roundtable 2005).

In clinical application, advantages of PDT over other forms of tumor therapy are its little invasiveness causing only restricted acute impairment such as local burning. This, together with the ease of handling, allows treatment in an outpatient setting (Triesscheijn et al. 2006, Vogl et al. 2004). To be mentioned also are (Brown et al. 2004, Hopper 2000, Triesscheijn et al. 2006): low systemic toxicity (mostly a time limited photosensitization of the skin (Harrod-Kim 2006) ); sparing of the tissue architecture in the treated area, thereby limiting scarring; no significant cumulative adverse effects upon repetitive application; no systemic immunosuppression; no direct mutagenicity or teratogenicity because nuclei and DNA of cells are usually not reached by the photosensitizer (Buytaert et al. 2007); and last but not least its affordability. Furthermore, PDT has in preclinical experiments been shown to enhance the host's immune response against the PDT-targeted neoplasia – a possible issue for anti-tumor vaccination (Castano et al. 2006, Gollnick et al. 2002, van Duijnhoven et al. 2003). Even if, in the case of malignancies, patients' survival is not necessarily prolonged, impairment due to tumor-caused obstruction, such as dyspnea, dysphagia or cholestasis, can be relieved and quality of life thereby improved (Brown et al. 2004, Hopper 2000, Moghissi 2004), which is still an issue, considering that patients admitted to clinical studies for PDT are often inoperable or else not suited for other classical treatments. Thus, PDT is believed to be a valuable tool in palliative medicine.

In internal medicine, neoplasiae on the surface of hollow organs, with little depth into the surrounding tissue, have typically been addressed by PDT research. Unlike radiotherapy, even big surfaces, such as the inner bladder or mesothelia (Du et al. 2010), as well as precancerous affectations can be treated without excessive systemic toxicity or adverse reactions (Hopper 2000). Moreover, with growing expertise in the use of interstitial irradiation devices, the confinement to organ surfaces can be overcome, and three-dimensional tumors of inner organs are becoming accessible. Amongst others, investigations are aimed at primary tumors or metastases of the liver (Kujundzic et al. 2007, Vogl et al. 2004) or the pancreas (Bown et al. 2002, Fan et al. 2007). The irradiation device can be placed

interstitially in the tumor and, owing to its missing side effects, irradiation can be repeated as required.

Last but not least, combination of PDT with surgery as well as radio- or chemotherapy is possible.

Thus, several applications of PDT with various sensitizers have in the last years been approved for clinical use by health agencies throughout the world or are in clinical trials (Brown et al. 2004, Filonenko et al. 2008, Juzeniene et al. 2007, Miller et al. 2007, Triesscheijn et al. 2006, Trushina et al. 2008).

## ***1.2 Lasers as Light Source for PDT***

Irradiation of the photosensitizer for PDT in clinical applications is classically performed with a laser (Alexiades-Armenakas 2006, Harrod-Kim 2006). One important advantage compared to other light sources is the monochromaticity of its light: the irradiation wavelength is chosen to be the most efficiently absorbed by the photosensitizer, hereby avoiding ineffective light contributing to total irradiation dose, which would be susceptible to damage the tissue in a non-specific way. Furthermore, coherence (one phase in time and space), collimation

(light propagation parallel in space), high achievable power-density (or irradiance), as well as the possibility to couple the source to optical fiber systems and specific applicators in order to access internal organs or even the interstitium (*Figure 4*) are properties that render the laser the most convenient light source for clinical applications. Especially diode lasers offer the advantage to be still more compact and cheaper.

In clinical applications where the lesion to be treated is three-dimensional, the tissue penetration of both, the drug and the light, is determinant for the effectiveness of the method, as are light absorption and scattering properties of the tissue. Typically, care has to be taken to avoid for example the promotion of cell growth or cell migration under conditions of low light dose or dysfunctional vasculature at a tumor edge, which has been reported as disastrous side effect by some authors (Chen et al. 2006). In cell culture experiments, we usually

circumvent such inhomogeneity by working with adherent monolayer cells, where all cells in a dish are, in principle, submitted to identical conditions of incubation and irradiation.

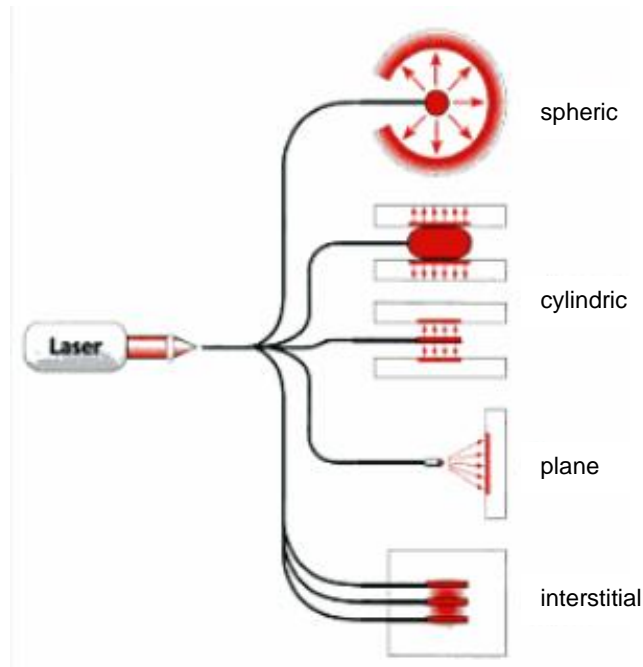


Figure 4 Schematic representation of the possibilities to apply laser light to tissue.  
( From Stepp 2003, Copyright Urban & Vogel GmbH )

### 1.3 Modes of Cell Death – Apoptosis and Necrosis

Wider medical application of PDT is still impaired by missing possibilities to thoroughly control specific effects in the targeted cells. The mechanisms by which PDT induces cell death have been object of extensive studies as reviewed by Oleinick (Oleinick et al. 2002), Almeida (Almeida et al. 2004) or Juzeniene (Juzeniene et al. 2000).

*In vivo*, besides direct cell damage, PDT can lead to the destruction of tumor vasculature (Chen et al. 2006) and activation of non-specific immune responses (Huang et al. 2008):

PDT-induced direct cell damage has been reported to proceed via different pathways (Almeida et al. 2004, Buytaert et al. 2007, Nowis et al. 2005): While

frequently necrotic cell death is occurring, characteristic features of the so-called programmed cell death or apoptosis have been observed.

In apoptosis, certain stimuli can incite cells to start a cascade of transformations that result in DNA fragmentation and finally lead to cell death (*Figure 5*). This has been shown to take place in physiological processes involving organ remodeling, such as embryonic development.

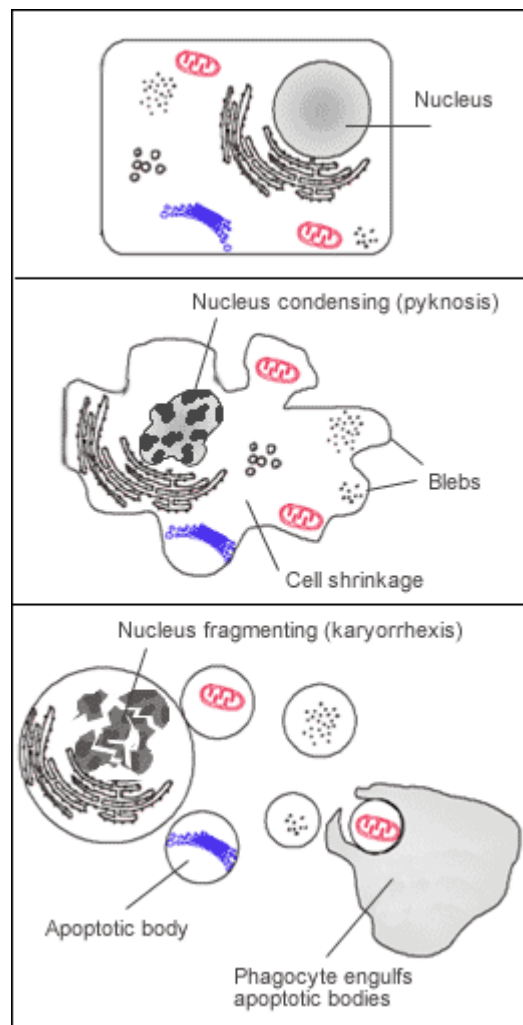


*Figure 5* Schematic Illustration of apoptotic cell death. ( From Farmer 2006 )

*In vivo*, the possibility to kill cells specifically by this means has the advantage of being well organized: Cells are not disrupted; hence, there is no inflammation by leakage of intracellular material to the interstitium (Hug 1998). On the other hand,



this mode of cell death requires a functioning genetic program that is sensitive to mutations as are frequently encountered in cancers: Cells might thus be or get resistant to apoptosis (Hug 1998, Terada et al. 2003) and/or to PDT (Singh et al. 2001):

Caspases play a key role in the initiation of apoptosis (Hug et al. 1999). Fourteen enzymes of this family, having in common a cysteine residue in their active center and specifically cutting peptides after an aspartate residue, are known in mammalian cells (Chauvier et al. 2007). They are usually present in form of pro-caspases that can be activated by proteolytic cleavage either by other enzymes or auto-catalytically. Furthermore, they are divided into two groups according to their position in the caspase cascade: the so-called initiators and the effectors.

Three distinct pathways are known to activate this cascade:

- In the *extrinsic pathway*, extracellular signals can be transmitted via a membranous death receptor, e.g. CD 95 (also known as Apo-1 or Fas), acting on caspase 8 in the first place.
- The *intrinsic pathway* is usually considered to be initiated via mitochondrial damage, leading to loss of mitochondrial membrane potential and release of cytochrome c from the mitochondrial intermembranous space to the cytosol, where it contributes, together with the protein Apaf-1, to the formation of the so-called apoptosome that activates caspase 9.

The transcription factor p53 can interfere at this level by preventing a heat-shock-protein, Hsp70, to bind Apaf-1, thus being pro-apoptotic. Another protein, bcl-2 (B-cell lymphoma rearrangement protein), prevents apoptosis by inhibiting leakage of mitochondrial proteins into the cytosol (Green et al. 1998).

- A third pathway, induced by stress, leads to calcium release from the endoplasmic reticulum and consecutively to the activation of caspase 12.

Either pathway finally leads to the activation of caspase 3 that has many substrates, like PARP (Poly-Adenosyl Ribose Phosphatase), an enzyme necessary for DNA repair. Late signs of apoptosis are DNA-laddering.

Upon PDT (cf. *Figure 6*) both, the intrinsic pathway with apoptosome formation as well as the extrinsic pathway through cell-death receptors have been observed

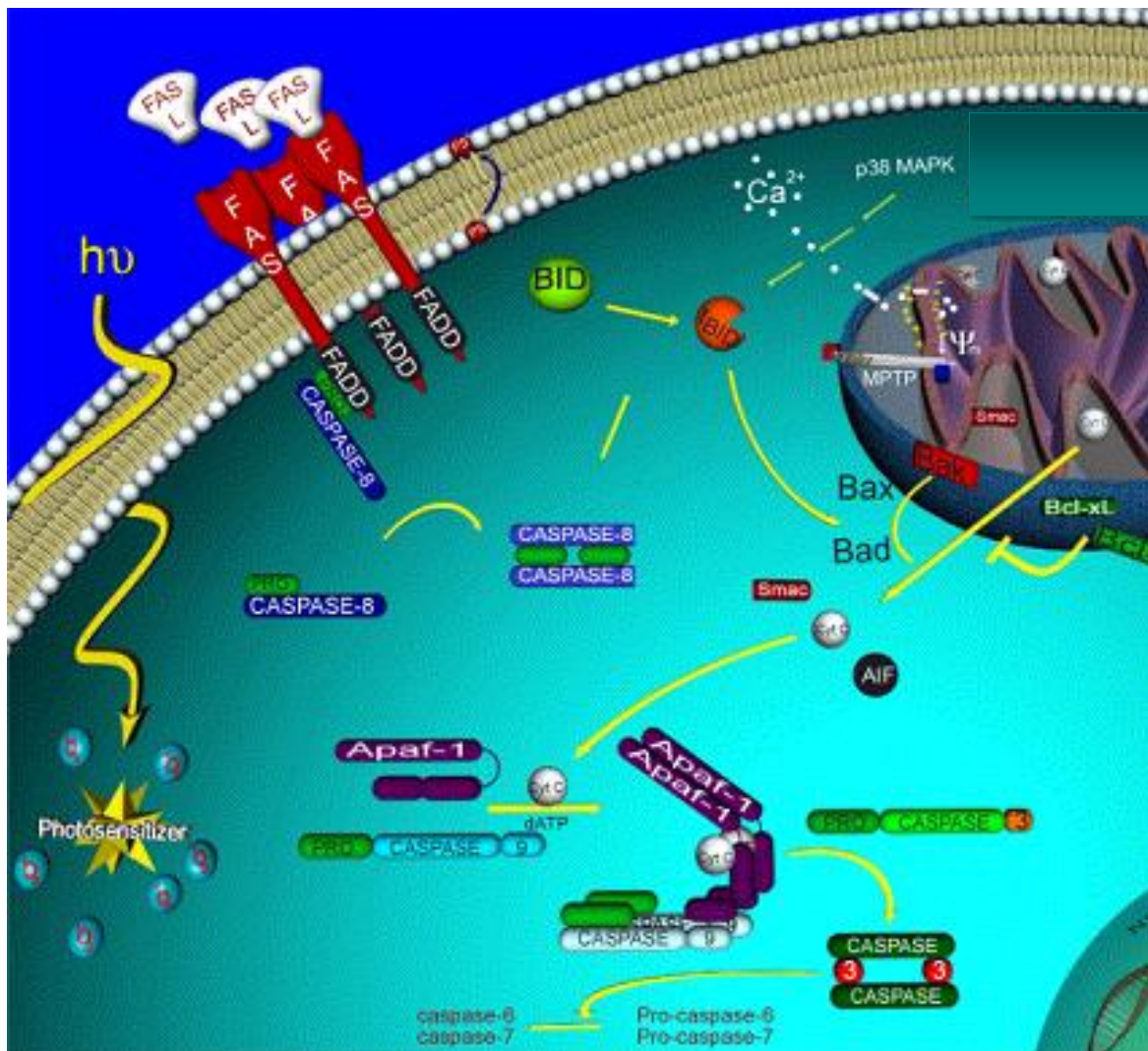


Figure 6 Major molecular events leading to cell death in cells treated with photodynamic therapy (PDT). The two major apoptotic pathways, the death receptor-mediated, extrinsic pathway, and the mitochondria-mediated, intrinsic pathway are presented. The diagram summarizes the results obtained in different tumor models using various sensitizers. ( From Almeida et al. 2004 , reprinted with permission from Elsevier ): The extrinsic pathway can be influenced by interaction of the irradiated photosensitizer (PS) with the transmembrane receptor FAS, leading to its clustering independently of the specific ligand FAS-L, and subsequent binding of FADD-protein and activation of caspase 8. The latter can also be directly activated by the PS. The intrinsic pathway involves perturbation of the mitochondrial transmembrane potential  $\Psi$ , formation of pores (MPTP) and leakage of mitochondrial proteins, e.g. cytochrome c (cyt c), Smac or AIF. Several Bcl-2-family proteins, such as Bak, Bax, Bad, Bcl-xL and Bcl-2, are susceptible of interfering at this level. Interaction of both pathways via caspase 8-induced cleavage of the protein BID or interference with calcium-levels has been shown. Cytochrome c release to the cytosol induces apoptosome formation around the Apaf-1-protein and subsequent activation of the caspase cascade (caspases 9, 3, 6 and 7).

(Miller et al. 2007, Almeida et al. 2004). The path followed depends on the photosensitizer used, its concentration, the localization of its intracellular photoactivation, the cell type and its protein endowment as well as on the irradiation mode (dose and irradiance).

Extensive attention has been given to the presence of the above-mentioned proteins known to interfere in tumor growth or apoptosis induction such as the tumor suppressor protein p53, caspases or members of the bcl-2-family (including Bak and Bax). These proteins are typically mutated in tumor cells (e.g. 50% of cancers exhibit mutated p53 (Harrod-Kim 2006)). Thus, the outcome of treatments like PDT, interfering with cell processes involving these proteins, can be expected to depend on the mutation status of the latter. Astonishingly, experiments provided evidence that, although their presence may favor a certain cell death pathway, the overall PDT-induced cell-killing does not seem to depend on them (Miller et al. 2007). Lately too, besides the mentioned proteins, mitochondrial phospholipids were found as possible early targets of PDT (Miller et al. 2007).

Among the proteins susceptible of interfering with apoptosis and relevant in tumor biology, p53 and bcl-2 have been mentioned here because the cell lines used in this work differ in the expression of these proteins.

Besides, not only apoptosis versus necrosis but intermediate pathways have since been described as possible modes of cell death: A mechanism referred to as paraptosis was characterized by Sperandio (Sperandio et al. 2000), which, although lacking several specific features of apoptosis, is genetically controlled; that is, it does require transcription and translation, and it seems to be caspase 9 dependent. On the other hand, this paraptosis involves neither DNA-fragmentation nor chromatin-condensation, nor does the formation of apoptotic bodies occur. Typically, it can bear some morphologic characteristics of necrosis, such as cytoplasmic vacuoles and swelling of mitochondria. And, unlike apoptosis, TUNEL assay (which is used to quantify apoptosis) is negative, and caspase-inhibitors or Bcl-xL, known to inhibit apoptosis, do not block this mode of cell death.

Last but not least, autophagy is a new-found mechanism by which a cell can recycle dysfunctional organelles while it can lead to cell death if ultimately the repair fails. Kessel (Kessel et al. 2007) found features of autophagy leading either to cell death or photodamage repair following PDT. It depends on functioning lysosomes and occurs independently of apoptosis.

## **1.4 This Work**

Our group has been working on the photobiological properties of different photosensitizers (Kinzler et al. 2007, Kress et al. 2003, Rück et al. 2003) and on their use in photodynamic therapy (Orth et al. 2000, Pfaffel-Schubart et al. 2006) or diagnosis (Malik et al. 2000). The present work is aimed at establishing a cell culture model for further investigation of the photobiological effects of tetrasulfonated aluminum phthalocyanine (AlPcS<sub>4</sub>) that had been assayed already before in cooperation with Russian researchers (Edinak et al. 1996).

Hepatocellular carcinoma cell (HCC) cultures were chosen (1) because the results might potentially be transferable to an *in vivo* model of a still difficult to treat neoplasia and (2) because three different cell lines were easily available for comparison purpose. Indeed, the three cell lines used differ, amongst others, in the expression of p53 and bcl-2 (cf. 'Material and Methods' and 'Results'), proteins which are, as has been mentioned above, potential interferers in apoptosis.

As photosensitizer our group originally used *Photosens*, a preparation obtained by courtesy from the General Physics Institute of the Russian Academy of Sciences (Moscow), which was said to be chlorine-free AlPcS<sub>4</sub> (N. Akgün, personal communication). Later on, we purchased it from Frontier Scientific (Lancashire, UK), where a much less expensive chloride form was regularly available too. In the following work, we will compare both substances.

Initially, phthalocyanines, such as AlPcS<sub>4</sub>, gained some interest as alternatives to the then mostly used porphyrins (of which porfimer sodium was the first photosensitizer to be approved for clinical use in 1993 (Triesscheijn et al. 2006) ) because of their typical light absorption maximum above 650 nm, which makes them useful in the PDT of living tissue that is relatively transmissive to light at this wavelength (Pushpan et al. 2002). Naphthalocyanines absorbing light around

770 nm have even been investigated for the treatment of pigmented melanomas. Moreover, due to their central metal atom, aluminum-, zinc- or silicon-phthalocyanines have a high singlet oxygen generating efficiency, a prerequisite for PDT. Furthermore, the long wavelength fluorescence exhibited makes this group of photosensitizers convenient for microscopic studies and co-analyzing of other fluorochromes the fluorescence maxima of which are commonly at shorter wavelengths.

While zinc- and silicon-phthalocyanines (Pc4) underwent clinical phase I/II trials in Switzerland respectively in the USA (Miller et al. 2007, Pushpan et al. 2002), AlPcS<sub>4</sub> itself, besides for experimental purposes (Almeida et al. 2004), has been used in the PDT of different neoplasiae in Russia, where it was first approved for clinical use in 1994 under the name *Photosens* (Sokolov et al. 1996, Filonenko et al. 2008, Trushina et al. 2008).

Various degrees of sulfonation of the phthalocyanine basic cycle allow to modulate its hydrophilicity. Several other derivatives have been synthesized and investigated, e.g. polymer-conjugates to enhance water solubility (Brasseur et al. 1999), AlPc encapsulated in (transferrin-conjugated) liposomes (Derycke et al. 2004), substituted with alkyl or peptide chains to modulate lipophilicity (Allen et al. 2002, Ke et al. 2012) or else coupled to monoclonal antibodies (Vrouenraets et al. 2001) to improve tumor-selectivity.

An interesting new application has recently been described by Norum (Norum et al. 2009), who used AlPcS<sub>2</sub> to promote photochemical internalization of bleomycin, a chemotherapeutic, in tumor cells. Furthermore, aluminum phthalocyanine has also proved effectiveness against *Leishmania* species, parasitic protozoae that cause severe systemic infections in humans still defying medicamentous treatment (Dutta et al. 2005).

To briefly outline the presented work, first toxicity of the photosensitizer alone was assessed as a function of concentration. As mentioned, two forms of AlPc, the chloride and the chlorine free form, were compared. Then, phototoxicity of AlPc, that is PDT, was investigated, again as function of concentration, but also in dependence of irradiation conditions.

These experiments were conducted with the help of a viability assay quantifying the amount of neutral red uptake ('Neutral Red Assay').

The responses of two viability assays based on different metabolic processes, neutral red uptake versus MTT transformation ('MTT Test', MTT = 3-(4,5-Dimethylthiazol-2-yl)-2,5-diphenyl-tetrazolium Bromide ), were then compared in a time course after PDT.

Localization of the photosensitizer was characterized in vital cells by laser scanning microscopy after co-incubation with organelle specific fluorochromes, and effects of PDT were visualized by optical and electron microscopy.

We explored the possibilities of surveying cells during dye-uptake or photodynamic therapy with our newly acquired LSM 510 meta (Zeiss).

Furthermore, the influence of caspase inhibitors and of different anti-oxidants or radical scavengers was assayed in the context of AIPcS<sub>4</sub>-PDT.

Cytochrome c release from mitochondrial intermembranous space being a characteristic step in mitochondria involving apoptosis, this was assayed by Western Blotting technique under PDT conditions, using a commercial kit that will be detailed further in 'Materials and Methods'. The physiological function of the proteins involved as well as the principle of the method is subject of the following section (1.5).

For comparison purpose, another cell line was submitted to the evaluation of cytochrome c release upon a specific trigger: We used murine L929 cells in parental (L929 Par) form as well as transfected with Apo-1 (L929 Apo):

Exposition of the transfected cells, expressing Apo-1, with agonistic anti-Apo-1 antibody leads to aggregation of the Apo-1 in the cell membrane that in turn launches the extrinsic caspase cascade (Green et al. 1998).

The following two sections describe the biochemical background for experimental settings, namely monitoring of mitochondrial cytochrome c release and the use of caspase inhibitors that are indispensable for the results' interpretation.

## **1.5 Cytochrome c and COX4 in Mitochondria**

As has been stated earlier, mitochondria are typically affected by apoptosis induction in the intrinsic pathway: Increase of outer membrane permeability by pore proteins leads to loss of membrane potential and of molecules usually found in the space between the inner and the outer mitochondrial membranes.

This can be monitored by the following method: Cells under investigation are destroyed mechanically, and their mitochondria and cytosol separated (fractionation). Then, a typical soluble mitochondrial protein, here cytochrome c, is detected in both fractions. If cytochrome c can be detected in the cytosol, this means, it has been released *ex ante* from the mitochondria. Because this can be caused also by severe mechanical damage, another mitochondrial protein, that usually remains in the mitochondrial membrane even after permeability transition, COX4, is monitored in parallel, to discern apoptotic effects from artifacts.

The physiological *in vivo* functions of both proteins considered in our kit, cytochrome c, and COX4, the control protein, are outlined here, referring to Saraste (Saraste 1999): Cytochrome c is a water-soluble hemoprotein, found in the space between the inner and the outer mitochondrial membrane. It donates electrons to the complex IV of the cytochrome c oxidase (COX4), which is, for its part, located in the mitochondrial inner membrane, and in turn generates a transmembrane proton gradient. *Figure 7* depicts the whole protein complex involved in oxidative phosphorylation with the cytochrome c and the subunits of cytochrome c oxidase.

During mitochondria-involving apoptosis, the mitochondrial outer membrane becomes permeable, allowing cytochrome c to diffuse into the cytosol, while the membrane-bound COX4 remains in the mitochondria.

Release of cytochrome c from the mitochondrial intermembrane space to the cytosol does not by itself impair mitochondrial function: Waterhouse (Waterhouse et al. 2001) report persistence of the mitochondrial transmembrane potential and survival of the cells, provided that in particular (1) cytochrome c is not allowed to diffuse out of the cell, and (2) induction of the caspase cascade provoking apoptosis is prevented.

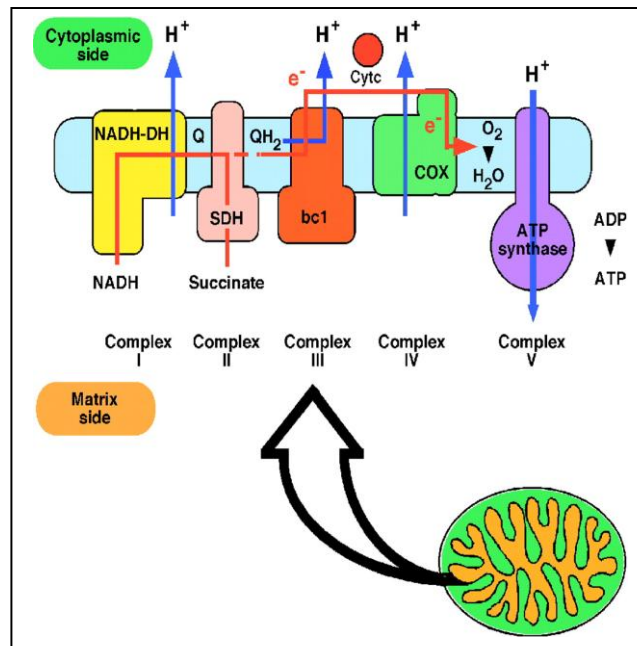


**Figure 7** The enzymes of the mitochondrial inner membrane involved in oxidative phosphorylation: NADH-dehydrogenase (DH), succinate dehydrogenase (SDH), cytochrome bc1, and cytochrome oxidase (COX) form the electron transfer chain to  $O_2$ . With the exception of SDH, these enzymes translocate protons across the membrane. The proton gradient is used by ATP synthase to make ATP. ( From Saraste, *Science* 283: 1488-1493 (1999), reprinted with permission from AAAS )

## 1.6 Caspase Inhibitors – General Considerations

For assessing how caspases are involved in the process of cell damage after PDT, cells were treated with two broad spectrum caspase inhibitors prior to PDT: z-VAD-fmk and boc-D-fmk (cf. 'Material & Methods').

Both inhibitors, acting as pseudosubstrates, contain a peptide part (D = Asp, respectively VAD = Val-Ala-Asp), that is specifically recognized by the active centre of caspases, combined with a fluoromethylketone (fmk) group reacting covalently (and thus irreversibly) with the caspases' cysteine (Chauvier et al. 2007). Furthermore, a benzoyloxycarbonyl- (z-) or a t-butoxycarbonyl- (boc-) group renders the inhibitor irreversible by preventing unspecific cleavage at the N-terminal end.



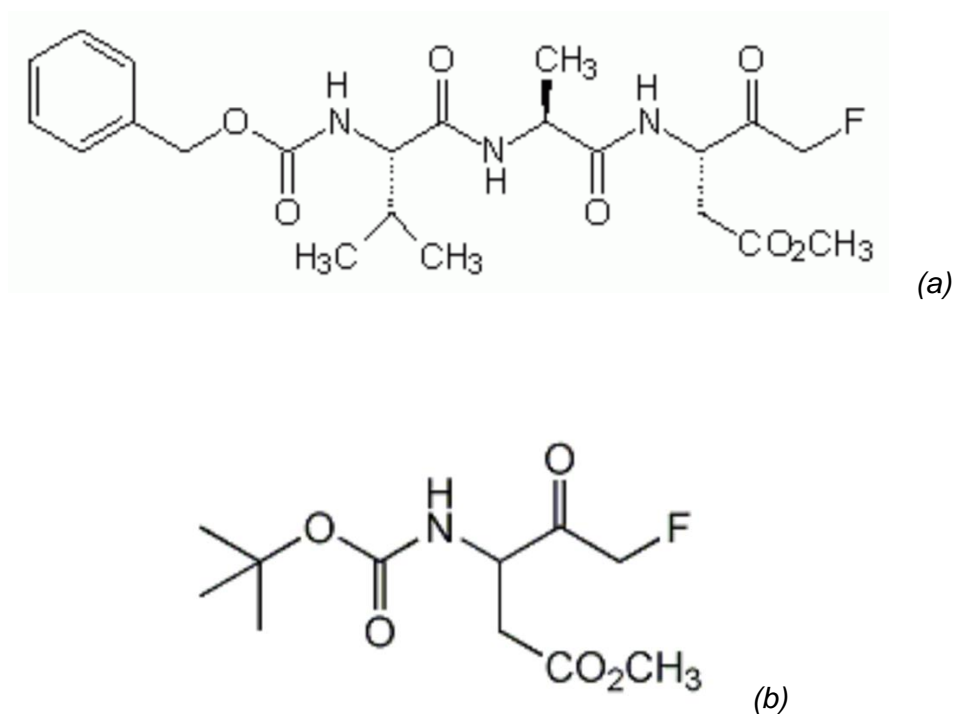


**Figure 8** Caspase inhibitors z-VAD-fmk (a) and boc-D-fmk (b).  
( From: EMD Millipore Chemicals, product information )

Linkage to the fmk-group as well as the O-methylation of the Asp side chain also enhances cell permeability that is poor for the unsubstituted peptidic inhibitor alone (Ekert et al. 1999, Chauvier et al. 2007).

The formulae of both caspase inhibitors are depicted in *Figure 8*.

## 2 Materials and Methods

### 2.1 General

Table 1 (a) and (b) list the reagents and tubes used for the different procedures described herein. Reagents used solely for Western blotting are itemized later (Table 3).

Furthermore were used:

- Double distilled water (ddw) as provided by the laboratory.
- Sterile double distilled water obtained by autoclaving the latter.
- 1x PBS prepared by adding 50 ml 10x PBS to 450 ml sterile ddw.

Adjusting the pH:

When the pH of solutions had to be adjusted, this was done with a pH-meter pH 537 equipped with a glass pH-electrode SenTix 61 (WTW GmbH / Germany).

Table 1 (a) Tubes and their characteristics. PP: polypropylene, PS: polystyrene.

Tubes	Material	Volume	Provider
		[ml]	
1.5ml	PP	1.5	Eppendorf
10ml PS	PS	10	Greiner
15ml PP	PP	15	Nunc
50ml PP	PP	50	Greiner

Table 1 (b) Reagents and their characteristics. (cf. Table 3 for Western reagents.)

(1) AOx: anti-oxidant or radical scavenger; cell: cell culture; dye: stains or color markers. LSM: laser scanning microscopy. MW: molecular weight; PBS: phosphate buffered saline.

Substance	Provider	Cat.#	MW [g/mol]	Characteristics	Used for (1)
Ascorbic acid	Merck		176.13		AOx
Acetic acid 100%	Merck	1.00063	60.05	1.05 g/ml	dye
Dimethylsulfoxide (DMSO)	Sigma	D-2650	78.13	1.10 g/ml	LSM
Dulbecco's Modified Eagle Medium (DMEM)	Gibco	31885-023			cell
Ethanol, denatured	Laboratory		46.07	0.79 g/ml	
EDTA (Versen) solution	Biochrom	L 2113		1 % w/v in PBS	cell
Fetal bovine serum (FCS)	Biochrom - Gibco -	- S 0115 - 10270-106			cell
Hydrochloric acid, min 37%	Riedel-de-Haen	30721	36.46	1.19 g/ml	
N-Acetyl-L-Cysteine (NAC)	Sigma	A-8199	163.2		AOx
Neutral Red (NR)	Biochrom	L 6313		0.3 % w/v	dye
10x PBS	Life Technologies, GibcoBRL	14200-067		sterile, without Ca <sup>2+</sup> , Mg <sup>2+</sup>	
Penicillin/Streptomycin (P/S)	Biochrom	A 2213		10'000 U/10'000 µg/ml	cell
Pyrrolidinedithiocarbamate (PDTTC), ammonium salt	Sigma	P-8765	164.3		AOx
RPMI 1640 Medium	Gibco	21875-034			cell
Sodium ascorbate	Fluka	11140	198.11		AOx
Sodium hydroxyde pellets	Merck	1.06482	40.00		
NaOH solution, min. 32%	Merck		40.00	1.35 g/ml	
Trypan Blue solution	Biochrom	L 6323		0.5 % w/v in 0.9 % NaCl	dye
Trypsin solution	Biochrom	L 2133		2.5 % w/v in PBS	cell

## 2.2 Cell Culture

### 2.2.1 Cell Lines

Cells utilized for this work were human hepatocarcinoma cells **Hep3b** (ATCC# HB-8064), **HepG2** (ATCC# HB-8065) and **HuH7** (provided by the Department of Experimental Anesthesiology; origin of the cells cf. Nakabayashi 1982).

Besides being carcinoma cells, i.e. of those that are potential targets of PDT *in vivo*, these three cell lines give the opportunity to compare cells with different protein expression pattern while originating from the same tissue.

Amongst others, the cell lines considered differ in the expression of p53: Thus, HepG2 are reported to be p53 wild type, whereas Hep3b are p53 negative and HuH7 are p53 mutated (Hug et al. 1997).

Concerning bcl-2, another protein susceptible of interfering in apoptotic pathways, data in literature is quite inconsistent concerning its presence in the afore mentioned HCCs. This will be dealt with further in the discussion.

### 2.2.2 Cell Handling

Cells were grown in Nunc (Denmark) cell culture flasks (growth surface: 75 mm<sup>2</sup>, called hereafter 'big'; or 25 mm<sup>2</sup>, called 'small') using RMPI 1640 Medium supplemented with 50 ml (10 %) Fetal Bovine Serum (FCS) and 5 ml Penicillin/Streptomycin (P/S) per 500 ml medium. Medium volume was 6 ml in small, respectively 16 ml in big flasks. Cultures were maintained in a humidified atmosphere at 37 °C and 5 % CO<sub>2</sub> in a Heraeus 6000 incubator.

All manipulations with these cells were done under sterile conditions, working on a laminar flow bench (Biohit), with sterile reagents. Solutions, if not purchased in a sterile form, were sterilized by vapor sterilization or filtering over 0.2 µm (Sartorius Minisart single use sterile syringe filter, Cat.# 16543 ).

Exception was made when cell growth was not to be assessed afterwards.

For removal of the adherent cells from the flasks, a trypsin/EDTA (T/E) solution was used, containing 0.125% of each, prepared from the Biochrom stock solutions by dilution in 1x PBS.

Cells were re-seeded in new flasks when confluent. For this purpose, medium was removed, 1 ml (small) respectively 2 ml (big flask) of T/E were added, and the flask left in the incubator for a few minutes until cells would go into suspension upon gentle clapping of the flask. 4 ml (small) respectively 8 ml (big flask) of fresh medium were added to stop the action of trypsin, cell suspension was pipetted several times through a one-milliliter pipette to avoid clumping of the cells, then the cell suspension was diluted about tenfold, depending on initial density, and introduced in a new flask.

For experiments, cells were cultured in 4 -, 24 - or 6 - well plates. Characteristics of these plates are given in *Table 2*. Unless otherwise mentioned, cells were seeded with an initial density of 100 - 200 cells /mm<sup>2</sup> and allowed to grow for two days prior to further treatment.

### **2.2.3 Cell Quantification**

To control cell density, counting of the cells at a proper dilution was performed with a Neubauer counting chamber (Brand, Germany).

For use with the Laser Scanning Microscope (cf. Chapter 2.12), cells were grown in 4 - well plates, each well of which had been tipped with a breamed round cover slide of 10 mm diameter (Merck Eurolab 631 9490) or on 75x25 mm<sup>2</sup> vapor sterilized microscope slides (Marienfeld/Germany) placed in Quadriperm plates (cf. *Table 2*).

*Table 2*      *Plates used: Surface, volume, T/E-volume; each per well.*  
*T/E: trypsine / EDTA - solution.*

	surface / well	medium / well	T/E per well	Provider
	[mm <sup>2</sup> ]	[ml]	[μl]	
<b>4 - well</b>	190	0.5	100	Nunc
<b>6 - well</b>	960	2.5	200	Becton-Dickinson
<b>Petri dish</b>	960	2.5	200	Nunc
<b>24 - well</b>	200	0.8	100	Nunc
<b>Quadriperm</b>	2180	5	n.a.	Vivascience
<b>96 - well</b>	32	0.1	n.a.	Greiner

## **2.3 Cell Growth Curve**

Cell growth was assessed by seeding the cells in Petri dishes with a specified initial density (100 cells/mm<sup>2</sup>) and hand counting cells at specified times. Special care was taken to achieve quantitative flaking and homogeneous resuspension. Cell densities in the dishes were calculated taking into account the applied dilution. At every time point two Petri dishes were appraised. Medium was exchanged in all dishes every two to three days.

A preliminary experiment evaluated cell recovery after seeding: Cells were seeded with a known density and hand counted two days later.

For further experiments cell counting by hand as described here was replaced by the use of viability assays which allow to process the cells faster when many samples are to be analyzed at the same time. The procedure as well as the validation of these assays is the theme of the following chapter.

## **2.4 Viability Assays**

Cell viability was quantified with the Neutral Red (NR) Assay and/or the MTT Test two days after accomplishment of the treatment that was to be assayed, unless otherwise mentioned. If the medium contained any reagents other than the ones used for common cell culture, it was exchanged with fresh one prior to the addition of the assay's reagent, in order to avoid possible interferences.

For these assays, cells were cultured and treated in 4-well plates when irradiation was involved and in 4-well or 24-well plates when not irradiated during the procedure.

Correlations were made, using untreated cells, between results obtained by the assays and seeded cell densities respectively hand-counted cell numbers, in order to assure linearity of the methods and to optimize the quantity of reagent (NR or MTT) necessary.

Hand-counting was performed on appropriately diluted cell suspensions, obtained by treatment of the adherent cells with T/E (0.1 ml/well) followed by addition of fresh medium (0.4 ml/well), with a Neubauer chamber (Brand, Germany). Special care was taken to achieve quantitative flaking.

Specific experimental conditions for each assay (NR and MTT respectively) are described hereafter. Common treatment at the end and evaluation are explicated below for both.

### **2.4.1 Neutral Red Assay**

The Neutral Red (NR) Assay was obtained as Gamma Kit from Biochrom (Cat.# D-7004) and the assay was performed as described bellow.

When the Gamma Kit was not available anymore, the solutions were homemade in the following way:

#### ***Neutral Red Solution***

4.5 g NaCl and 5 ml 0.3 % w/v NR (Biochrom Cat.# L 6313) were completed to 500 ml with ddw after adjusting the pH to 7.4 with NaOH solution.

Thus, final concentration was 0.03 % NR in 0.9 % NaCl.

The solution was stored at 4°C and protected from light. It was filtered over a folded paper filter (Schleicher&Schuell Cat.# 10 311 647) when crystals precipitated, and discarded when its color changed.

*Washing Solution*

1x PBS (prepared from commercial 10x PBS)

*Lysis Solution*

Mixture of the following:

500 ml ethanol (denatured), 500 ml ddw and 10 ml acetic acid 100 %.

500 µl of NR solution were added to the medium of each well and incubated for 1 - 4 h in the incubator. (Incubation time was kept constant for samples that were to be compared). The liquid was then removed, the cells carefully washed with 100 µl washing solution and then lysed with 100 µl lysis solution. (Volumes are given per well.) The plates were left on a shaker for 10 min at RT, then the solution from every well was transferred to a 96 - well plate and quantified (cf. 2.4.3).

**2.4.2 MTT Assay**

The MTT Assay was purchased as Alpha Kit from Biochrom (Cat.# D-7002) and the assay was performed as follows.

50 µl of MTT solution were added to each well and incubated for 2-4 h in the incubator (time being constant for samples to be compared). The liquid was then removed and the plates allowed to dry for 30 min at 37 °C. 25 µl of SDS-solution per well were added followed by 100 µl of lysis solution (containing isopropanol). It was desisted from washing because early experiments showed that the cells tended to be removed from their support through this procedure, leading to irreproducible results.

Plates were shaken for 5 min prior to transfer of 100 µl of each well onto a 96 - well plate. If color density was very high, volume of lysis solution was increased and/or volume transferred to the 96 - well plate was reduced. In these cases, optical density was corrected for the volume.

**2.4.3 Photometry for Viability Assays**

The solutions on 96 - well plates were analyzed by the following procedure:

Optical densities were measured in a microplate luminometer (Lucy 1, Anthos Instruments/ Austria) at 570 nm and 690 nm for specific and unspecific absorption respectively. Data were transferred to Excel and further evaluated.



Empty wells of the 96 - well plates were measured under the same conditions to verify the blank values.

Results obtained were evaluated and compared as values of optical densities (O.D.) or relative optical densities in percent of the control values (% of ctrl). Unless otherwise mentioned, control values were obtained from 'untreated' cells, i.e. cultured in medium with FCS and P/S; change of medium was performed at the same intervals as for the treated cells.

For several wells treated in the same way, values obtained were characterized by the median and the median absolute difference (MAD) if there were less than thirty values. If there were more, the mean and the standard deviation were used for characterization.

For some experiments, time course of optical densities was observed after PDT for either test. In these cases, particular care was taken to incubate with the dyes for a constant short time. The time of every point was defined to be the middle time of incubation.

## 2.5 Photodynamic Therapy (PDT)

### 2.5.1 The Photosensitizer

For PDT, cells are incubated with a dye, called the photosensitizer, during a certain time and then submitted to light of a wavelength specific for the photosensitizer, usually close to the absorption maximum of the latter. Concentration of the photosensitizer and duration of incubation on the one hand, irradiance of the light [ $\text{W}/\text{m}^2$ ] and duration of irradiation (the product of both giving the overall dose of irradiation, or radiant exposure  $H_e$  in [ $\text{J}/\text{m}^2$ ]) on the other hand, are the parameters to be controlled.

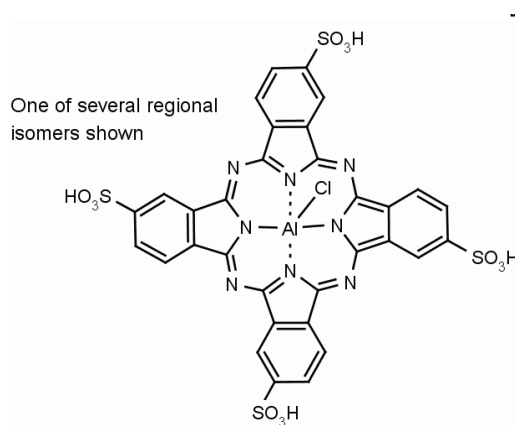


**Figure 9**      *Molecular structure of the photosensitizer aluminum phthalocyanine tetrasulfonate chloride,  $\text{AlPcS}_4\cdot\text{Cl}$  (Formula weight: 895.21 g/mol)*  
( Figure from Frontier Scientific online catalogue )

In our case, PDT was performed using tetrasulfonated aluminum phthalocyanine ( $\text{AlPcS}_4$ , hereafter abbreviated  $\text{AlPc}$ ; *Figure 9*) purchased from Frontier Scientific (Lancashire, UK). Originally, our group used *Photosens*, a preparation obtained by courtesy from the General Physics Institute of the Russian Academy of Sciences (Moscow), which was said to be free of chlorine. Such a substance could be specially synthesized by Frontier Scientific upon request, but it is far more expensive than the catalogue product containing a chlorine ligand (Cat.#  $\text{AlPcS}$ -834, FW 895.21 g/mol). Therefore, both substances (from Frontier Scientific) were compared anent their dark and photo-toxicity on the cell lines used

(cf. 'Results'). Besides toxicity, absorption and fluorescence spectra of both substances were recorded as described hereafter.

*Note: For ease of writing, we will refer to the photosensitizer as AlPc throughout the chapters Material & Methods and Results, thereby meaning the tetrasulfonated form which was the only one used.*

### **2.5.2 AlPc - Absorption and Fluorescence Spectra**

Absorption spectra of both, AlPc-Cl and AlPc-OH, were recorded with a Kontron Uvikon 810 spectrometer, using ddw as reference.

Fluorescence spectra of both AlPc-compounds were recorded at two different concentrations (in the mM and  $\mu$ M range respectively) using the laser scanning microscope LSM 410 (Zeiss), with the 633nm line of a helium-neon-laser as excitation source and a grid adapted on the detector side for wavelength resolution.

Fluorescence spectra were smoothed by an automated procedure, which defines the fluorescence value at a certain wavelength as the mean of the fluorescence values measured at the following five wavelengths.

To compare the spectra, absorbances respectively fluorescence intensities were normalized to the highest maximum value.

### **2.5.3 AlPc Stock Solutions**

For use in cell experiments, solutions of AlPc were prepared by dissolving a weighted amount in ddw at a concentration of 1-5 mg/ml (approximately 1-5 mM) and sterile filtered over 0.2  $\mu$ m (Sartorius Minisart single use sterile syringe filter, Cat.# 16543). Higher concentrations showed to be in the region of solubility limits. The stock solution was stored at -20 °C.

Because (1) the hydration of the substance significantly varies from one batch to the other; (2) the solution has to be filtered; and (3) no formula weight is provided by the manufacturer for the chlorine free compound, the concentrations of the stock solutions were standardized by measuring the optical density at 675 nm (Kontron Uvikon 810) of a diluted solution (approximately 1-5  $\mu$ M) prepared

thereof using ddw as reference. With the help of a molar extinction coefficient of 170'000 L/mol/cm, given in the literature (Darwent et al. 1982), the concentration of the stock solution was determined (see 'Results' for further details).

#### **2.5.4 Cells' Incubation with the Photosensitizer**

From the stock solution, the appropriate amount was added to the culture medium of the cells and incubated for at least 24 h. It had been shown previously that after this time the intracellular concentration was stable (N. Akgün, personal communication).

The medium was then removed, cells were washed twice with medium and supplied with fresh medium (containing only FCS and P/S).

All cells treated with AIPc were protected from light (besides controlled irradiation for PDT) by keeping the flasks or the plates wrapped in aluminum foil, and by working under dimmed light throughout the procedures following incubation with the photosensitizer.

Dark toxicity was evaluated with the help of NR Assay two days later.

#### **2.5.5 Photodynamic Therapy - Procedure**

For PDT, the cells were submitted to light of 676 nm provided by a diode laser (Applied Optonics Corp.) equipped with an optical fiber. The irradiance at the end of the latter was measured with the help of a power meter (TPM-310 from Gentec/Canada). The size of the spot was adjusted to the size of the well to be irradiated (190 mm<sup>2</sup> for 4 - well plates, 960 mm<sup>2</sup> for 6 - well plates) and the total power emitted was adjusted to 190 respectively 960 mW to yield an irradiance of 1 mW/mm<sup>2</sup> (= 100 mW/cm<sup>2</sup>) that was used for all experiments unless otherwise mentioned. Irradiation was performed during various times to submit the cells to different light doses (radiant exposure, H<sub>e</sub> [J/cm<sup>2</sup>]).

Some experiments served to evaluate the effect of different irradiances with equal overall doses.

When the cells had been incubated with a dye, in particular the photosensitizer, the colored supernatant was removed and the cells washed twice before adding fresh medium, thus avoiding uncontrollable absorption of irradiation by additives in the medium.

Furthermore, to cut off scattering of light from one well of the plate to the others, 2 ml of trypan blue solution (with an absorption maximum at 607 nm) were filled in the space between the wells during irradiation. This solution was obtained by diluting a commercial stock solution, 0.5 % w/v in physiological saline (Biochrom Cat.# L 6323), threefold in 1x PBS. It was removed from the plates after irradiation.

Following irradiation, the plates were returned to the incubator, and NR and/or MTT Assay was carried out two days later, or further processing was undertaken as explained in the corresponding sections.

## 2.6 Cytochrome c Release from Mitochondria

### 2.6.1 Procedure

In order to assess cytochrome c release from mitochondria after PDT as an early sign of apoptosis, mitochondrial and cytosolic fractions of cells were separated with the help of the ApoAlert Cell Fractionation Kit (Clontech Cat.# K2016-1). The kit provides (1) a *1x washing buffer*, to be diluted with ddw from a tenfold concentrate, and (2) a *fractionation buffer*, the latter being completed with 1 µl DTT and 2 µl protease inhibitor per milliliter buffer to form the so-called *fractionation buffer mixture*.

After separation, both fractions are analyzed by Western Blotting with the help of a cytochrome c specific antibody. To control the proper separation of the fractions, they are also assessed with a COX 4 -specific antibody, that recognizes a protein (namely the subunit 4 of the cytochrome c oxidase) remaining in the mitochondria even when the cells undergo apoptosis.

For performing this assay, cells were left to grow in 6 -well plates until almost confluent, then subjected to the desired treatment. Cells were collected from five 6 -well plates by removing the medium, adding 0.2 ml of T/E, incubating at 37 °C for a few minutes, adding 0.8 ml medium and helping suspending the cells with a cell scraper (Nunc) (Volumes given per well). Contact time with T/E was kept to a minimum in order to avoid artifacts by this treatment. From then on, cell suspensions as well as all reagent solutions were kept on ice or at 4 °C.

Cells were collected in a 50 ml PP centrifuge tube (Greiner), submitted to centrifugation for 5 min at 600 g (Heraeus Omnifuge 2.ORS), the supernatant was removed and the pellet re-suspended in 1 ml of *1x washing buffer*, centrifuged again at the same conditions, the supernatant removed and the cells re-suspended in 0.8 ml of *fractionation buffer mixture* (see above for preparation). The suspension was left on ice for 10 min, then homogenized with the help of a 7 ml Dounce tissue grinder (Fisher Scientific Cat.# B 245 050 80), using sixty passes with the tight pestle. The suspension was transferred to a 1.5 ml tube (Eppendorf 3810X) and centrifuged for 10 min at 700 g (Heraeus Bifuge stratos). The supernatant was transferred to a new Eppendorf tube, while the pellet was discarded. The supernatant was centrifuged for 25 min at 10'000 g, to separate the

supernatant cytosolic fraction, which was transferred to a fresh Eppendorf tube, and the pellet corresponding to the mitochondrial fraction, which was resuspended in 0.1 ml of the *fractionation buffer mixture* for storage.

The obtained fractions were kept at -20 °C until further analysis by gel electrophoresis and Western blotting; then thawing was performed at 4°C.

Cytochrome c release was compared for cells (1) untreated; (2) treated with AIPc alone; and (3) submitted to PDT; exact conditions will be detailed with the results.

Cells not irradiated were cultured in the usual cell culture flasks as described, instead of 6 -well plates, for greater ease of handling. Two to three flasks of 75 mm<sup>2</sup> were used for one sample.

Cells incubated with AIPc were washed twice with 10 ml 1xPBS prior to treatment with the ApoAlert Kit.

Cells submitted to PDT were left at 37 °C for 15 min after irradiation. Then isolation according to the ApoAlert Kit was undertaken.

*Table 3 Reagents used for protein analysis (protein quantification, gel electrophoresis, Ponceau S staining, Western blotting and immunodetection). MW molecular weight*

<b>Substance</b>	<b>Provider</b>	<b>Cat.#</b>	<b>MW [g/mol]</b>	<b>Characteristic</b>
<b>Bicinchoninic acid (BCA)</b>	Sigma	B-9643		
<b>Bromophenol blue, Na-salt</b>	Roth	A512.1	691.9	
<b>Copper sulfate solution</b>	Sigma	C-2284		4% w/v
<b>Dimethylsulfoxide (DMSO)</b>	Fluka	41648	78.13	1.10 g/ml
<b>Ethylenediamine tetraacetic acid, disodium salt, dihydrate (EDTA)</b>	Fluka	03677	372.24	
<b>Glycerin</b>	J.T. Baker	7044	92.10	
<b>Glycine</b>	Sigma	G-6388	75.07	
<b>HEPES</b>	Biochrom	L 1613		1 M, pH-buffer 7-8
<b>Hydrochloric acid, ≥ 37%</b>	Riedel-de-Haen	30721	36.46	1.19 g/ml
<b>2-Mercaptoethanol</b>	Roth	4227.1	78.13	1.12 g/ml
<b>Methanol</b>	Merck	1.06009.	32.04	0.79 g/ml
<b>Ponceau S</b>	Merck	1.14275		
<b>Protease Inhibitor Cocktail</b>	Sigma	P-8340		
<b>Skim Milk Powder</b>	Fluka	70166	n.a.	
<b>Sodium chloride</b>	Fluka	71379	58.44	
<b>Sodium dodecylsulfate (SDS)</b>	Fluka	71725	288.38	
<b>Sodium hydroxide pellets</b>	Merck	1.06482	40.00	
<b>NaOH solution, ≥ 32%</b>	Merck		40.00	1.35 g/ml
<b>Trichloroacetic acid (TCA)</b>	Merck	1.00807		
<b>Tris-Base</b>	Roth	5429.3	121.14	pH 10-12
<b>Tris-HCl</b>			157.60	pH 2-4
<b>Triton X-100</b>	Sigma	T-8787		
<b>Tween-20</b>	Merck	1.09280.		
<b>Bovine Serum Albumin (BSA)</b>	Sigma	P-0914		1 mg/ml in 0.15 M NaCl



## 2.7 Western Blotting

The substances used for Western analysis of proteins are listed in *Table 3*.

### 2.7.1 Determining Protein Concentration

Protein concentration was determined in each sample with the help of the Biuret reaction, by photometric detection of the formed copper(I) using bicinchoninic acid (BCA) according to the Sigma procedure TPRO-562.

For this assay, all reagents as well as the samples were kept on ice prior the final incubation.

Standard protein solutions were prepared using the BSA standard (1 mg/ml) according to the *Table 4*. They were kept at -20°C for further use.

*Table 5* gives the composition of the lysis buffer mixture (lbm).

Aliquots of the samples to be assayed were diluted 25-fold in ddw to a total volume of 50 µl.

Reagent solution was prepared by mixing the BCA and the copper(II) sulfate solutions at a ratio of 50:1 .

1 ml of this reagent was added to each 50 µl sample (samples and standards).

The mixtures were allowed to incubate at 37 °C for 30 min; then optical densities were measured at 562 nm (Kontron Uvikon 810) with ddw as reference.

*Table 4* Preparation of protein standards. lbm: lysis buffer mixture (cf. *Table 5*); ddw: double distilled water; BSA: bovine serum albumine.

Std #	endconc. [µg/ml]	lbm [µl]	ddw [µl]	BSA [µl]	m(Prot.) [µg]	m/50 µl [µg]
P1	0	20	480	0	0	0
P2	100	20	430	50	50	5
P3	200	20	380	100	100	10
P4	300	20	330	150	150	15
P5	400	20	280	200	200	20
P6	500	20	230	250	250	25
P7	600	20	180	300	300	30

Table 5      *Lysis buffer mixture (lbm).*

Vol.	of	stock-conc.	pH	endconc.
[ $\mu$ l]		[M]		[mM]
200	Hepes	1	7.4	20
300	NaCl	5		150
100	EDTA	0.5	7.5 (NaOH)	5
1000	glycerin	100%		10%
100	Triton X-100	100%		1%

The mixture was completed to a final volume of 10 ml with double distilled water (8.3 ml). Of this lysis buffer, 1 ml aliquots were kept at  $-20^{\circ}\text{C}$ . Prior to use,  $20\ \mu\text{l/ml}$  protease inhibitor cocktail (Sigma) were added to yield the final lysis buffer mixture (lbm),  $20\ \mu\text{l}$  of which were added to each protein standard solution (cf. Table 4).

A linear regression curve was calculated from the standards, and the concentration of each sample was determined with its help. Figure 10 exemplifies a calibration curve obtained as described.

If the samples' concentration values were not in the range of the regression curve, the procedure was repeated with an appropriate dilution of the samples, total volume always being adjusted to  $50\ \mu\text{l}$ .

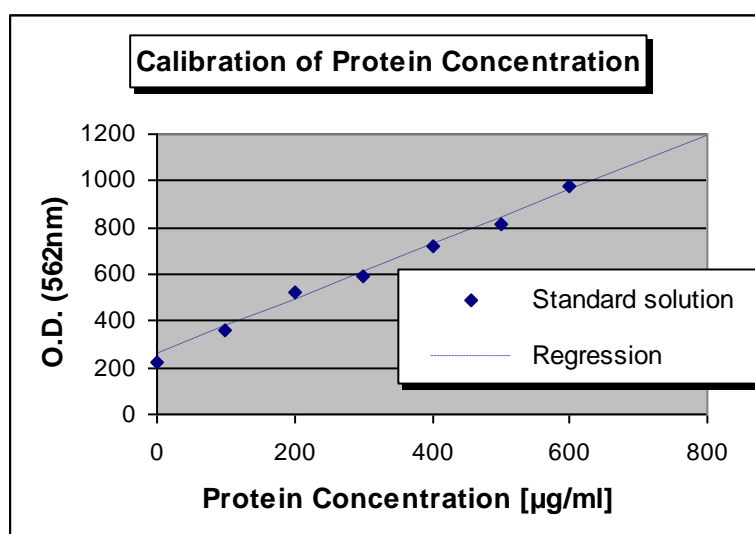


Figure 10      *Calibration of Protein Concentration according to the Sigma procedure TPRO-562 (cf. text). Linear regression yields: slope  $1.17\ \text{ml}/\mu\text{g}$ , y-axis intercept 257, correlation coefficient  $r^2\ 0.9965$ . (O.D. = optical density)*

### 2.7.2 Preparing Stock Solutions

Solutions and buffers were prepared according to the following protocols:

#### (1) Stock solutions (in ddw)

- (a) **SDS** 10 % (w/v) 10 g for 100 ml solution
- (b) **EDTA** 0.5 M, pH 8.0 18.61 g + 2 g NaOH pellets, for 100 ml solution;  
pH adjusted with NaOH or HCl
- (c) **NaCl** 5 M 146.1 g for 500 ml solution.
- (d) **Tris-HCl** 1 M, pH 7.5 60.57 g of Tris-Base for 500 ml solution,  
pH adjusted with 37 % HCl
- (e) **Tris-HCl** 1.5 M, pH 6.8 18.17 g of Tris-Base for 100 ml solution;  
pH adjusted with 37 % HCl

Solutions (b) - (e) were autoclaved before further use and kept in sterile vessels.

(2) Loading buffer (2x LoadB) was prepared to be diluted twofold with a sample.

	stock	volume [ml]	final conc. for load (1x)	
<b>SDS 10 %</b>	10 %	2	1.60	%
<b>Tris-HCl, pH 6.8</b>	1.5 M	1.66	0.20	M
<b>EDTA, pH 8.0</b>	0.5 M	0.01	0.40	mM
<b>Glycerin</b>	100 %	2	16.03	%
<b>Bromophenol blue</b>		few grains	n.a.	
<b>total Volume</b>		5.67	(12.47 ml) *	
<b>Mercaptoethanol</b>	100 %	0.57	10	%

\* after addition of mercaptoethanol and sample.

Aliquots of 200 µl were kept at -20 °C before addition of mercaptoethanol. The latter was added just before usage.

(3) **Running buffer** (RunB) was prepared to be diluted tenfold with ddw before use for gel electrophoresis.

	stock	m [g]	1x conc.	
<b>Tris-Base</b>	solid	15.14	25	mM
<b>Glycine</b>	solid	72.07	192	mM
<b>SDS</b>	10 % (w/v)	50 ml	0.1	%
<b>total Volume</b>		500 ml		

The volume was filled up with ddw, and the final solution kept at RT.

(4) **Transfer buffer** (TransfB)

	stock	m [g]	conc.	
<b>Tris-Base</b>	solid	2.9	48	mM
<b>Glycine</b>	solid	1.45	39	mM
<b>SDS</b>	10 % (w/v)	1.85 ml	0.037	%
<b>Methanol</b>	100 %	100 ml	20	%
<b>total Volume</b>		500 ml		

The volume was adjusted with ddw. The buffer was kept at RT and used without further additions for blotting.

(5) **TBS, TBST and blocking buffer** (BlockB)

10x TBS buffer:

	stock	V [ml]	10x conc.	
<b>Tris-HCl</b>	1 M, pH 7.5	500	0.5	M
<b>NaCl</b>	5 M	300	1.5	M
<b>ddw</b>				
<b>total Volume</b>		1000		

From this, 1x TBST buffer was prepared by tenfold dilution in ddw and addition of Tween-20 at a ratio of 0.25 ml per 500 ml. The final blocking buffer was then obtained by adding skimmed milk powder to 1x TBST buffer at a ratio of 12.5 g per 250 ml (5 %).

While TBS and TBST buffers were kept at RT, blocking buffer was kept at 4°C.

### **2.7.3 Protein Gel Electrophoresis**

For gel electrophoresis the following pre-cast gels were used:

10-20 % Tris-glycine acrylamide gels,  
cassette size 10 x 10 cm<sup>2</sup>, thickness 1.0 mm, 12 wells  
(Zaxis, Hudson, USA, Cat.# 110-1020T212)

The electrophoresis chamber was from Owl Separation Systems (Portsmouth, USA).

Samples were thawed at 4 °C. The volume containing 10 µg of protein (as determined by the BCA assay) was added to the same amount of 2x LoadB. If the total volume obtained was less than 3 µl, more 2x LoadB was added for greater ease of manipulation. The samples, in firmly closed Eppendorf tubes (to avoid evaporation), were heated to 95 °C on an Eppendorf Thermomixer for 5 min, then immediately put on ice.

The gel was mounted in the chamber which was then filled with running buffer. The wells of the gel were rinsed with running buffer prior to loading the samples. As size standard the wide range Sigma Color Marker (Cat.# C-3437) was used to run aside the samples during electrophoresis. 10 µl of this standard marker were loaded in a separate well.

Care was taken to perform electrophoresis of the cytosolic and mitochondrial fractions of each sample on the same gel for comparison.

Electrophoresis power supply (Consort E835)

Running conditions for one (two) gels:

80 V	15 (30) mA	until penetration of the samples in the gel.
100 V	35 (70) mA	for the separation.

Electrophoresis was stopped when the bromophenol blue added to the samples (in the 2x LoadB) was seen to have reached the end of the gel.

Gels were then removed from their support and kept for the blotting following immediately.

#### **2.7.4 Blotting**

Semi-dry blotting was performed with a semi-dry blotting chamber from Owl Separation Systems (Portsmouth, USA). All materials were soaked with transfer buffer. On the (negative) bottom platter electrode three 10 x 10 cm<sup>2</sup> pieces of filter paper (Whartman /England, Cat.# 1001 917) were placed, upon which was laid the gel and a 10 x 10 cm<sup>2</sup> piece of nitrocellulose membrane (Hybond ECL RPN 203 D, Amersham Pharmacia). On top of these followed three more pieces of filter paper. Air was removed by impregnating every layer with transfer buffer and then rolling a glass bar over the layers of paper in several directions. The chamber was closed with the cover containing the (positive) top electrode.

Transfer of the proteins was performed with the help of an electrophoresis power supply (Consort E835), applying 3 V and 80 mA (for one gel) during 1.5 h.

The blotting membrane was retrieved, briefly washed with ddw and assessed for protein loading with Ponceau S staining as follows.

#### **2.7.5 Ponceau S Staining**

In order to verify successful electrophoresis and blotting of the proteins, the proteins on the blotting membrane were reversibly stained with Ponceau S.

A solution of Ponceau S in trichloroacetic acid (TCA) was prepared by dissolving Ponceau S and TCA in ddw to a final concentration of 0.2 % w/v Ponceau S and 3 % w/v of TCA. This solution was kept at 4 °C when not in use.

The blotting membrane was shaken in this solution for 10 - 20 min after washing in several changes of ddw to remove the transfer buffer, then again in ddw to remove excess of dye until the protein bands appeared.

Documentation of the protein loading was done by photocopying the stained membrane. The bands of the size marker were marked with a pen.

To remove the Ponceau S staining, the membrane was shaken in basic Tris solution (approximate pH 9-10) until decolorized and washed in several changes of ddw.

### **2.7.6 Immunostaining for Cytochrome c and COX 4**

After blotting (and staining/decolorizing with Ponceau S) or after stripping (cf. 2.7.7), the membrane was transferred into blocking buffer and shaken for 30 min at RT.

The primary antibody was incubated overnight at 4 °C:

For cytochrome c, the rabbit antibody (provided with the ApoAlert Kit) was used at a concentration of 100 µl in 10 ml blocking buffer (1:100).

For COX 4, the murine antibody (provided with the ApoAlert Kit) was used at a concentration of 20 µl in 10 ml blocking buffer (1:500).

Solutions of primary antibodies were kept at 4 °C to be reused up to four times.

After incubation with the primary antibody, the membrane was washed twice in blocking buffer (15 min at RT), then transferred for 1 h at RT into the corresponding HRP-marked secondary antibody solution (goat anti-rabbit, Santa Cruz Cat.# sc-2004 or goat anti-mouse, Santa Cruz sc-2005; concentration 4 µl in 20 ml of blocking buffer, i.e. 1:5'000).

Finally, the membrane was washed twice 15 min at RT in blocking buffer.

Substrates for the bioluminescent reaction of the HRP were added in form of the ECL solutions 1 and 2 (Amersham Pharmacia, ECL Western Blotting Detection Reagents, RPN 2106): For one membrane of ca. 7 x 5 cm<sup>2</sup>, 2 ml of each solution (recommended: 60 µl/cm<sup>2</sup>) were mixed and then dropped on the membrane lying on a cling-film until fully covered. The membrane was left for 1 min, then the substrate solution was drained and the membrane wrapped in a new piece of cling-film avoiding air pockets. The wrapped membrane was introduced in an X-ray film cassette (Hypercassette 18 x 24 cm<sup>2</sup>, Amersham Pharmacia Cat.# RPN 11642) and covered with an autoradiography film (Hyperfilm ECL 18 x 24 cm<sup>2</sup>, Amersham Pharmacia Cat.# RPN 2103K). Exposition time had to be optimized and was noted. The film was developed thereafter by an automated process. All manipulations involving the film prior to development were done in the absence of light or under red light.

The molecular weights of cytochrome c and COX 4 are 15 and 17 kD respectively.

Because of problems encountered with the detection of COX 4 (cf. 'Results'), proteins from a different cell line, the L929, were used as 'positive control'. Properties of the L929 are detailed in the next section.

Cytosolic and mitochondrial proteins of these cells were separated with the ApoAlert Cell Fractionation Kit as described. The mitochondrial fraction was used as positive control for COX 4.

#### ***2.7.7 Stripping***

For further marking with different antibodies, the membrane was stripped according to the following procedure carried out at RT:

The membrane was shaken in 0.2 M NaOH solution for 5 min, then in ddw for another 5 min and finally blocked again for 30 min in blocking buffer.

Membranes were kept in blocking buffer at 4 °C between the procedures. Stripping and reuse of one membrane with different antibodies was allowed for up to three times.



## **2.8 L929 Cells and anti-Apo-1**

For other investigations on PDT in our laboratory, we had been using the murine fibroblasts L929 (ATCC# CCL-1) in parental form (L929 Par), as well as transfected with Apo-1 (L929 Apo). As mentioned above, these cells served to compare their behavior to the cell fractionation procedure described, and, in particular, as 'positive control' for the detection of COX 4.

Incubation of the transfected cells, expressing Apo-1, with the agonistic anti-Apo-1 antibody (1µg/ml in the presence of 10ng/ml protein A as cross-linker, (H. Hug, personal communication)) leads to aggregation of the receptor in the cell membrane that in turn launches apoptosis via the extrinsic caspase cascade (Hug 1998). Mitochondrial cytochrome c release has been reported to be a downstream event in this pathway (Green et al. 1998).

The incubation with the antibody will hereafter be termed 'induction'.

Cytosolic and mitochondrial proteins of the parental as well as the transfected cells, w/o or after induction, were separated with the ApoAlert Cell Fractionation Kit as described. Besides studying the results of the fractionation and the effect of anti-Apo-1 induction, the mitochondrial fraction turned out to be a useful positive control for COX 4.

## 2.9 Caspase Inhibitors (C.I.)

### 2.9.1 Characteristics of the Inhibitors

For assessing how caspases are involved in the process of cell damage after PDT, cells were treated with two broad spectrum caspase inhibitors prior to PDT.

The following characteristics are reported for them by the provider:

- *Caspase Inhibitor I* (C.I.1) (Calbiochem Cat.# 627610)

**z-VAD-fmk**, MW 467.5 g/mol

A cell-permeable, irreversible inhibitor of caspases 1, 3, 4 and 7.

- *Caspase Inhibitor III* (C.I.3) (Calbiochem Cat.# 218745)

**boc-D-fmk**, MW 263.3 g/mol

A cell-permeable, irreversible broad spectrum caspase inhibitor; said to be more efficient than Caspase Inhibitor I (D'Mello et al. 1998).

### 2.9.2 Procedure

Both inhibitors are supplied as 1 mg of solid. They were dissolved in DMSO to give a stock solution of 25 mM. These stock solutions were kept at -20 °C. Experimental conditions were adapted from D'Mello (D'Mello et al. 1998) concerning concentrations and incubation times.

First, toxicity of the inhibitors was assessed. Cells seeded according to the protocol described were subjected to different concentrations (25, 50 or 100 µM) of either inhibitor for two days. The medium was then exchanged with fresh one and NR Assay performed.

Then, combined toxicity of the inhibitor in the presence of AIPc was assessed. For this purpose, cells were incubated two days after seeding with 400 µM AIPc-Cl for 24 h, then washed and the medium replaced. Then, either inhibitor was added to a final concentration of 100 µM. After two days, exchange of medium and NR Assay were performed as described.

Phototoxicity of the inhibitors was tested by incubating the cells with 100 µM of either inhibitor for 12 h and then irradiating with 100 mW/cm<sup>2</sup>, 50 s (i.e. 5 J/cm<sup>2</sup>) as described. After two days, exchange of medium and NR Assay were performed as described.

The conditions for preliminary toxicity tests were chosen to be more strenuous than those used for PDT; so that, under PDT conditions, effects of inherent toxicity would be in any case lesser.

Effect of PDT on HuH7 cells was compared in the absence and in the presence of either inhibitor. For this purpose, cells were processed as described before (AIPc 100  $\mu$ M, 24 h; H<sub>e</sub> 5 J/cm<sup>2</sup>). Caspase inhibitor was added 15 min prior to irradiation, after washing of the cells. Two days after irradiation, NR Assay was performed as described.

## **2.10 Antioxidants and Radical Scavengers**

Several substances were tested for a potential protective or enhancing effect with PDT by means of their reductive and/or radical scavenging properties. They will be referred to as 'antioxidants' hereafter. These substances were pyrrolidine dithiocarbamate (PDTC), N-acetyl-cysteine (NAC) and ascorbate. The latter was used as free acid (ascorbic acid) or as sodium salt (sodium ascorbate).

First cytotoxicity of these compounds was assessed. For this purpose cells were incubated with different concentrations of the antioxidant after two days of growth. Stock solutions were 10 mM in ddw, filtered over 2  $\mu$ m for sterilization, added in the appropriate amount to the cell culture medium. Incubation was carried out over at least 24 h, then the cells were washed twice and allowed to grow in fresh medium for another two days. Viability of the cells was then assessed by NR assay.

Concentrations that were non toxic under these conditions were used for assessing concomitant toxicity of the antioxidants with AIPc or with irradiation. AIPc was co-incubated with the antioxidant at a concentration of 100  $\mu$ M. Irradiation was performed after replacing the antioxidant and/or AIPc containing medium with fresh one. Irradiation conditions were 100 mW/cm<sup>2</sup>, 50 s (i.e. 5 J/cm<sup>2</sup>). Viability was assessed after two days with the NR assay.

Concentrations shown to be non toxic under these conditions were then used to observe an eventual effect on PDT. AIPc concentration was 100  $\mu$ M for 24 h, then irradiation with 100 mW/cm<sup>2</sup>, 50 s was performed. Viability according to NR assay was tested two days later. As in the preliminary experiments, antioxidants were incubated concomitantly with AIPc.

## **2.11 Electron Microscopy**

### **2.11.1 Transmission Electron Microscopy (TEM)**

Following PDT (according to the procedure described before with AIPc 24 h 100  $\mu$ M and  $H_e$  1 J/cm<sup>2</sup>, HuH7 cells harvested 15 respectively 30 min post PDT), cellular morphology was examined by transmission electron microscopy. The cells were fixed in the culture dishes (4-well plate) with 2 % glutaraldehyde/2 % formaldehyde in 0.1 M cacodylate buffer and embedded in epoxy resin. Semi-thin sections for light microscopy were stained with the Richardson fast stain.

Ultrathin sections for electron microscopy were stained with uranyl acetate and lead citrate.

### **2.11.2 Scanning Electron Microscopy (SEM)**

From HuH7 cells submitted to PDT as above, the cytokeratine skeleton was prepared according to the method described by Beil (Beil et al. 2003) to be imaged by high resolution scanning electron microscopy (Hitachi S-5200 in-lens SEM; Tokyo, Japan): After a pre-fixation extraction with 2.2 % polyethylene glycol, followed by actin depletion with gelsolin, cells were fixed with 2 % glutaraldehyde in 0.1 M cacodylate buffer, gradually dehydrated in alcohol, then stained with uranyl acetate, subjected to critical point drying and finally coated with 3 nm of platinum.

For both EM techniques, samples of untreated cells were obtained for comparison following the same protocol as for the PDT-treated cells.

## 2.12 Laser Scanning Microscopy (LSM)

### 2.12.1 The Microscope System

For localizing and studying morphological changes after PDT, confocal laser scanning microscopy with the LSM 510 meta system (Zeiss) was used, to observe the living cells submitted to specific treatments. *Figure 11* illustrates the main components of the microscope with the excitation and detection devices.

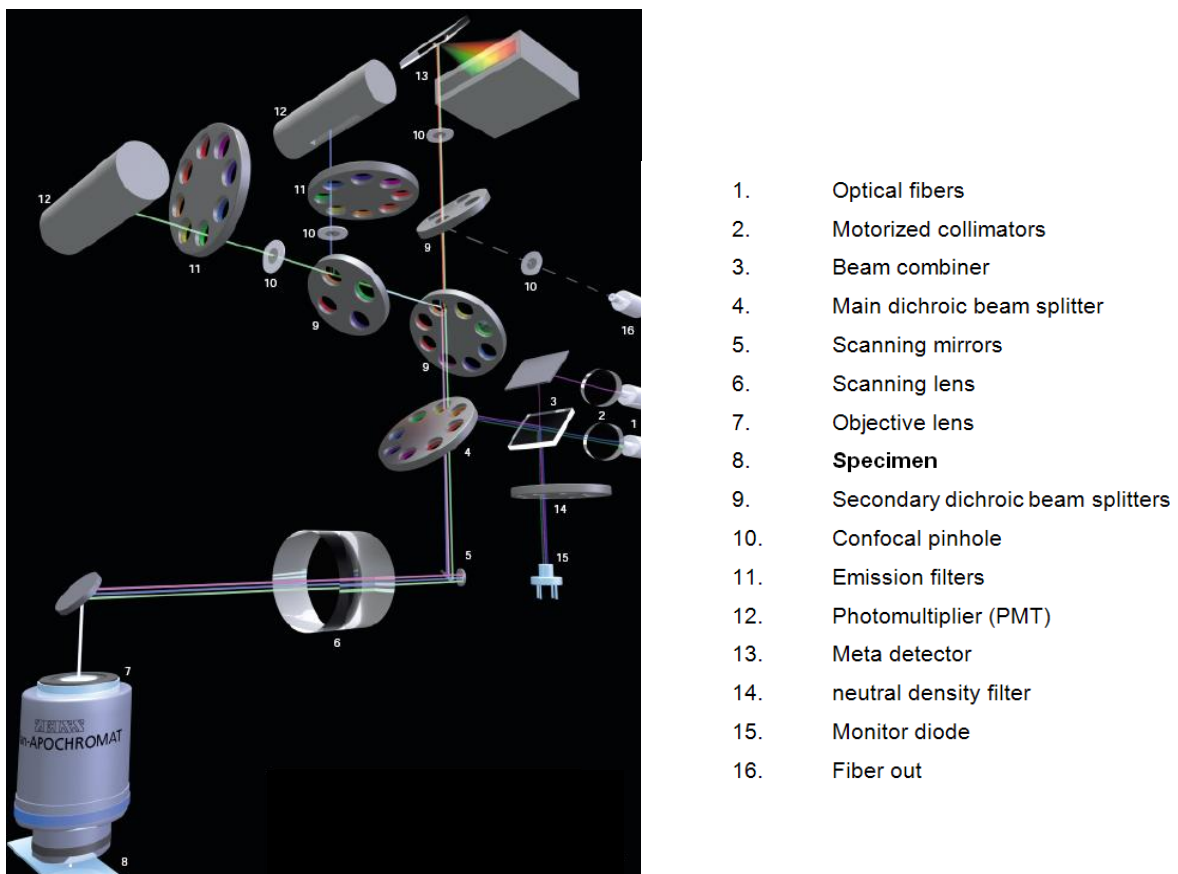


*Figure 11* Scheme of the LSM 510 meta system (from Zeiss Product Information).  
For explanation cf. text.

The specimen down left (8) is illuminated by the incoming laser light from the middle right (1), that is scanned over it linewise with the help of the scanning mirrors (5) and scanning lens (6). Several lasers of different wavelengths are

available for selective excitation of the dyes and/or markers present in the sample.

The pathway for the detection of the transmission image (conventional optical microscopy) is not shown in the scheme. Fluorescence is detected by sending back the emitted light that is scanned from the specimen through the scanning lens (6), then separating it from the incoming light through the main dichroic beam splitter (4) and dividing it through several secondary beam splitters (9) into regions of defined wavelengths that can be further adapted to the wavelength bands of interest by bandpass filters (11), before being detected by the photomultipliers (12).

The pinholes (10), that are the main device for assuring confocality, have to be closed as much as possible (which is restricted by the necessary sensitivity) and precisely positioned in the horizontal plane to allow the most selective detection of the fluorescence emitted by the region of the incoming light's focus in the specimen. This enables three dimensional imaging of the specimen by scanning the position of the focus through the vertical direction. A maximum of vertical resolution versus sensitivity is achieved when the pinholes are approximately the size of the axial Airy disc (projected on the confocal aperture) which depends on the objective's numerical aperture and on the considered wavelength (Sheppard et al. 1997, Zeiss product information).

Another important parameter influencing confocality is the spherical aberration due to oil-glass-water refraction at the interfaces between the objective and the specimen. This can be circumvented by the use of water-immersion objectives.

The meta system (13), containing thirty-two photomultipliers covering a range of 340 nm, besides being necessary for detection with spectral resolution (that is recording a whole spectrum from every point scanned), allows an individualized detection in a certain wavelength region (up to eight regions) and may hence be complementary to the photomultipliers combined with the emission band- (BP) or longpass (LP) filters (11,12) which serve as fixed, invariable band detectors.

### **2.12.2      Modes of Detection**

The LSM 510 meta system allows several detection modes with the above mentioned setting:

(1.a.) In the channel mode (ChMo), the specimen is irradiated by the chosen lasers and light returning is detected in several wavelength bands, each of which is assigned to a specific fluorochrome and is represented in its own color. The image thus represents the distribution of the fluorochromes in the specimen. Crosstalk, i.e. fluorescence of one substance in a wavelength region assigned to another, is a limiting factor for this mode.

(1.b.) In the multitrack mode, the conditions of irradiation and detection can to some extent be varied from one scanned line of the specimen to the next. Again, each color in the resulting image represents one wavelength band or substance, with the advantage that crosstalk may be reduced.

(2) The meta or lambda mode (LaMo) records at every point, line by line, of the specimen, the whole visible spectrum (or a predefined part of it), giving the emission intensities at every wavelength (more precisely: wavelength bands of 11 nm). Every point of the resulting image therefore contains the sum of the spectra of the substances fluorescing at that point. The information can be represented in form of a stack of intensity pictures of the specimen at the wavelengths considered ( $\lambda$ -stack).

Further processing of this information then allows in particular:

(a) Extracting a wavelength band (e.g. the emission maximum of a fluorochrome) and assigning it a channel and a corresponding color.

(b) Extracting known spectra of specific substances from the image (linear unmixing, LiUMx): The intensity of the spectrum can then be represented in its own color, imaging the substance to which it belongs.

(c) Extracting a defined number of spectra calculated from points of high light intensities at a certain wavelength (ACE = Automated Component Extraction). The result is very similar to that in (b) although the compounds may not necessarily be well defined.

Usually the extraction procedures significantly reduce the spatial resolution.

Moreover, time series and scans in vertical direction (resulting in z-stacks) do further enlarge the possibilities of imaging a given specimen.



Reduction of background noise, and thus resolution enhancement, can be achieved by scanning the same specimen several times and creating a mean image of all the scans. Limitations however are imposed by photobleaching of the fluorochromes and if the specimen is not an inert system but for instance a living cell, susceptible to change during the scanning.

### **2.12.3 General Experimental Conditions**

Optical microscopy of the living cells mounted on appropriate glass slides was performed with a 63x oil or water immersion objective with a numerical aperture of 1.4 and 1.2 respectively. LSM settings were chosen according to the fluorochromes used in order to achieve maximal sensitivity with best spacial and spectral resolution. Special care was taken to avoid crosstalk, i.e. detection of fluorescence of one compound in a wavelength domain attributed to another. In the mostly utilized channel mode (ChMo), this implies the use of different excitation wavelengths (i.e. lasers lines) and detection in narrow wavelength domains (through bandpass filters) that are far apart. Typically, a photosensitizer like ALPc with a fluorescence in the far red upon excitation with red light readily combines with fluorochromes excited by a blue laser and fluorescing in the blue or green region.

The next section describes more in detail the fluorochromes used and their LSM-relevant spectral characteristics.

The pinholes were set between 100 and 150  $\mu\text{m}$ ; in some cases with very bright fluorescence, they could be reduced to about 50  $\mu\text{m}$ . This is the range where the resulting vertical resolution is equal in size to the Airy disc (about 400nm) that defines the best achievable axial resolution based on the optical properties of the microscope.

### **2.12.4 Fluorochromes and Fluorophores**

Table 6 gives the LSM-relevant spectral characteristics of the fluorochromes and fluorophores used, according to the supplier's specifications (Molecular Probes Handbook).

A few remarks are to be made concerning these substances:

Fluo-3 is introduced in the cells in form of the acetoxymethyl (AM) ester which is cell permeant but not fluorescent. It is hydrolyzed to the free acid by intracellular esterases and consequently trapped inside the cells. The latter fluoresces in the presence of calcium ions ( $K_d = 390 \text{ nM}$ , fluorescence increase about hundredfold). Alternatively, it can be hydrolysed in vitro, by NaOH for example, to assess spectra of the solution.

LysoTracker Green Br<sub>2</sub> is fluorescent in acid environment. Spectra of the solution were recorded in acidified aqueous environment.

The MitoTracker Red CMXRos exists in a reduced form, CM-H<sub>2</sub>XRos that is not fluorescent. It can be oxidized in active mitochondria to the fluorescent form, and hence serve as an indicator of functioning mitochondria.

Neutral Red was tested as a lysosomal marker too, although it is not a commonly used fluorochrome.

Stock solutions of the fluorophores (Molecular Probes / Life Technologies GmbH, Darmstadt) were prepared as advised by the manufacturer and stored at 4 °C, shielded from light. Volumes added to the medium for cells' incubation and incubation times were adapted to obtain the desired staining with a sufficient intensity. Cell medium was kept to a minimum during incubation to minimize the volumes needed.

From every fluorochrome aqueous solutions were prepared to measure the fluorescence spectra with the meta detector of the LSM.

Fluo-3-AM was first hydrolysed to the free Fluo-3 by addition of equimolar quantities of NaOH, the final solution was buffered with HEPES and an excess amount of calcium chloride was added.

The solution of LysoTracker Green Br<sub>2</sub> was acidified by adjunction of diluted HCl.

**Table 6** *Data related to the fluorochromes used for Laser Scanning Microscopy (Molecular Probes Handbook).*

<b>Fluorochrome</b>	<b>Abs.max</b>	<b>Ex</b>	<b>Em.max</b>	<b>Em</b>	<b>Type</b>	<b>Molecular Probes</b>	<b>MW</b>	<b>Solution</b>
	<b>[nm]</b>	<b>[nm]</b>	<b>[nm]</b>	<b>[nm]</b>		<b>Cat.#</b>	<b>[g/mol]</b>	<b>in</b>
AlPcS <sub>4</sub>	675	633	680	650-710 643-717	PS	Frontier Scientific	(895.22) <sup>1</sup>	ddw
Fluo-3 (+Ca)	503	488	525	500-550	Calcium Indicator	F-1242		DMSO
MitoTracker Red CMX Ros	578	543	599	565-615 557-621	Mitochondria	M-7512	531.52	DMSO
MitoTracker Red CM- H <sub>2</sub> XRos (oxidized)	578	543	599		active Mitochondria	M-7513	497.08	DMSO
LysoTracker Green Br <sub>2</sub>	532	488 514	545	LP 505 535-590	Lysosomes	L-7542		DMSO
Neutral Red	530	514	640	525-621 LP 560	Lysosomes	Biochrom		0.9% NaCl
Rhodamine 123	508	488	529	500-550	Mitochondria	Sigma R 8004	380.8	ddw

<sup>1</sup> Formula weight

Note: Abs.max refers to the maximum of the absorption spectrum, while Ex gives the wavelength actually used to observe fluorescence, which is usually imposed by the laser available or other fluorochromes concomitantly used. Accordingly, Em refers to the band of wavelengths actually detected, the maximal fluorescence occurring at the value given as Em.max.

LP: long pass (filter); PS: Photosensitizer; MW: molecular weight; ddw: double distilled water, DMSO: Dimethylsulfoxide.

### **2.12.5      Preparation of the Cells and Processes Studied**

For use with the Laser Scanning Microscope, cells were grown in 4 - well plates, each well of which had been tipped with a breamed round cover slide of 10 mm diameter (Merck Eurolab 631 9490), or on 75 x 25 mm<sup>2</sup> vapor sterilized microscope slides (Marienfeld /Germany) in Quadriperm plates (cf. *Table 2*).

Just before imaging, the slides were removed from the medium, washed with isotonic sodium chloride solution or PBS, covered with another slide to prevent drying and mounted on the LSM specimen support.

Still, with this probing, viability and, more importantly, metabolic stability of the cells was limited by drying, depletion of CO<sub>2</sub> and excess of oxygen, as well as by low temperature. At the time when these experiments were conducted, no flow-through chamber, gas supply or warming device had been adapted to our LSM system. Therefore, imaging, and in particular online monitoring, was restricted to about half an hour after retrieving the cells from the incubator.

To prevent drying, cells could be mounted on the slides fixed together with Vaseline that would allow a larger volume of liquid and prolong the possible observation time.

Photosensitizer uptake was monitored by incubating cells with 100 µM AIPc for various defined durations, then washing the cells and analyzing by LSM. Automated optimization of the detection parameters allowed using the detector gain as indirect quantification parameter of AIPc fluorescence intensity.

In another experimental setting, the cells mounted on the slides for LSM were incubated with small volumes of 100 µM AIPc containing medium and observed online for up to 20 min. Care was taken to close the pinhole as much as possible to reduce the detection of the medium's fluorescence by high confocality, even if this would impair detection of low (early) cellular AIPc uptake.

Morphology of cells and intracellular distribution patterns of AIPc were then compared for cells before and after PDT (H<sub>e</sub> 5 J/cm<sup>2</sup>) and with specific organelle markers. Details of experimental conditions will be described with the results.

## 3 Results

Note: In the following, the term 'treatment of cells' applies to every adjunction made to the cells' medium besides FCS and P/S; i.e. in particular, addition of photosensitizer, caspase inhibitor, antioxidants etc., with or without subsequent irradiation.

### 3.1 Preliminary Experiments

#### - Cell Growth and Viability Assays

Normal cell growth was assessed by establishing growth curves of each cell line. *Figure 12* depicts the increase of cell density as function of time after seeding with a seeding cell density of 100 cells/mm<sup>2</sup>.

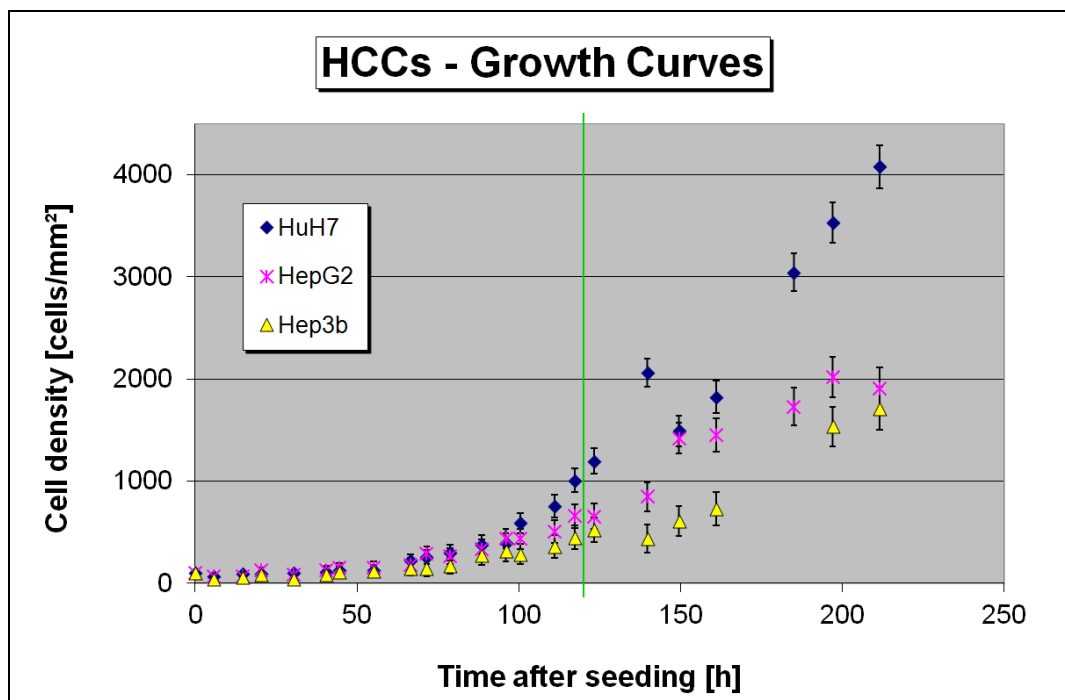


*Figure 12* Growth curve of the human hepatocellular carcinoma cell lines (HCC) HuH7, HepG2 and Hep3b: Cell density as function of time after seeding ( $t$ ). All cell lines. Cell density at  $t=0$  is the seeding density. The vertical bar delimits the time range used for the subsequent experiments.

Thus, exponential growth started about 50 h and continued for at least up to 150 h after seeding. Cell densities at that time were in the order of 1000 cells/mm<sup>2</sup>. Growth rates of three cells lines differed markedly, HuH7 cells being the fastest and Hep3b the slowest.

At higher densities or after longer times, growth curves deviate from exponential. Nutrient depletion is one factor contributing to flattening of the curves, while reduced cell adhesion to the vial probably accounts for curve irregularities, because of irreproducible cell loss during exchange of medium.

Considering this, the general procedure for the subsequent experiments was set as follows: Cells were incubated with the photosensitizer two days after seeding, left for one day, then irradiated and left again for two days before evaluation of toxicity, yielding a total time of 120 h after seeding.

Recovery of cells through hand-counting shortly after seeding was evaluated (Figure 13) and proved to be reasonably accurate for cell densities less than 50'000 /well.

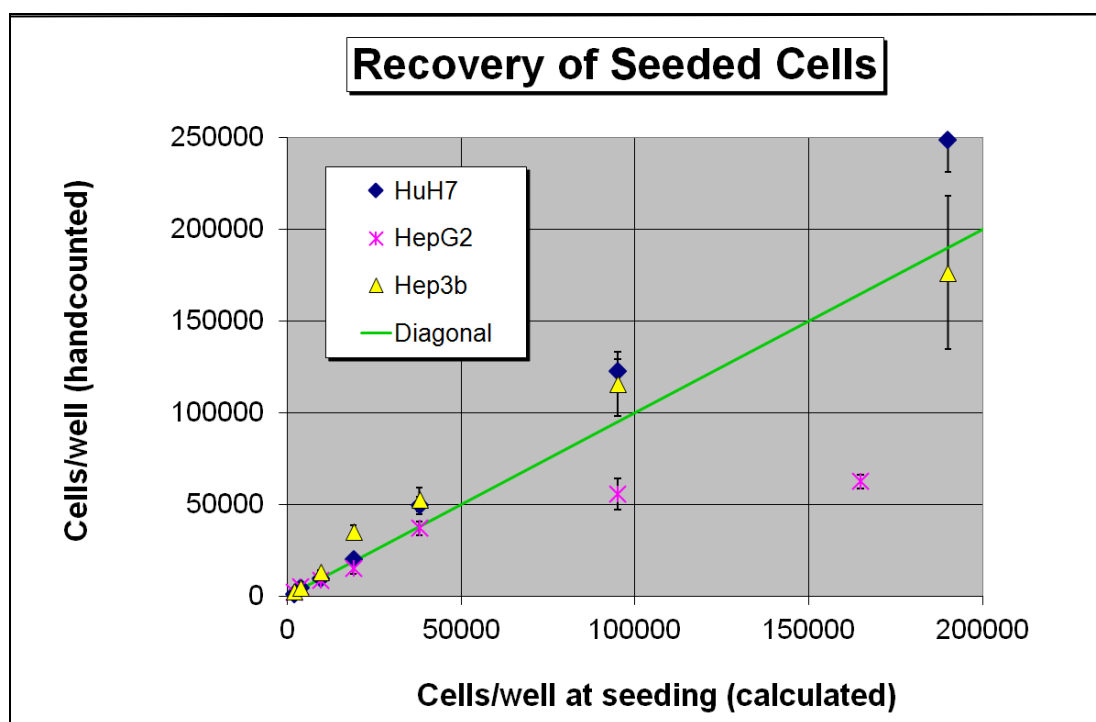


Figure 13 Recovery of seeded cells as determined by hand-counting. All cell lines. The diagonal bar represents (theoretical) 100 % recovery.

It should be noted that, as has been described in the literature (Ball et al. 2001), after PDT, cells are more difficult to detach from the culture dishes. Therefore, quantitative flaking is most important. The use of viability assays for quantification of PDT effects circumvents this problem.

Still, the most important reason for replacing cell quantification through hand-counting (HC) by viability assays using neutral red and/or MTT was the possibility to analyze more samples in less time.

In preliminary experiments, proportionality between cell numbers, as determined by hand-counting, and MTT conversion, as measured by optical density (O.D.) of the supernatant of lysed cells, was demonstrated for the three cell lines used (*Figure 14.a*). The same correlation was demonstrated using Neutral Red when the amount of NR solution added was sufficiently high, i.e. more than 500  $\mu$ l/well (data not shown).

Furthermore, O.D. from MTT conversion was in good linear correlation to the O.D. from NR uptake (*Figure 14.b*).

Hence, the O.D. (NR or MTT) could be used as a measure of cell density, while correlating NR uptake or MTT transformation of untreated cells with the one of treated cells would be a measure of the treatment's toxicity.

Because cell densities and/or incubation times with NR or MTT might slightly vary from one experiment to another, O.D. values are usually given as percentage of the O.D. of non-treated cells grown in parallel [% of ctrl].

Toxicity (either dark- or photo-toxicity) of a treatment was evaluated by means of neutral red (NR) uptake *reduction* after two days of growth in normal medium. It was assumed that after this time, cells were either living or dead, but not otherwise impaired in NR uptake by the preceding treatment.

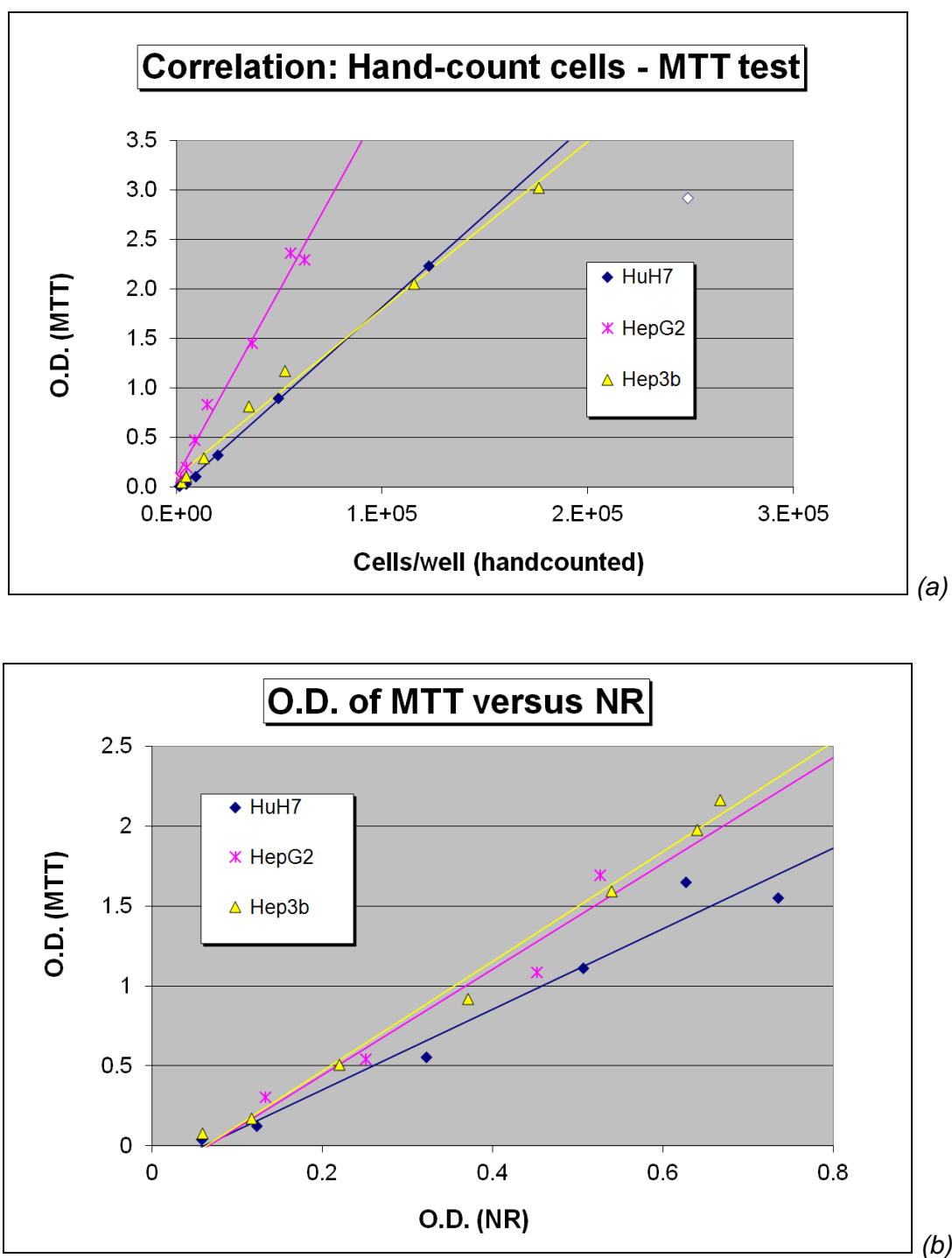


Figure 14

Comparison of hand counting and viability assays NR and MTT for cell quantification; all three cell lines:

(a)  $O.D.(MTT) = f(\text{cell density}) [\text{cells/well}]$ . All cell lines.

Cell density was determined by hand counting.

(b)  $O.D.(MTT) = f(O.D.(NR))$ . All cell lines.

The straight lines are the corresponding linear regression curves, without the point marked by an open rhomb. O.D.: optical density. NR: Neutral Red, MTT: 3-(4,5-Dimethylthiazol-2-yl)-2,5-diphenyl-tetrazolium bromide



## **3.2 Characterizing AlPc and Comparing AlPc-Cl and AlPc-OH**

### **3.2.1 Photometric Characterization of AlPc-Cl and -OH**

Two forms of AlPc were compared as described in 'Methods': one (AlPc-Cl) bears a chlorine ligand, whereas in the 'free' form (AlPc-OH) the chlorine is replaced by a hydroxide group.

The solids of these two compounds differ in color, the chloride being greenish, the free form rather turquoise. In dilute solution both turn turquoise, which indicates that the chlorine ligand might be lost upon solubilization.

To evaluate if significant differences would have to be taken into account while working with either compound, absorption as well as fluorescence spectra were recorded for both. These show to be identical for dilute solutions (*Figure 15*). It was therefore concluded that both compounds are very similar; in particular their molar extinction coefficient was assumed to be the same, and it was used to standardize the concentration of the stock solutions.

At higher concentrations, the fluorescence maximum of AlPc is gradually red-shifted. This has been described by Juzenas (Juzenas et al. 2004) and attributed to inner filter effects.

*Note: The seemingly higher background noise in the fluorescence of the more concentrated solutions (Figure 15.b, spectra for AlPc in millimolar range) is due to a high attenuation needed during the measurement and subsequent mathematical amplification of the spectrum to normalize the values for greater ease of comparison.*

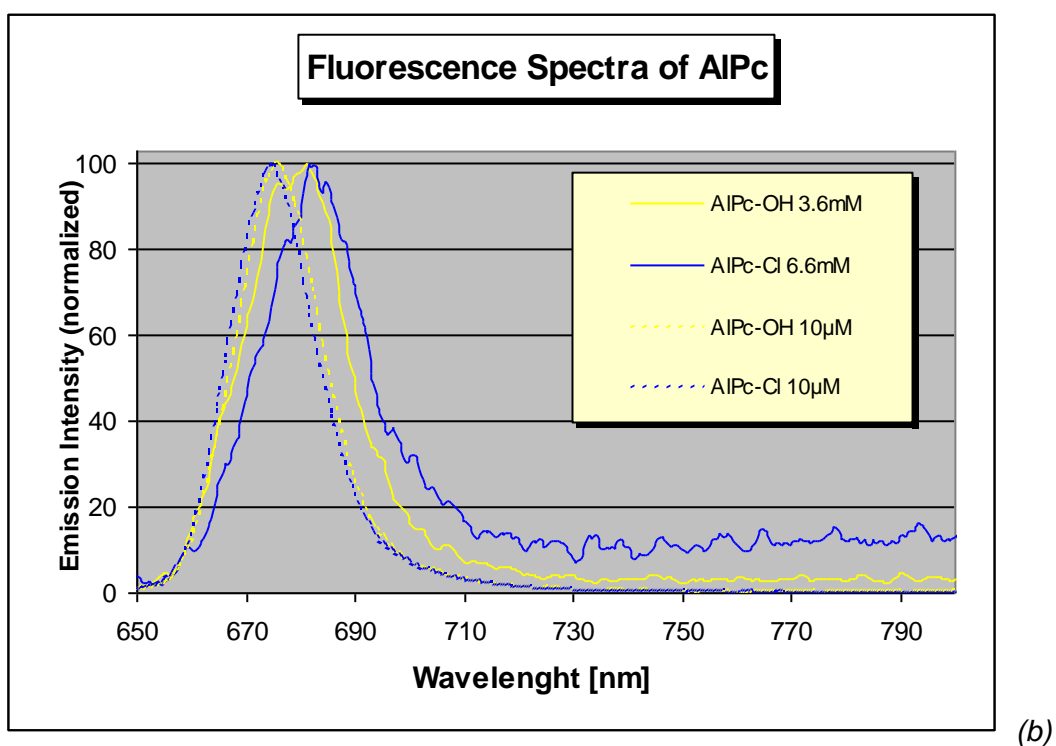
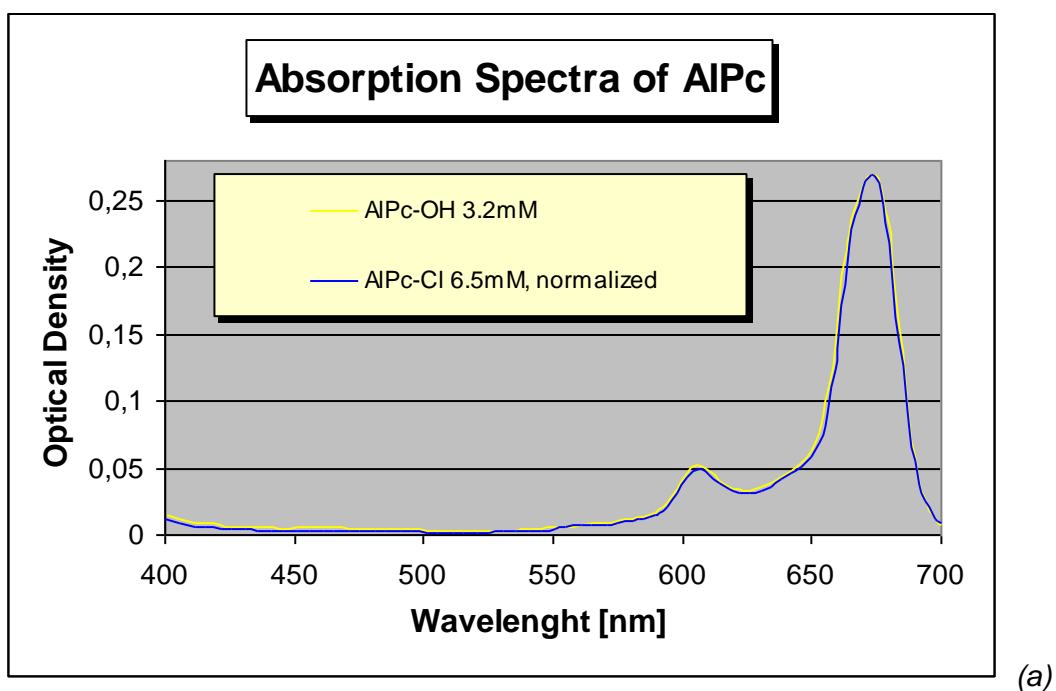


Figure 15 (a) Absorption Spectra of AlPc-Cl and -OH.  
 (b) Fluorescence Spectra of AlPc-Cl and -OH. Excitation 633 nm.  
 Absorbance and fluorescence intensities are normalized to the respective maximum value. (AlPc-Cl / -OH = aluminum phthalocyanine chloride / free)

### **3.2.2 Quantification of AIPc**

Absorption maximum of both compounds (AIPc-OH and -Cl) was at 675 nm, so that photometric quantification was performed at this wavelength using the molar extinction coefficient of 170'000 L/mol/cm given by Darwent (Darwent et al. 1982). They determined this extinction coefficient for a substance that is a mixture of di-, tri- and tetrasulfonated derivatives with an average of three sulfonic groups per molecule. However, the absorption spectrum given by the authors is very similar to the one of our compound. Therefore, the extinction coefficient was supposed to be at least very close. Furthermore, it was assumed to be the same for the chlorine free and the chlorine containing compound, regarding that the absorption as well as the fluorescence spectra of diluted solutions from either were virtually identical.

As described below, the two compounds did not significantly differ as to their dark or photo-toxicity under these conditions. This was the case for all three cell lines investigated (*Figure 18*).

These findings justified the further experiments to be carried out with the chlorine containing AIPc (AIPc-Cl) unless otherwise mentioned.

### **3.2.3 PDT with AIPc**

Irradiation of cells pretreated with AIPc was performed at 676 nm as described in 'Methods'. Because this is very close to the absorption maximum of the photosensitizer, the photodynamic yield should be close to maximum too.

On the other hand, other substances added to the cells, especially other fluorochromes, can be expected to be little susceptible to excitation by such a long wavelength, meaning that the phototoxicity of these should be negligible. Nevertheless, addition to the cells of any other substance, besides AIPc, was avoided prior to PDT; or if this was not possible, phototoxicity of the substance was tested separately.

### **3.2.4 AIPc in Laser Scanning Microscopy**

The laser of the LSM410 and 510 meta systems with the emission wavelength closest to the absorption maximum of AIPc is the HeNe laser with a line at 633 nm. Excitation at this wavelength produces a strong fluorescence with a maximum at 676 nm (*Figure 15.b*). Very concentrated solutions ( $> 3.5$  mM) show a shift in the spectrum to 683 nm, that disappears upon dilution.

Most fluorochromes used for cellular diagnostic have their absorbance and fluorescence maxima at shorter wavelengths and therefore are not excited by the 633 nm laser.

On the other hand, laser of shorter wavelengths do cause AIPc to fluoresce but to a lower extent (data not shown.) This is of no relevance for separate imaging if, on the detection side, the detection channels can discriminate properly the wavelength bands (cf. Chapter 3.10 for further considerations).

### **3.2.5 Dark Toxicity of AIPc-Cl and -OH**

Cells were incubated with AIPc for 24 h as described under 'Methods'. Concentrations used were between 1  $\mu$ M and 1 mM. All three cell lines showed a very low toxicity up to 500  $\mu$ M (*Figure 16*). As pictured later (*Figure 22*) results were similar for NR and MTT assay.

There was no significant difference between AIPc-Cl and AIPc-OH.

There was no significant difference between the three hepatoma cell lines either, with the exception of Hep3b that seems to be slightly more sensitive.

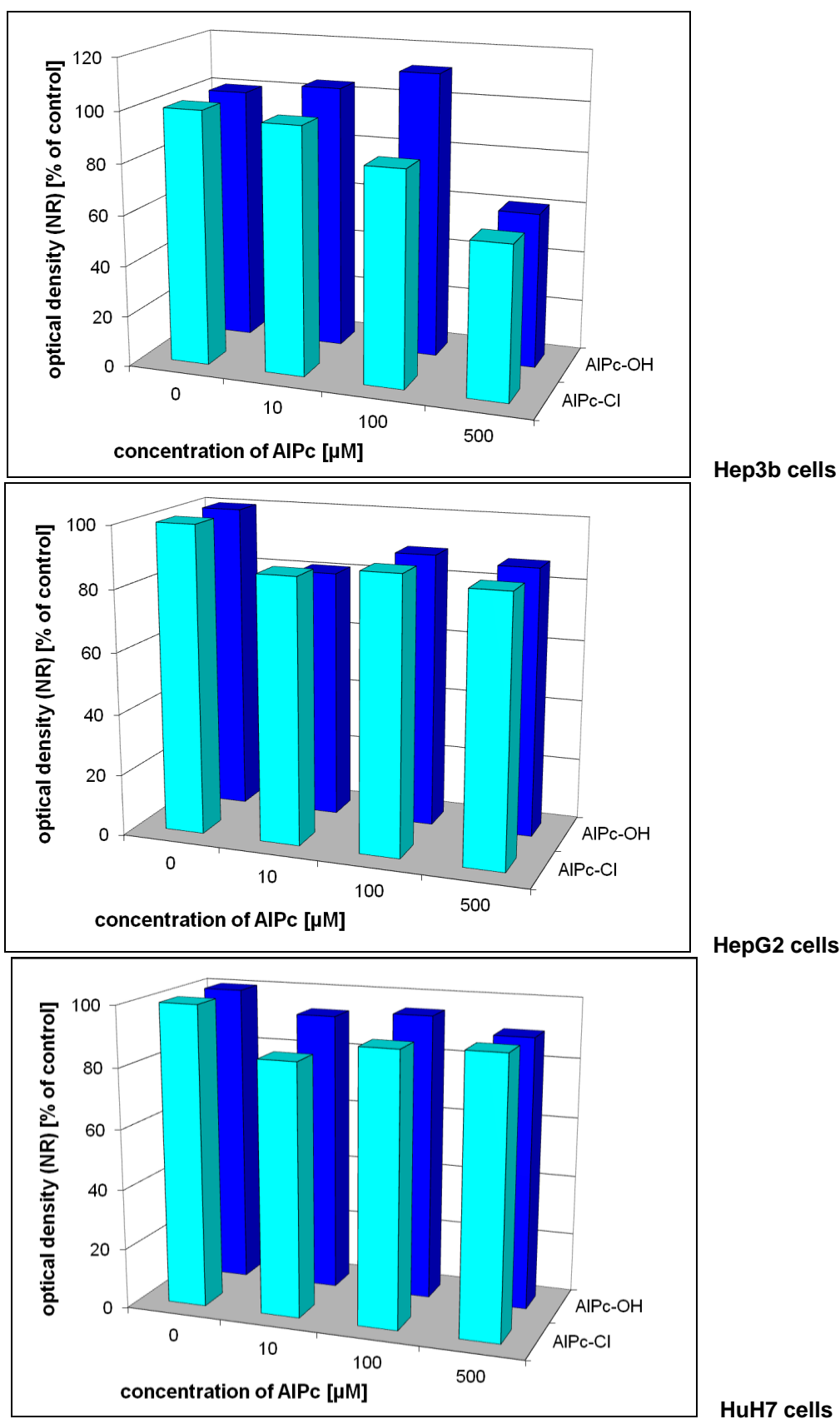
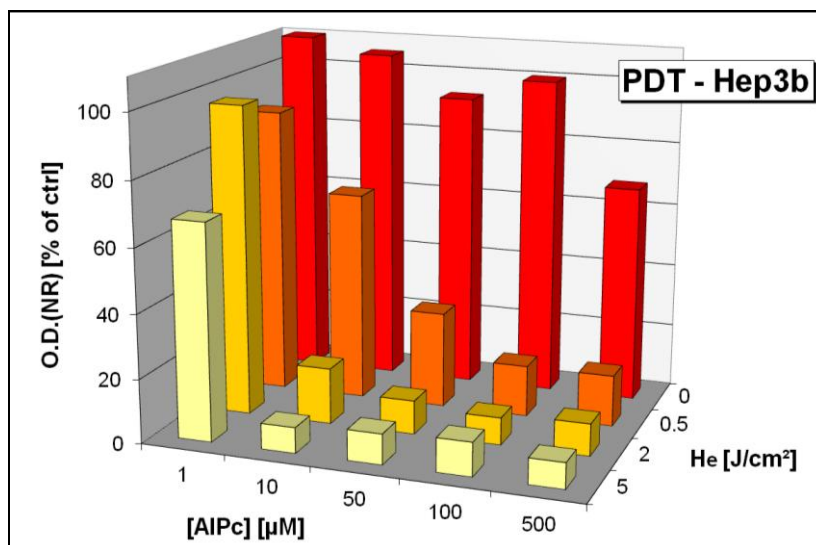


Figure 16 Neutral Red (NR) response after aluminum phthalocyanine (AlPc) incubation: Dark toxicity of AlPc as function of its concentration; comparison of AlPc-Cl and AlPc-OH. Median of absolute differences: MAD < 10 %.

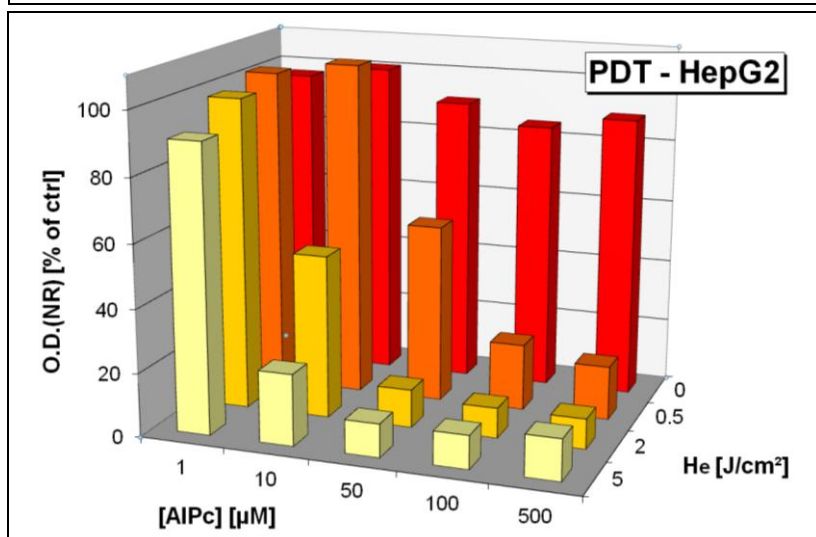
### **3.2.6 Phototoxicity of AlPc-Cl and -OH**

AlPc is phototoxic to all three cell lines investigated in a concentration and irradiation dose dependent manner (*Figure 17*). There is no significant difference between the three cell lines nor between AlPc-Cl and AlPc-OH (*Figure 18*).

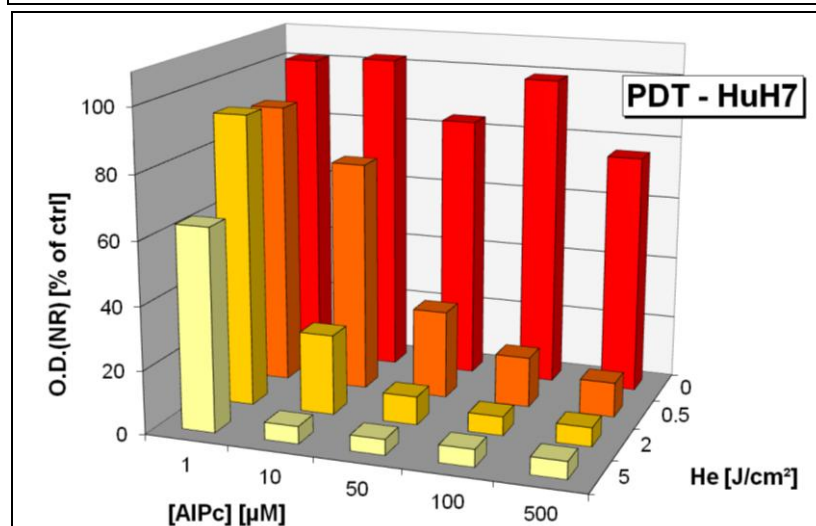
For further experiments, we chose such conditions of AlPc concentrations and irradiation doses that were surely yielding a high percentage of cell killing. This renders the results more reproducible and slight changes in experimental conditions are less likely to produce noticeable effects on the outcome. The implications of this procedure will be discussed in more details in the following chapter.



Hep3b cells



HepG2 cells



HuH7 cells

**Figure 17** Phototoxicity of aluminum phthalocyanine as function of its concentration [AlPc] and irradiation dose: Radiant exposures  $H_e$  are 0, 0.5, 2 and 5 J/cm<sup>2</sup>. Evaluation with Neutral Red (NR) Assay. (O.D.: optical density. ctrl: control.)

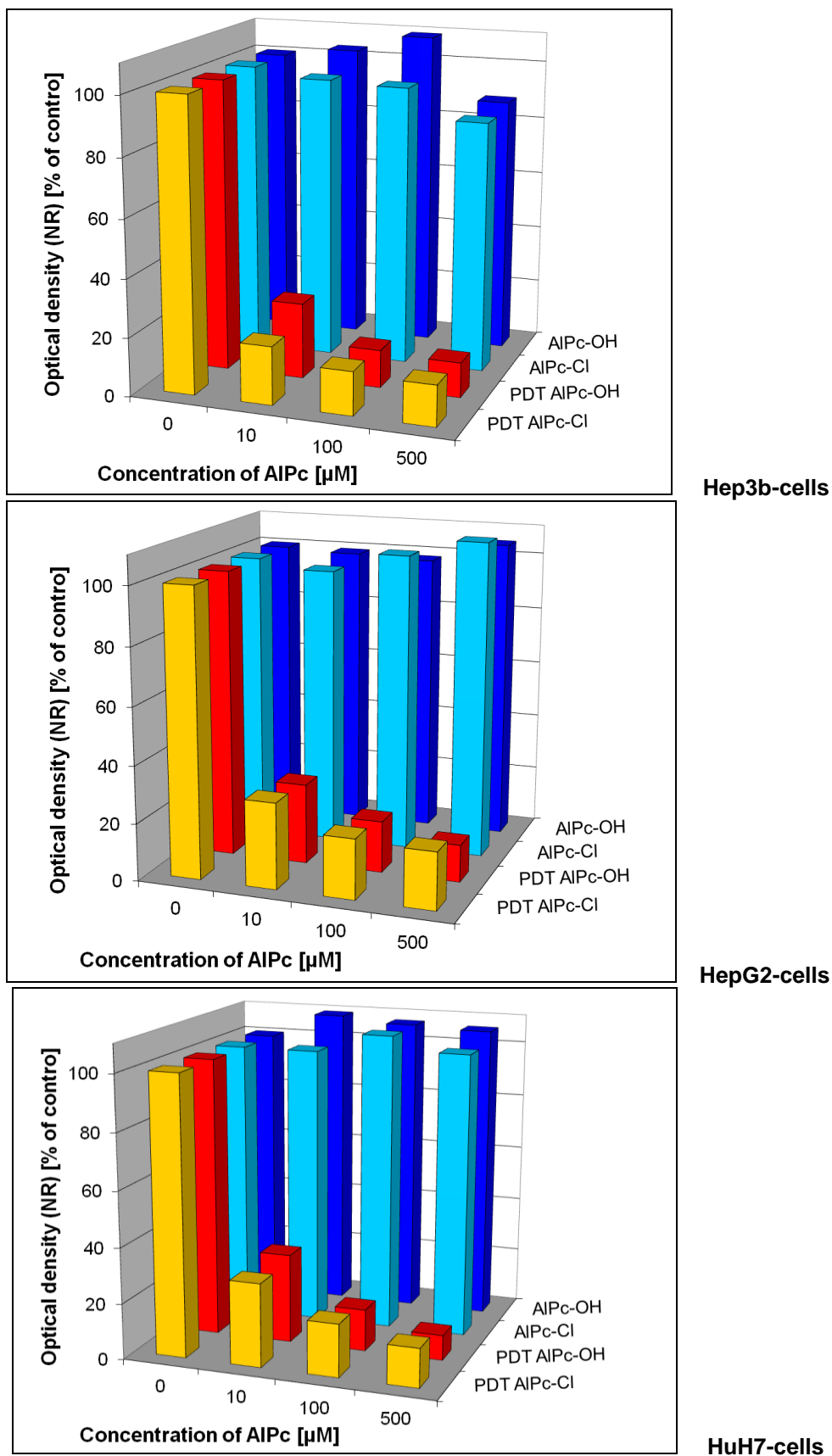
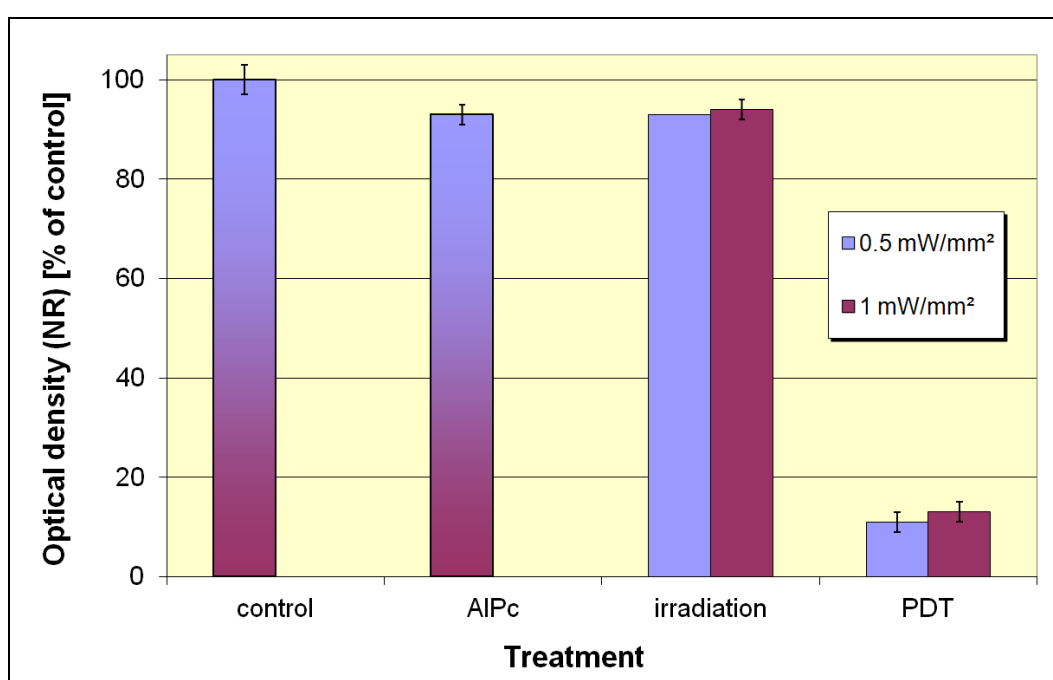


Figure 18 Comparison of dark and photo-toxicity of aluminum phthalocyanine forms AIPc-Cl and AIPc-OH. Radiant exposure  $5 \text{ J/cm}^2$ . Evaluation with Neutral Red (NR) Assay. PDT: photodynamic therapy. Median of absolute differences: MAD < 10 %.



### 3.2.7 Dependence of PDT-Toxicity on Irradiance

As some experiments had to be done with lower irradiance (power per surface [ $\text{W}/\text{cm}^2$ ]), influence of the latter on HuH7 cells was tested with constant overall radiant exposure ( $5 \text{ J}/\text{cm}^2$ ). It has been reported (Moor et al. 1997) that this can influence PDT efficiency, but in our case no significant difference was observed in the range tested (*Figure 19*).



*Figure 19* Comparison of two irradiances anent their toxicity to photodynamic therapy PDT. Aluminum phthalocyanine (AIPc)  $100 \mu\text{M}$  1d, radiant exposure He  $5 \text{ J}/\text{cm}^2$ . HuH7 cells. Evaluation with Neutral Red (NR) Assay.

### 3.3 PDT Effect in Dependence on Time of Incubation after Cell Seeding

AlPc (100  $\mu$ M, 1 d) was added to HuH7 cells at different times after seeding, in the range between zero hours (incubation with seeding) and eight days. No significant difference in PDT-toxicity ( $H_e$  5 J/cm<sup>2</sup>) could be observed in the range between one and four days (Figure 20). When more time elapsed between seeding and incubation/irradiation, PDT seemed to be less efficient. As will be discussed later in more detail, this might be due to the fact that higher cell densities prevent consistent monolayers in the cell dishes, leading to less efficient irradiation of the underlying cells.

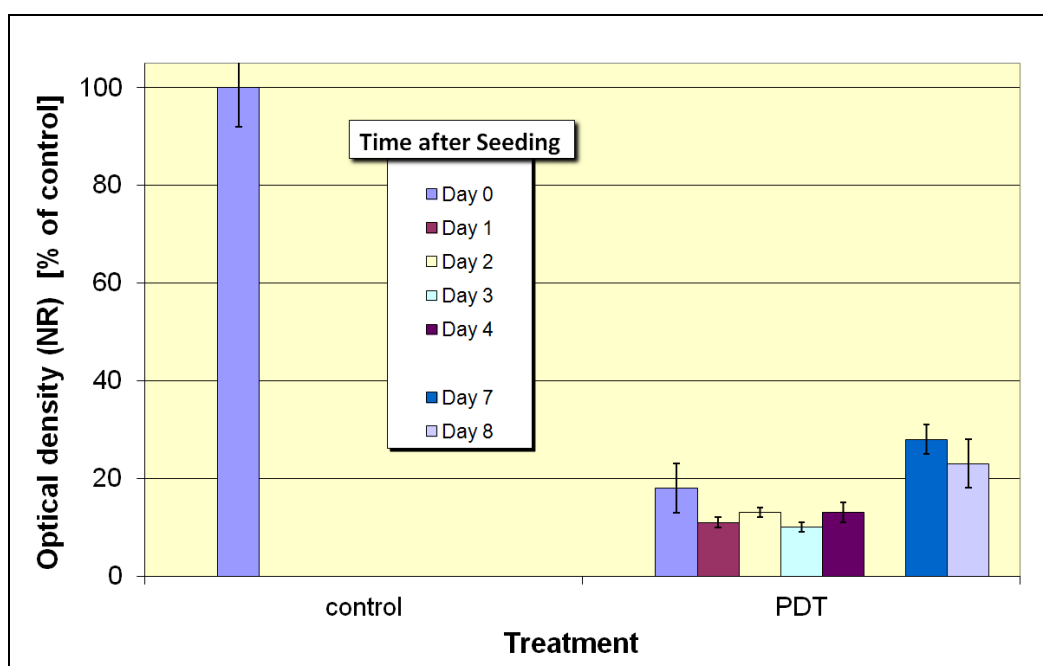
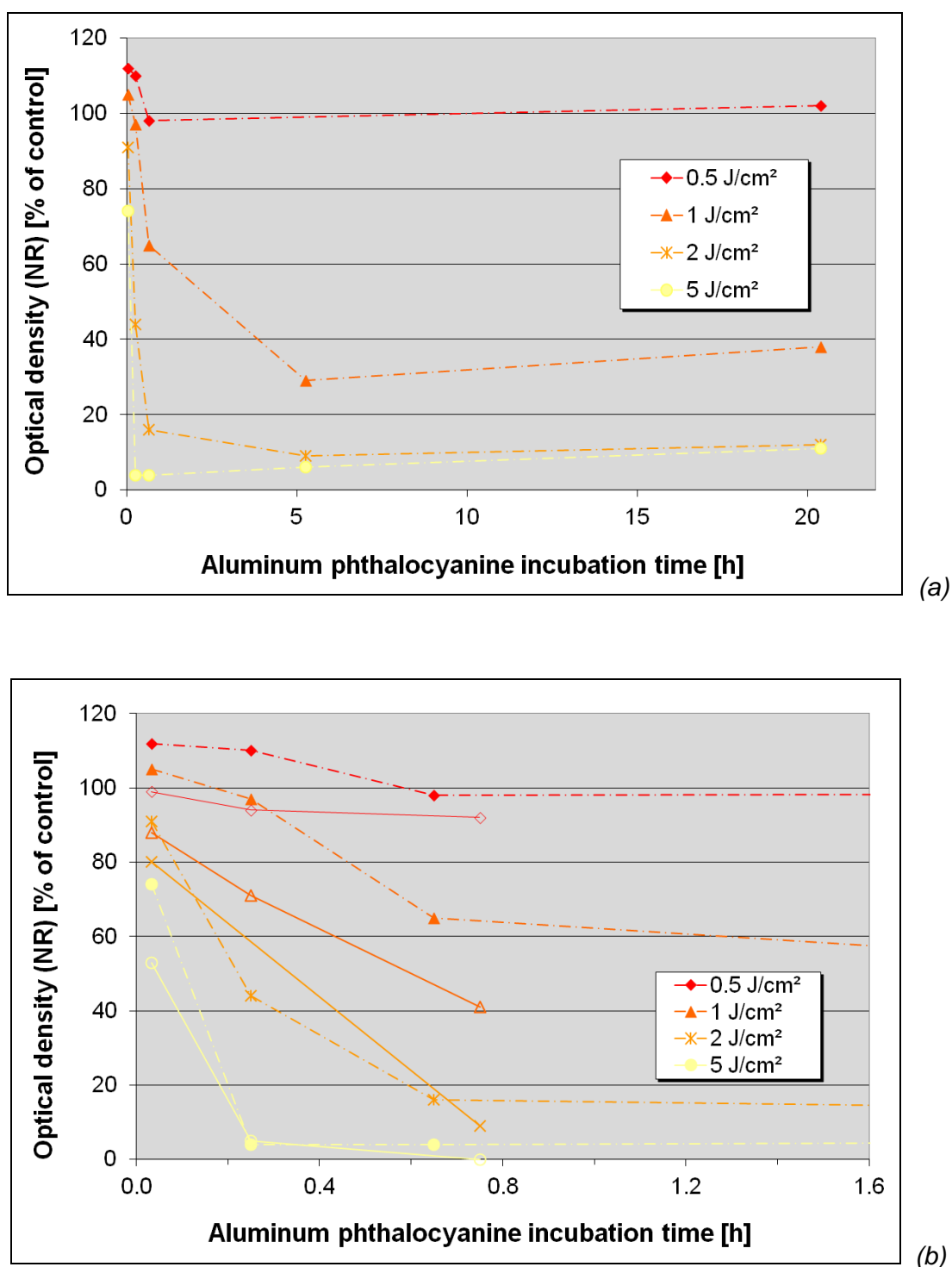


Figure 20 Toxicity of photodynamic therapy (PDT) with aluminum phthalocyanine (AlPc) as depending on time after seeding.  
HuH7 cells. AlPc 100  $\mu$ M 1 d, radiant exposure  $H_e$  5 J/cm<sup>2</sup>.  
Evaluation with Neutral Red (NR) Assay.

### ***3.4 PDT Effect in Dependence on Duration of AIPc Incubation***

AIPc (100  $\mu$ M) was added to Hep3b cells two days after seeding for time periods ranging from 2 min to 20 h. PDT toxicity increased (i.e. cell survival decreased) with AIPc incubation duration up to about five hours, then remained steady or even decreased slightly (*Figure 21*). Thus, there seems to be a maximum of PDT efficacy at intermediate incubation durations. This effect is reproducible for all the irradiation doses tested.

Another striking phenomenon is very clearly observed here: At short incubation times (2-15 min) combined with low irradiation doses (0.5-1 J/cm<sup>2</sup>), there is a slight increase in cell viability relative to the control, untreated cells. In the detail graph for the time range from 0 to 1.6 hours (*Figure 21.b*), an experiment conducted under seemingly the same conditions (open symbols) shows that this effect does not occur regularly, although it was observed in several different experiments involving low AIPc concentrations and low irradiation doses (data not shown).



**Figure 21** Toxicity of photodynamic therapy with aluminum phthalocyanine (AIPc) depending on duration of incubation (AIPc 100  $\mu$ M) and irradiation. Hep3b cells. Evaluation with Neutral Red (NR) Assay after 2 d.

(a) Whole time range (0-20 h).

(b) Detail of (a) in the range 0-1.6 h. The open symbols refer to a different experiment for comparison (cf. text).

### **3.5 Assaying PDT Effects with Viability Assays**

#### **3.5.1 Comparing the Viability Assays NR and MTT**

Although NR assay is a rapid and reproducible means of evaluating cell survival, NR uptake might not be a yes or no response considering that lysosomal function could be impaired without the cells being dead.

To further validate the results obtained with the NR assay, they were compared with those obtained by the MTT test, which is based upon a different cellular mechanism. It was presumed that a good correlation between both assays would prove the reliability of either method.

To emphasize briefly the differences between both assays: The NR assay relies on the uptake of NR in lysosomes that need a low pH in order to do so, which normally is the case solely in living cells. The cells are then lysed, so that the NR taken up is released in order to be quantified via the optical density (O.D.) of the supernatant.

In the MTT test, a yellow compound is taken up by living cells and converted to a violet product by a mitochondrial dehydrogenase (requiring functioning mitochondria). For the assay, this product too is released through cell lysis and measured via O.D. in the supernatant.

*Table 7* summarizes the differences between both methods.

The question is whether the NR assay, meaning the lysosomal function, or the MTT test, meaning the mitochondrial enzyme, can be (reversibly) impaired without the cell being dead; and, on the other hand, whether the mitochondrial enzyme can still be functional while the cell is already dead.

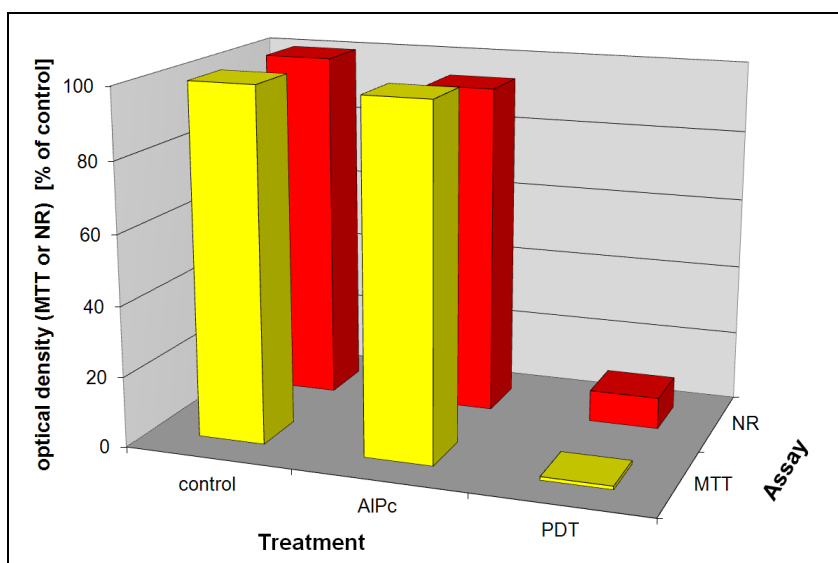
Implications and consequences of the two approaches will be further discussed together with other results.

Table 7      Comparison of NR and MTT viability assays.

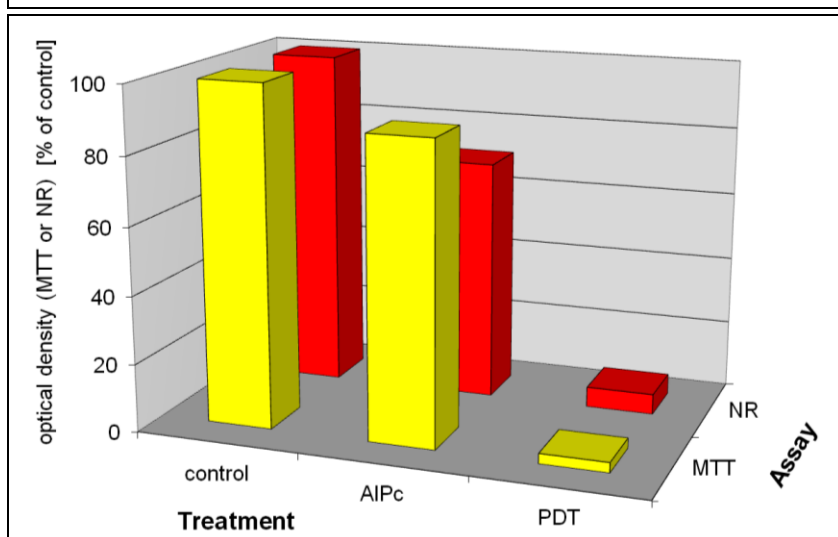
Neutral Red (NR) Assay	MTT Test
phenazine based dye	Me <sub>2</sub> -thiazol-2-yl-Ph <sub>2</sub> -tetrazolium bromide
active uptake by lysosomes	transformed by mitochondrial dehydrogenase into formazan
dependent on low pH	dependent on enzymatic activity

### **3.5.2 Dark and Phototoxicity of AIPc – Comparing NR and MTT**

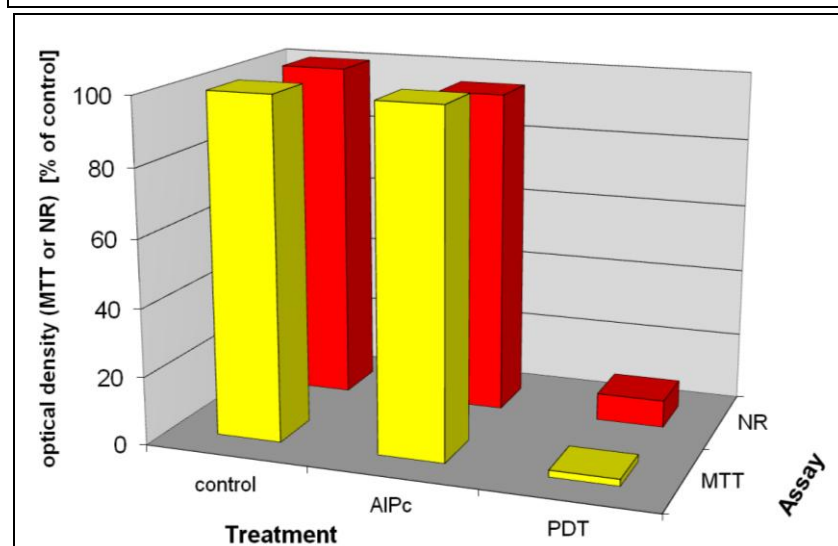
When cells were submitted to AIPc or PDT in the usual way, the viability assays NR and MTT gave virtually the same response, although the MTT test indicated a slightly lower relative cell survival following PDT (*Figure 22*).



Hep3b cells



HepG2 cells



HuH7 cells

Figure 22

Comparison of Neutral Red (NR) and MTT response 48 h after treatment with respect to dark- (AIPc) and photo- (PDT) toxicity of aluminum phthalocyanine AIPc. Median of absolute differences: MAD < 10%. (MTT: 3-(4,5-Dimethylthiazol-2-yl)-2,5-diphenyl-tetrazolium bromide)

### **3.5.3 Time Course of Neutral Red and MTT Response after PDT**

It has to be stressed that these viability assays, performed two days after treatment, do not allow to distinguish between slower overall growth of the cells and death of some cells with normal growth of the others; nor give information about the kinetics of cell killing after the applied treatment.

Still, we considered that comparison of both assays might give some insight in cell death pathways. For this reason, 'toxicity', as evaluated with the viability assays, was assessed as function of time after treatment (cf. 'Methods').

It could be shown (*Figure 23*) that following PDT, both assays react in a significantly different way; the NR uptake being impaired as soon as one hour after PDT, whereas the MTT test was not affected at such an early time. Not until about 40 h post-irradiation would both assays yield concordant results. This is the time frame of the results mentioned before, determining the toxicity after two days.

This finding could indicate that lysosomes are the primary target of AIPc-PDT in these cells and thus maybe also the intracellular region of accumulation, while mitochondria are affected only later.

In the case of HepG2 cells, the dotted lines refer to an experiment where evidently, for an unknown reason, PDT was not effective in the usual way: Shortly after irradiation, the Neutral Red response was strongly reduced as expected but recovered rapidly in the following hours, while the MTT response was practically unimpaired. The experiment concerned was carried out as a couple with (1) AIPc 100  $\mu$ M followed by H<sub>e</sub> 1 J/cm<sup>2</sup> that was more effective in reducing NR and MTT response than (2) AIPc 10  $\mu$ M followed by H<sub>e</sub> 2 J/cm<sup>2</sup>. It is interesting to remark, and would perhaps merit further studying, that obviously lysosomal Neutral Red uptake can be reversibly inhibited.



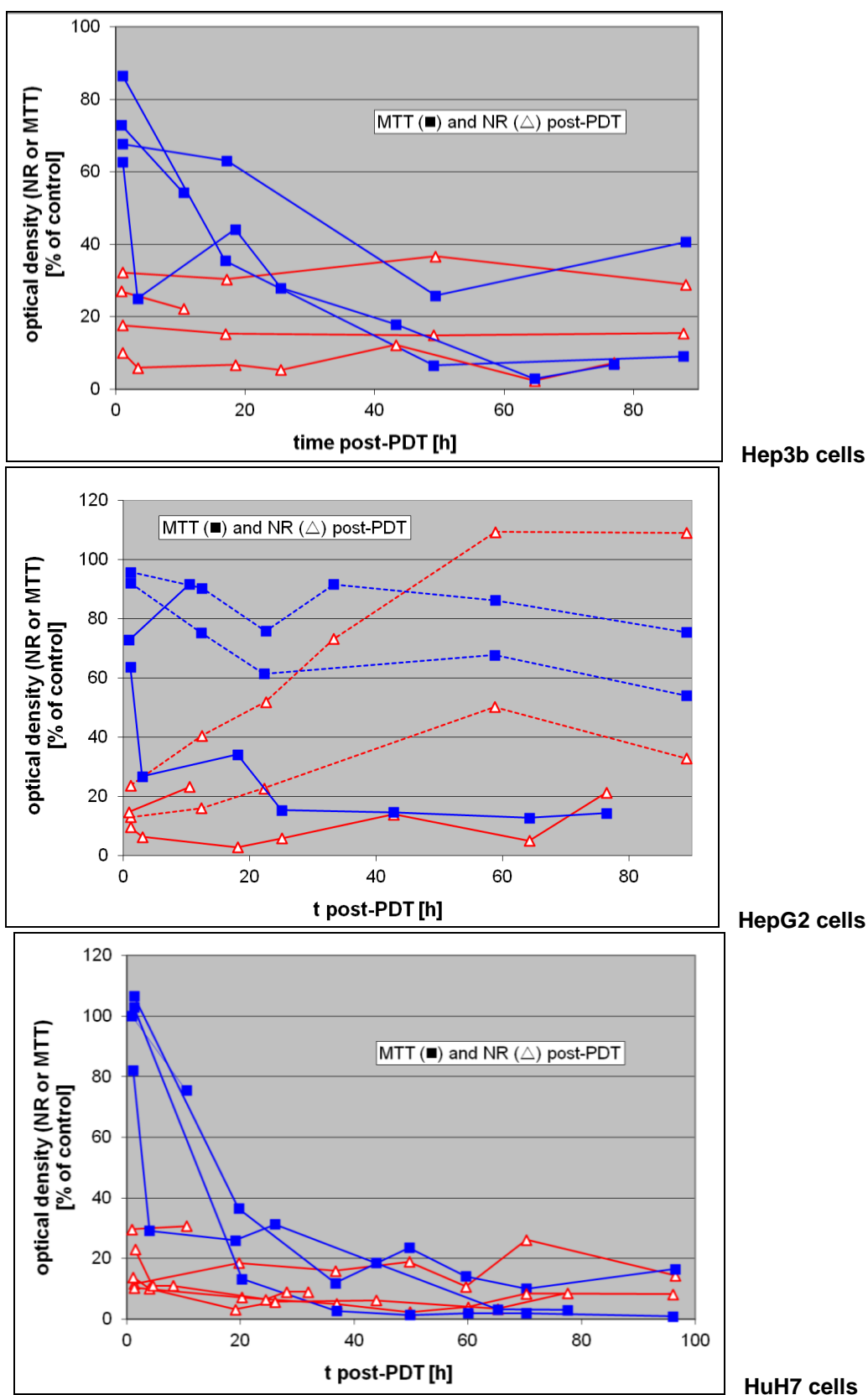


Figure 23

Time course of NR (△) and MTT (■) response after photodynamic therapy (PDT). Aluminum phthalocyanine AlPc 10 or 100  $\mu\text{M}$  20-40 h, radiant exposure  $H_e$  2 or 1  $\text{J}/\text{cm}^2$ . The lines correspond to individual experiments. For HepG2 cells the dotted lines are commented in the text. NR: Neutral Red; MTT: 3-(4,5-Dimethylthiazol-2-yl)-2,5-diphenyl-tetrazolium Bromide

Cells treated with ALPc alone showed in some cases a slight reduction in NR uptake shortly after the incubation with the photosensitizer that would recover in about the first ten hours, the cells then behaving as the ones not treated at all (data not shown). This again indicates that NR uptake might be reversibly impaired by ALPc and could be an indication of lysosomal accumulation of this photosensitizer too.

As mentioned, besides the missing response in one experiment with HepG2 cells, the observations described apply indifferently to all three cell lines although the results seem least disparate with HuH7 cells.

### **3.6 Electron Microscopy**

Electron microscopic features of HuH7 cells were compared between cells untreated and cells 15 respectively 30 min after PDT. Cells were prepared as described for analyses by conventional transmission electron microscopy (*Figure 24 a-b*) as well as for scanning electron microscopy to visualize the cytokeratine skeleton (*Figure 24.c.*).

PDT treatment leads to the formation of large vacuoles as soon as 15 min after PDT. This pattern does not significantly change between 15 and 30 min but the cytoplasm seems to become more homogeneous with time. This finding is in accordance to optical microscopic imaging showing vacuole formation too (cf. *Figure 35*).

The cytoskeleton seems to be affected by PDT in the same interval. Already 15 min after irradiation and even more after 30 min a clustering around the filaments can be observed.

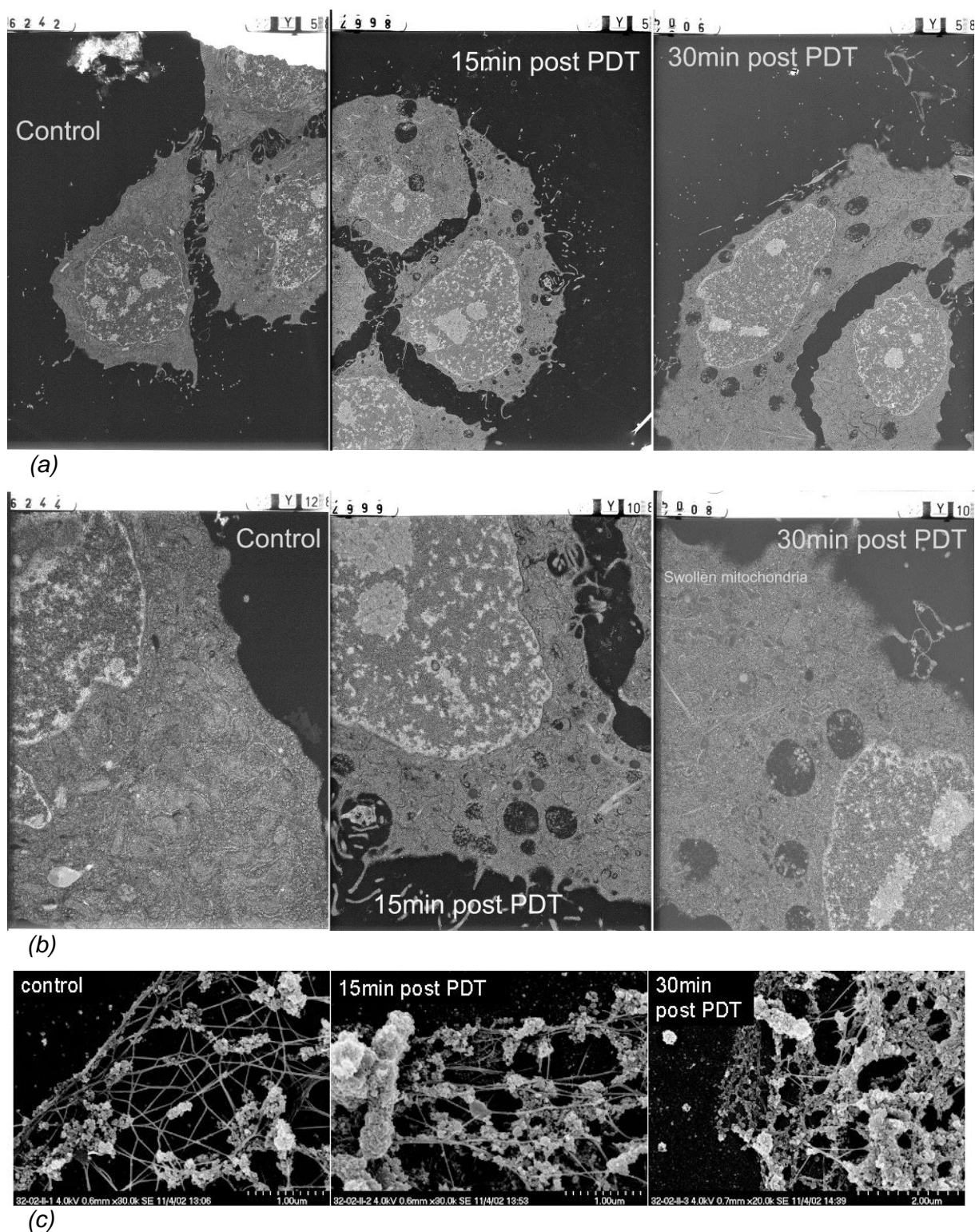


**Figure 24** Electron microscopy (EM) images of HuH7 cells following photodynamic therapy (PDT).

- (a) Transmission EM 1x: w/o PDT (control), 15min and 30min post-PDT,  
 (b) Transmission EM, 100x: w/o PDT (control), 15min and 30min post-PDT,  
 (c) Scanning EM: w/o PDT (control), 15min and 30min post-PDT.

### 3.7 Mitochondrial Cytochrome c Release

#### 3.7.1 PDT-Induced Cytochrome c Release from HCCs

Mitochondrial cytochrome c release was used as potential indicator of apoptosis: The following cell treatments were compared: untreated cells; cells treated with AIPc alone; and cells submitted to PDT (i.e. AIPc followed by irradiation).

*Figure 25 a-c* shows Western blottings of the cytosolic (c) and the mitochondrial (m) fractions of every sample of all three cell lines prepared as described in 'Methods'. Cells were collected 15 min after irradiation when PDT was to be assessed.

Proper separation of the mitochondrial from the cytosolic fraction was proved by the black and white pattern of cytochrome c distribution between both fractions in the control cells with respect to HuH7 and HepG2 cells. Under the same conditions however, untreated Hep3b cells presented cytochrome c in the cytosolic fractions too, just as did L929 cells, transfected or not, that were used to compare the behavior of another cell line under the mentioned fractionation procedure. For the latter, no noticeable cytochrome c release could be detected upon induction with anti-Apo-1 antibody (*Figure 26*).

Cytochrome c distribution in cells treated with AIPc (100  $\mu$ M, 2d) alone was the same as observed in the controls.

For all three HCC cell lines, PDT (AIPc 100  $\mu$ M 2d,  $H_e$  5 J/cm<sup>2</sup>) induced a distinct increase of cytochrome c in the cytosolic fractions when compared to the controls. This indicates loss of mitochondrial cytochrome c due to PDT. In the range between 1 and 5 J/cm<sup>2</sup> no quantitative difference in the effect could be detected for HuH7 or HepG2 cells (Western not shown).

It is interesting to remark that the observed cytochrome c release occurs as soon as 15 min after PDT while the mitochondrial enzyme on which relies the MTT test was virtually unimpaired for at least one hour more. Waterhouse (Waterhouse et al. 2001) already reported that, even after cytochrome c release, mitochondrial function and in particular the transmembrane potential can be maintained, meanwhile the *cytosolic* cytochrome c being used for the electron transport chains.

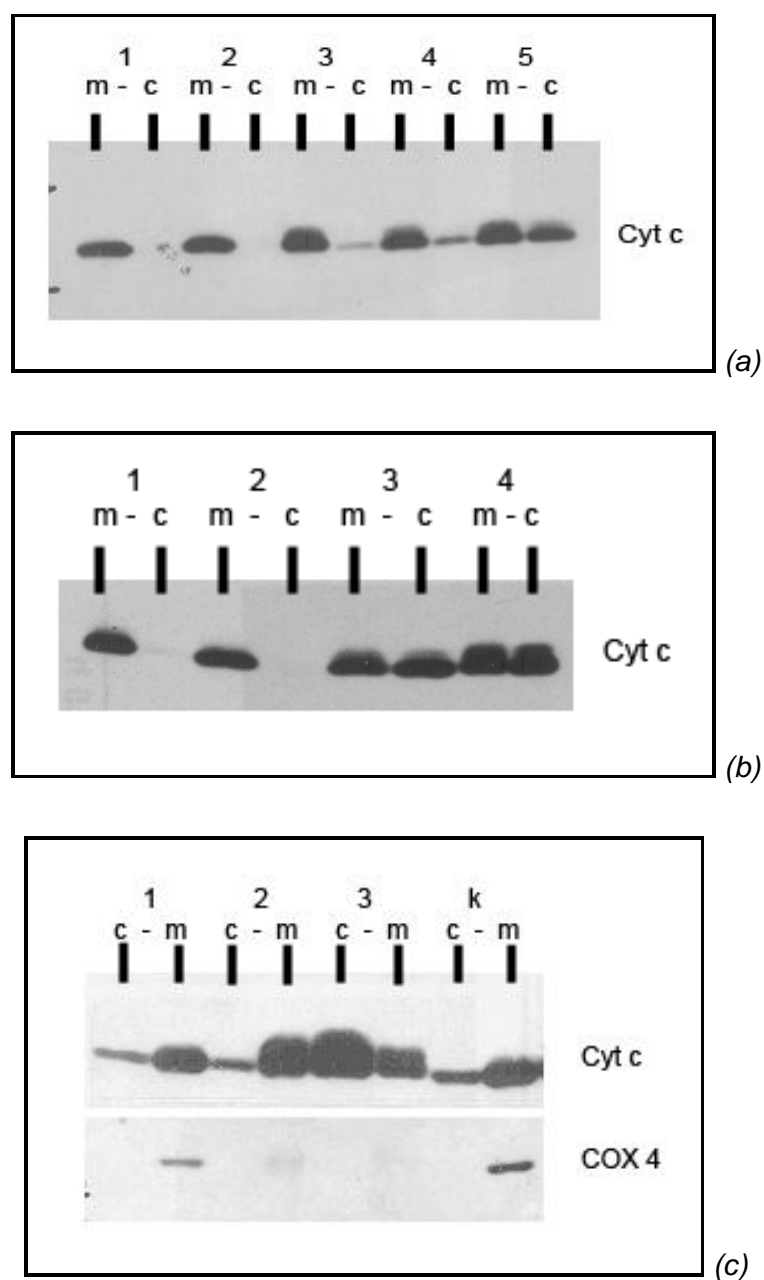


**Figure 25** Western blot of cytochrome c (Cyt c) release from mitochondria (m) to cytosol (c) in cells: (a) HuH7, (b) HepG2, (c) Hep3b (and L929 Apo) cells.

Lanes: 1 Control

2 Aluminum phthalocyanine (AlPc) 100  $\mu$ M, 2d

3-5 AlPc 100  $\mu$ M 2d,  $H_e$  5 J/cm<sup>2</sup>, 15 min post PDT

k L929 Apo cells, control (cf. Figure 26)

PDT: photodynamic therapy.  $H_e$ : radiant exposure

COX 4: Cytochrome c oxydase 4.

### **3.7.2 The Control Protein COX 4**

As mentioned in "Material and Methods", the kit used for these experiments includes a 'negative control': Mitochondrial as well as cytosolic samples are assessed for the presence of cytochrome c oxidase subunit 4 (COX 4). Unlike cytochrome c, COX 4 is not released from the mitochondria during apoptosis; only severe mitochondrial damage, as occurring during necrosis, or possibly through artifacts during sampling, results in cytosolic COX 4. Therefore, in principle, probing for cytochrome c and COX 4 allows to differentiate between apoptotic cells and necrotic or otherwise damaged cells; damage meaning destruction of mitochondria during processing the cells.

Here, detection of COX 4 was not possible in all but one sample tested (*Figure 25.c.*), although the mitochondrial fraction of another cell line, the murine fibroblasts L929 (transfected or not with Apo-1), probed under identical conditions, showed to be mostly positive (*Figure 26*). The latter was subsequently used as positive control to check the efficiency of the used reagents.

On request, the manufacturer confirmed that the COX 4 antibody provided in the kit we used is supposed to recognize, among others, the human as well as the murine protein.

Although for the above given reasons, COX 4 is a valuable parameter to control cell processing, most available detection kits for cytochrome c do not comprise such an option. Publications mainly rely on the results obtained for cytochrome c (e.g. Ali et al. 2002), so that we renounced here to investigate further the reason why we could not detect the COX 4 in hepatocellular carcinoma cells.

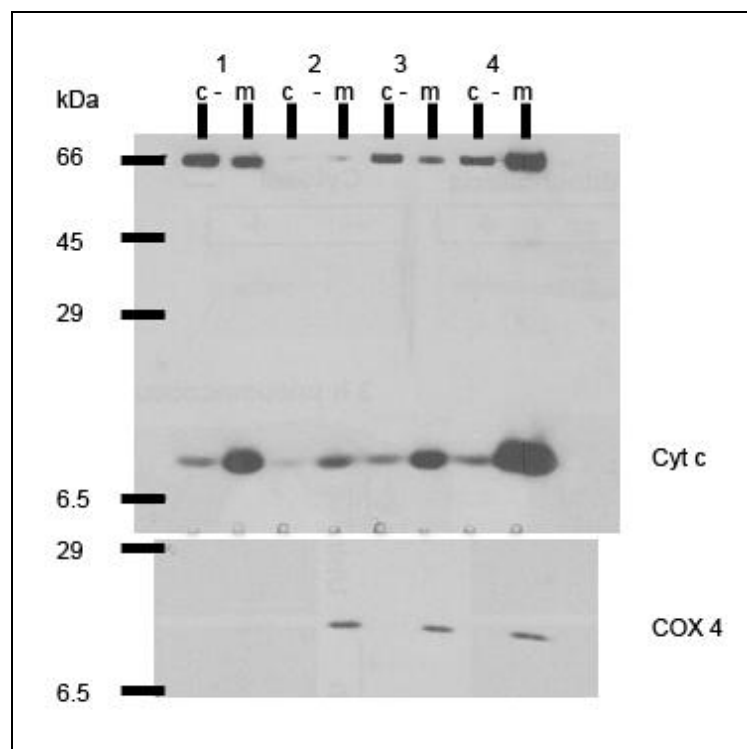


**Figure 26** Western blot of cytochrome c (Cyt c) and cytochrome c oxydase COX 4 after cell fractionation in parental (Par) L929 and L929 Apo transfected cells. Induction with anti-Apo-1 antibody. c = cytosol, m = mitochondria.

Lanes: 1 L929 Apo, control  
 2 L929 Apo, induction  
 3 L929 Par, control  
 4 L929 Par, induction



### **3.8 AIPc-PDT in the Presence of Caspase Inhibitors**

Two caspase inhibitors, acting on a broad range of caspases, were used to assess the possibility to prevent cell killing in AIPc-PDT by inhibiting the action of caspases. If this was possible, it would be an indication of caspases being involved in the underlying mechanism of cell dying, and hence, an indication of apoptosis induction.

#### **3.8.1 Caspase Inhibitors – Dark, Concomitant and Photo-Toxicity**

As caspase inhibitors have been reported to be cytotoxic themselves, dark toxicity as well as phototoxicity ( $5 \text{ J/cm}^2$ ) and combined toxicity with AIPc (24 h, 400  $\mu\text{M}$ ) were assessed for all cell lines. Results are shown here for HuH7 cells (*Figure 27*); no significant difference was observed when probing the two other cell lines (data not shown).

Both caspase inhibitors seem to be slightly toxic at concentrations of 100  $\mu\text{M}$  (cell survival about 80% of control), while at lower doses boc-D-fmk (C.I.3) leads to slightly lower survival rates than z-VAD-fmk (C.I.1) (*Figure 27.a*).

There was no significant additional toxicity of either caspase inhibitor upon irradiation or concomitantly with AIPc (*Figure 27.b and c*).

D'Mello (D'Mello et al. 1998) used 15 min incubation with boc-D-fmk (C.I.3) 25-100  $\mu\text{M}$ , and z-VAD-fmk (C.I.1) 50-100  $\mu\text{M}$ , to yield a 90 and 65 % protection against apoptosis respectively. They reported the protection to be effective for up to two days and boc-D-fmk to be slightly more efficient than z-VAD-fmk. Thus, conditions used herein are in the range of those used by the reference.

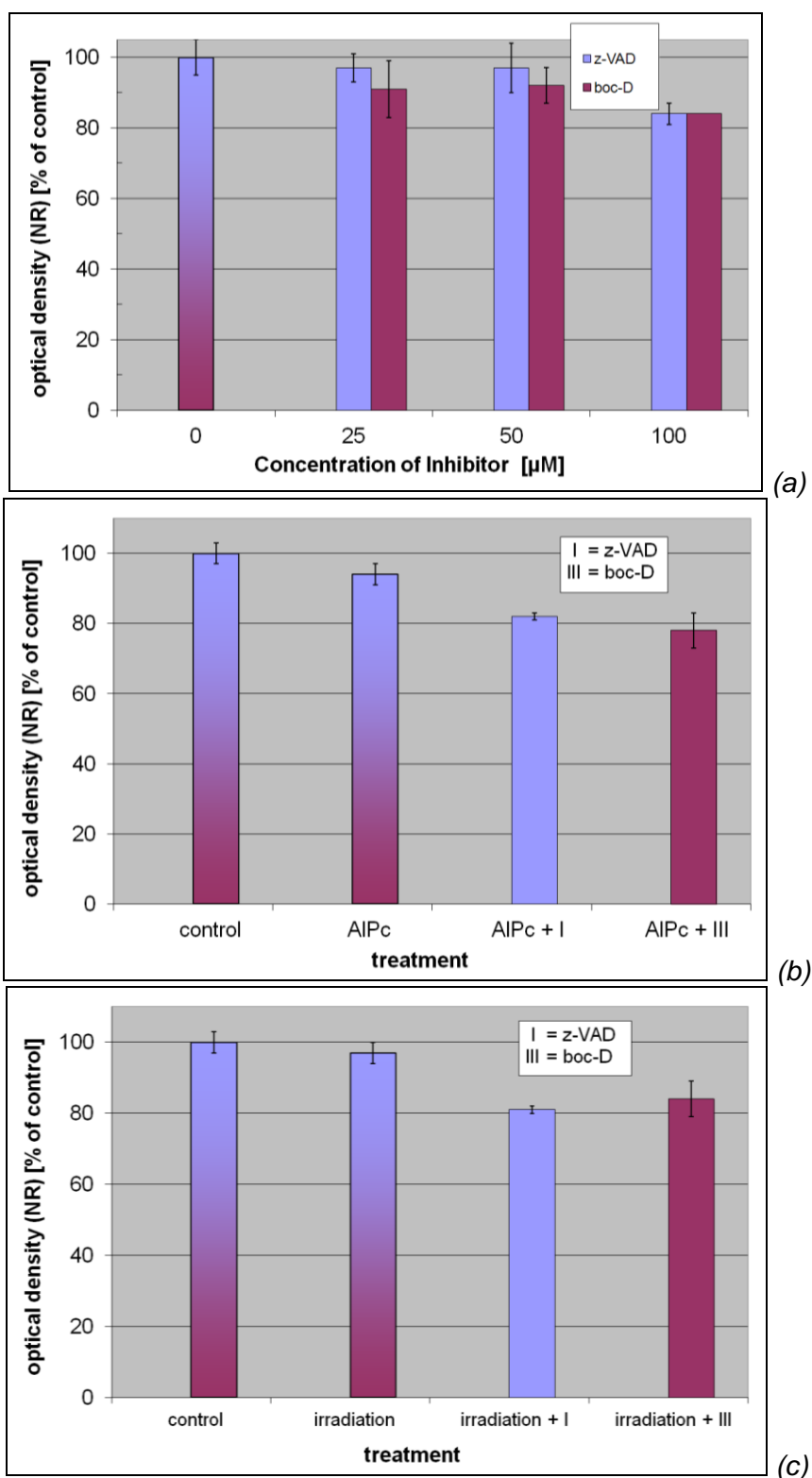


Figure 27

Evaluation of caspase inhibitors' (C.I.) toxicity on HuH7 cells.

(a) Darktoxicity of caspase inhibitors z-VAD-fmk (I) and boc-D-fmk (III).

(Concentrations as indicated for 2 d, then Neutral Red Assay (NR) )

(b) Concomitant toxicity of caspase inhibitors I and III with AIPc.

(aluminum phthalocyanine AIPc 400  $\mu\text{M}$  24 h, C.I. 100  $\mu\text{M}$  2 d, then NR )

(c) Phototoxicity of caspase inhibitors z-VAD (I) and boc-D (III).

(concentration 100  $\mu\text{M}$  12 h, radiant exposure  $H_e$  5  $\text{J}/\text{cm}^2$ , NR after 2 d )

### **3.8.2 PDT in the Presence of Caspase Inhibitor**

HuH7 cells were submitted to PDT (AIPc 100  $\mu$ M 24 h,  $H_e$  5 J/cm<sup>2</sup>) in the presence of either caspase inhibitor, added 15 min prior to irradiation, after retrieval of AIPc from the medium. Results are presented in *Figure 28*.

While the effect of PDT under these conditions is not noticeably modified by the presence of z-VAD-fmk (C.I.1) up to a concentration of 100  $\mu$ M, there seems to be a little protective effect by D-boc-fmk (C.I.3), that is concentration dependent in the range tested (O.R. 1.3 – 1.7). Cell survival upon PDT can thus be increased from 3 to 5 % in the presence of D-boc-fmk. In accordance to the results reported by D'Mello (D'Mello et al. 1998), D-boc-fmk is more efficient as protector but the high protection yielded in their experiments (60-95%) was by far not achieved in our case.

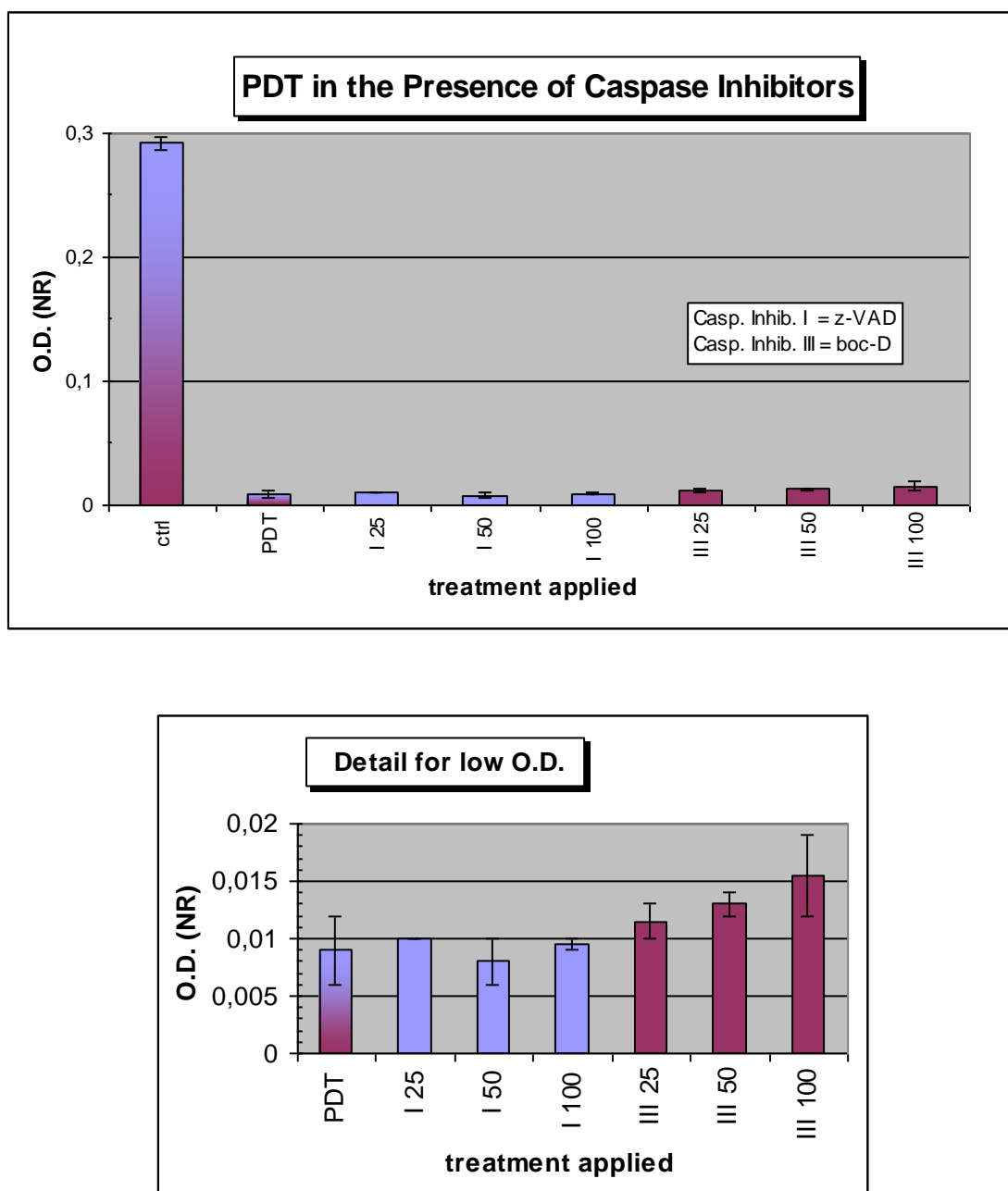


Figure 28

Effect of caspase inhibitors I and III (concentration as indicated in  $\mu\text{M}$ ) on photodynamic therapy (PDT) with aluminum phthalocyanine (AlPc). HuH7 cells, AlPc  $100 \mu\text{M}$  24 h, radiant exposure  $H_e$   $5 \text{ J/cm}^2$ , caspase inhibitor added 15 min prior irradiation, Neutral Red (NR) Assay after 2 d. The lower graph shows the PDT-results at a larger scale. O.D.: optical density.

### **3.9 Antioxidants**

Several substances, susceptible to interfere with initial production of reactive oxygen species or free radicals, were used to treat cells submitted to PDT. These antioxidants were: N-acetyl cysteine (NAC), pyrrolidine dithiocarbamate (PDTC) and ascorbate. The latter was used as free acid (ascorbic acid) and as sodium salt (sodium ascorbate) to evaluate the effect of pH.

As described for the investigation of caspase inhibitors in the previous chapter, dark toxicity of the compounds alone as well as combined toxicity with AIPc (100  $\mu$ M, 24 h) or irradiation (5 J/cm<sup>2</sup>) was evaluated with the Neutral Red Assay. Concentrations of the antioxidants were in the range 0-1 mM.

NAC as well as both forms of ascorbate showed no significant toxicity on either cell line neither alone nor combined with AIPc or irradiation (data not shown).

For PDTC, results varied largely: In some experiments PDTC did not seem to be toxic up to 100  $\mu$ M, whereas in others 5  $\mu$ M did suffice to kill 80 % of the cells. This was independent of the cell line treated. We concluded that the experimental conditions did not allow us a sufficient control of PDTC concentration, possibly because the compound is not stable in solution or not fit for our procedure of sterile filtering. This was not investigated further.

An influence of NAC or either form of ascorbate on PDT could not be demonstrated for any of the three HCC cell lines (data not shown).

As these compounds did not seem to have any noticeable effect on the PDT treatment we were investigating, no further experiments were made with them.

## 3.10 Laser Scanning Microscopy

### 3.10.1 General Considerations and Probing the Fluorochromes

Figure 29 shows the fluorescence spectra of the fluorophores utilized hereafter, as well as the fluorescence spectrum of AlPc-Cl as recorded from adequately prepared solutions with the meta-detector of the LSM 510.

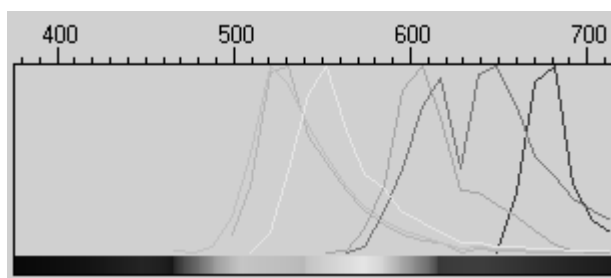


Figure 29 Fluorescence spectra of: (from left to right): Rh123 and Fluo-3, LysoTracker Green Br<sub>2</sub>, MitoTracker CMX Ros, Neutral Red (NR), Aluminum phthalocyanine. (The indentation at 630nm in the broad NR-spectrum is due to the exclusion of the 633nm laser from the detectors.)

As can be seen, Rhodamine123 and Fluo-3 cannot be discriminated by their spectra. Several other spectra overlap to an extent that makes them inappropriate for use with the channel detection mode, where a bandpass filter defines a certain region of the visible spectrum that is detected by one photomultiplier (PMT).

These fluorophores can eventually be differentiated in two ways: Either by combining the conventional channel mode (ChMo) with the multi-track mode; or by using the spectral mode (LaMo) of the meta system with online or offline extraction of the fluorophore-specific spectra (online fingerprinting or linear unmix):

The multi-track mode allows recording the fluorescence image line-wise under different conditions. For instance, the first line can be excited with the laser for one fluorophore with detection in the wavelength region specific for that one, while every second line is recorded in the band specific for the second fluorophore after excitation with the corresponding laser.

This multi-track mode is not useful, however, when both dyes emit significantly upon excitation with the same laser. In this case, extraction of the spectra is the

sole possibility to discern both fluorophores. The fluorescence image is recorded by the meta detector with spectral resolution, i.e. an intensity image every 11 nm (or further apart) is obtained. From the resulting lambda-stack a spectrum of every image pixel can be extracted. Regions where surely only either fluorophore is present can be used to define the spectrum of this species and extract it in the overall image (linear unmix). Alternatively, there is an automated extraction of components (ACE) mode, by which a defined number of spectra is extracted from the lambda-stack. Every spectrum (i.e. every compound) can then be represented in a different color.

*Note: In order to enhance clarity of the LSM images, transmission pictures of the cells are not included considering that they do not give additional information.*

### **3.10.2      Monitoring the Uptake and Localization of AIPc**

The uptake of AIPc by the cells is very rapid. Typical intracellular fluorescence increase can be observed as early as 2 min after addition of AIPc (*Figure 30.b*). The concentration seems to be increasing for about 5 h as can be seen by the decrease of the detector gain (D.G.) when using the 'find' function for optimizing the recording (*Figure 30.a*). Besides fluorescence intensity, which is thus indirectly monitored by the automated regulation of the detector gain, the density of fluorescent dots per cell does increase with time too (*Figure 30 b-g*).

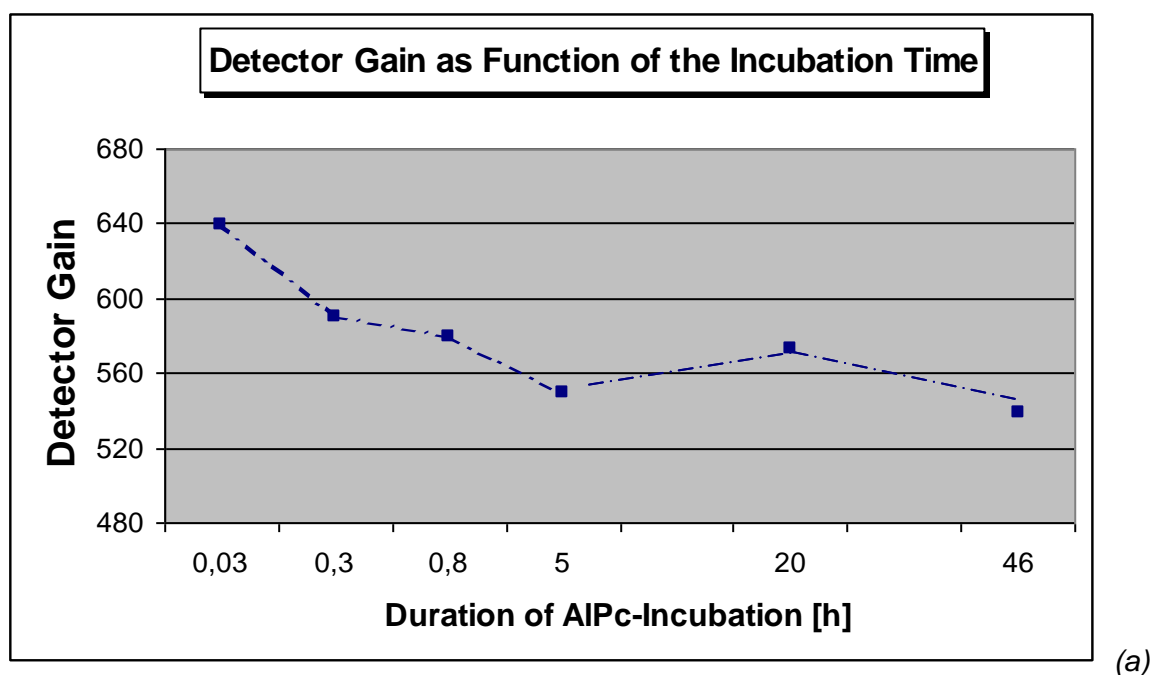
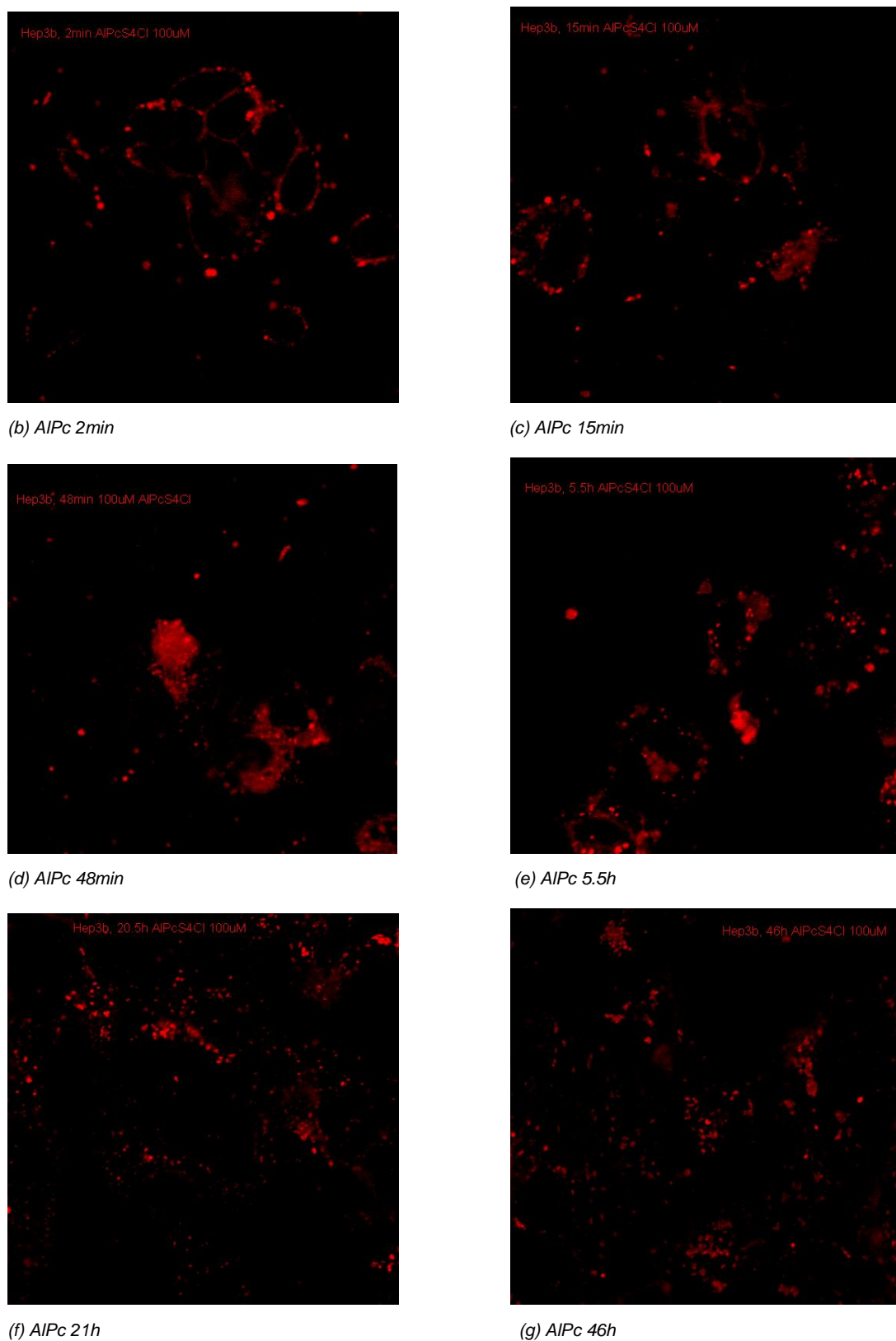


Figure 30.a Uptake of aluminum phthalocyanine (AlPc) in Hep3b cells over time monitored by laser scanning microscopic imaging:  
 Decrease of Detector Gain (D.G.) (optimized by 'find') with increase of AlPc incubation duration. (Non-linear time scale.)  
 (For the corresponding fluorescence images cf. Figure 30 b-g below.)





**Figure 30** Uptake of aluminum phthalocyanine (AlPc) in Hep3b cells over time, Detector Gain optimized by 'find' as shown in Figure 30.a.

Fluorescence images after (b) 2 min, (c) 15 min, (d) 48 min, (e) 5.5 h, (f) 20.5 h, and (g) 46 h of incubation with AlPc 100 $\mu$ M.

As mentioned before, in the observed time range, sensitivity to 676 nm light (i.e. phototoxicity or PDT efficiency) increases with incubation duration (cf. *Figure 21*). In different experiments, the AIPc distribution shows a granular versus a diffuse cytosolic pattern which does not depend solely on the duration of incubation with the photosensitizer. We suspect the phase of cell growth to play a role, because the distribution seems to be towards the more diffuse pattern in older culture plates. When addition of AIPc is done early after seeding, the AIPc-fluorescence is granular, similar to a lysosomal staining (*Figure 31 a-b*), while a diffuse cytoplasmic pattern is overlaid when time between seeding and AIPc-addition is longer (*Figure 31.c*).

Following PDT, the AIPc fluorescence pattern did not show such remarkable differences from one experiment to another (*Figure 35 c-d*).

Cellular uptake of AIPc could also be monitored online with the LSM by incubating Hep3b cells with AIPc-containing medium and scanning the specimen at a predetermined position with an almost closed pinhole to achieve the highest possible vertical resolution and minimize the fluorescence of the surrounding solution (*Figure 32*). Different cells were scanned for the image series to avoid bleaching or photo reaction through repeated irradiation.

As little as 10 min incubation with AIPc was sufficient to observe a granular pattern of AIPc fluorescence appear in the peripheral regions of the incubated cells. This would increase with time in number and intensity, while after longer incubation duration a more diffuse cytosolic AIPc fluorescence outlining the cells could be observed additionally. It should be noted that detection sensitivity in this method is restricted because of the high surrounding fluorescence of the incubation medium, but the LSM images show clearly that there is a concentration process taking place during the uptake.

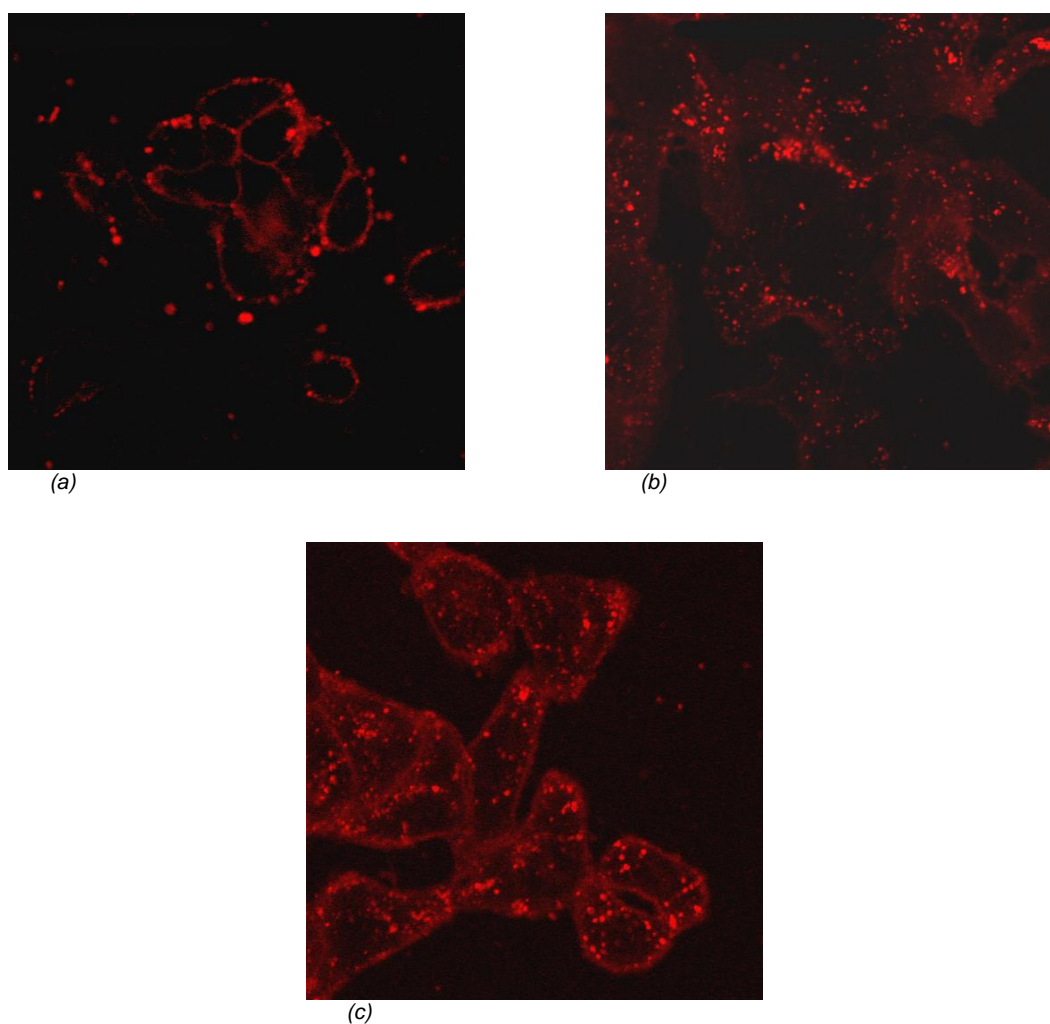


**Figure 31**     *Different intracellular aluminum phthalocyanine (AlPc) distribution pattern after incubation with 100  $\mu$ M at various times after seeding:*

- a. AlPc 100  $\mu$ M, 2min incubation, 14 h after seeding; granular pattern,*
- b. AlPc 100  $\mu$ M, 20.5h incubation, 14 h after seeding; granular pattern,*
- c. AlPc 100  $\mu$ M, 2 h incubation, 3 d after seeding; granular + diffuse pattern.*

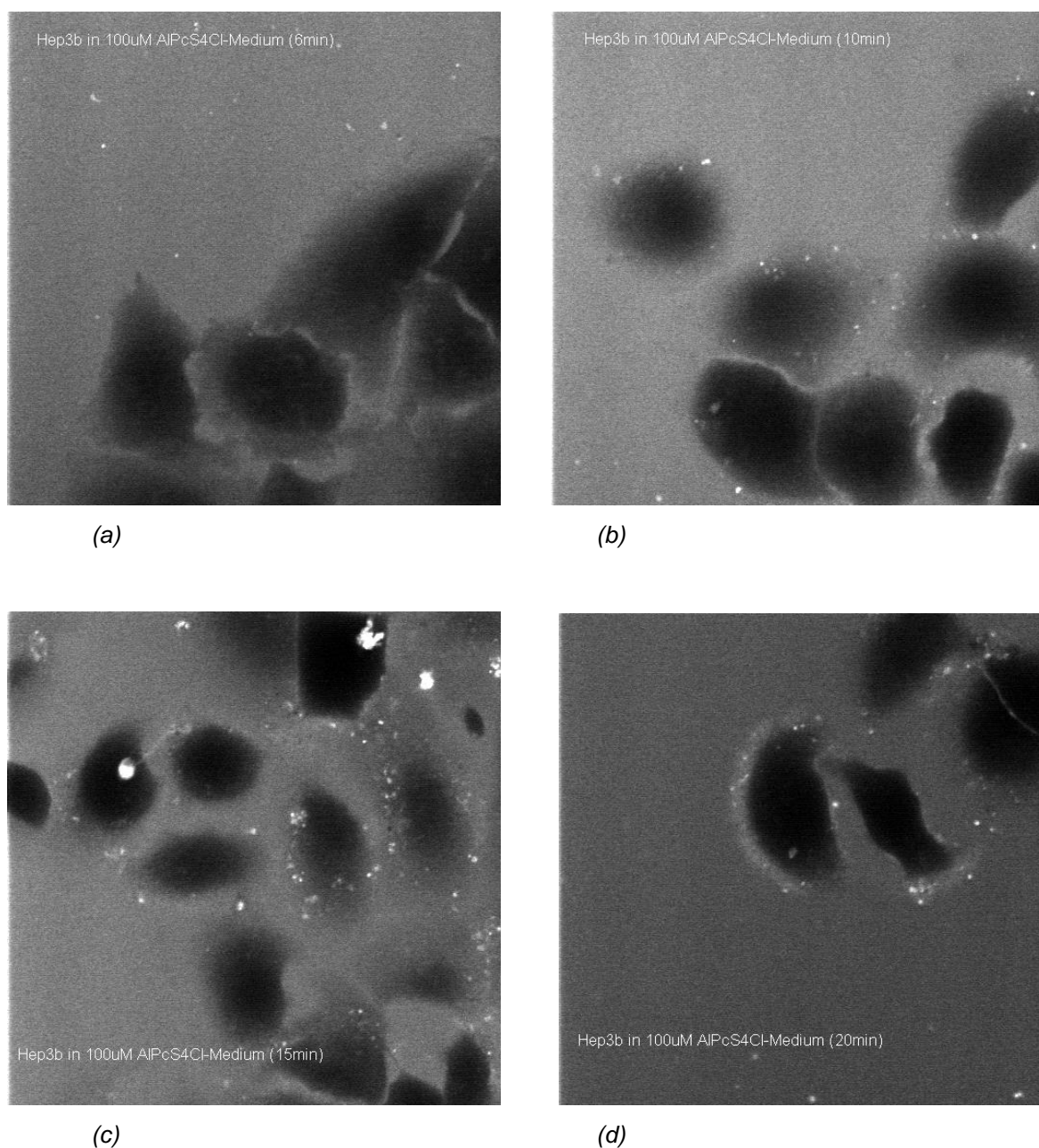
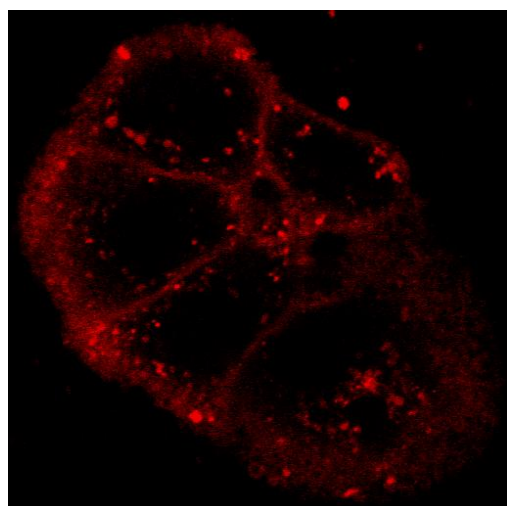
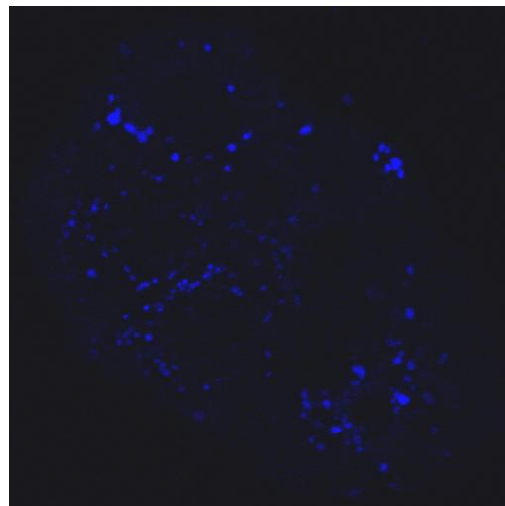


**Figure 32** Laser scanning microscopic online monitoring of aluminum phthalocyanine (AlPc) ( $100\ \mu\text{M}$ ) uptake in Hep3b cells. Time series: (a) 6 min, (b) 10 min, (c) 15 min, (d) 20 min after addition of AlPc.

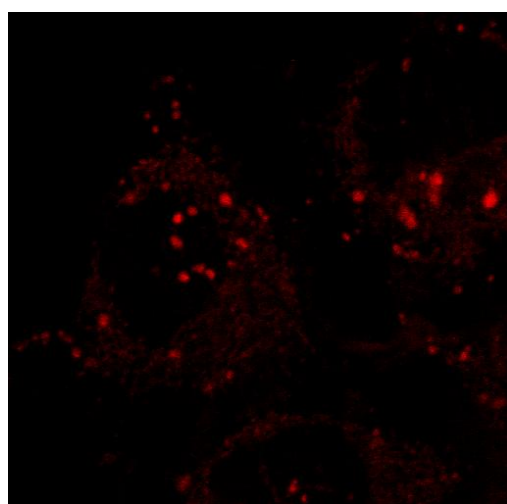
The granular pattern of AlPc strongly resembles fluorescence distribution of the lysosomal marker LysoTracker Green Br<sub>2</sub> (Figure 33.a), whereas it is not co-localized with Rhodamine 123 (Figure 33.b) or MitoTracker Red CMX Ros (data not shown).



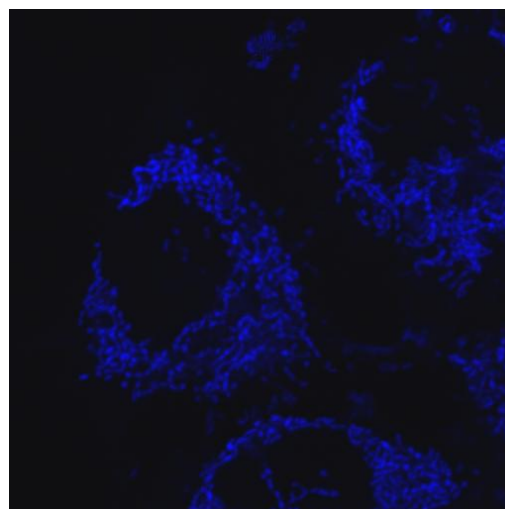
*(a) 1 h AlPc 100  $\mu$ M*



*3 h LysoTracker 50 nM*



*(b) 1 d AlPc 100  $\mu$ M*

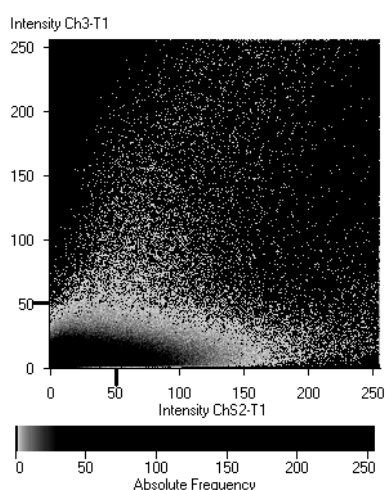


*30 min Rhodamine 123 40  $\mu$ M*

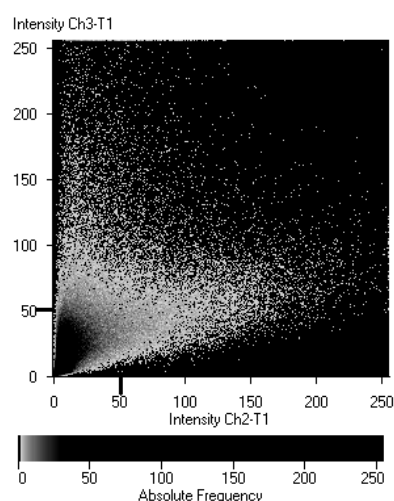
*Figure 33.a/b Comparison of fluorescence pattern and colocalization of aluminum phthalocyanine (AlPc) with*

*(a) LysoTracker Green Br<sub>2</sub> (3 h, 50 nM), Hep3b cells*

*(b) Rhodamine 123 (30 min, 40  $\mu$ M), HuH7 cells*



(c) AIPc versus LysoTracker



(d) AIPc versus Rhodamine 123

Figure 33.c/d Colocalization of aluminum phthalocyanine (AIPc) (Ch3-T1) with  
 (c) lysosomal marker LysoTracker (ChS2-T1)  
 (d) mitochondrial marker Rhodamine 123 (Ch2-T1)

Semiquantitative representation of the degree of colocalization can be automated by the LSM 510 software for any fluorescence image recorded in the channel mode and is shown for the couples AIPc/LysoTracker and AIPc/Rhodamine 123 in Figure 33 c and d. Although for Rhodamine 123 the different localization of both fluorochromes is quite evident, often the sensitivity of this representation is restrained because of low overall fluorescence intensities (lower with increasing confocality, i.e. vertical resolution). That is the case here with the data for the LysoTracker: the distribution is quite distinct from that for Rhodamine but the fluorescence intensities are too low to give evidence for colocalization.

Attempts to colocalize AIPc with NR (2 h, 0.02 %) failed, because NR leads to a diffuse cytosolic fluorescence while the lysosomes do not fluoresce at all, although in visual mode, they appear as deep red vacuoles (Figure 34). Indeed, fluorescence of NR seems to be quenched in lysosomes either by high concentration or by conditions inherent to these organelles (e.g. pH). Singh (Singh

et al. 1998) reported an unusual solvatochromism, i.e. important changes in absorption and fluorescence spectra, depending on solvent properties, that might account for our findings.

No further experiments were undertaken to find adequate experimental conditions, although it might be interesting to follow NR staining and fluorescence post-PDT.

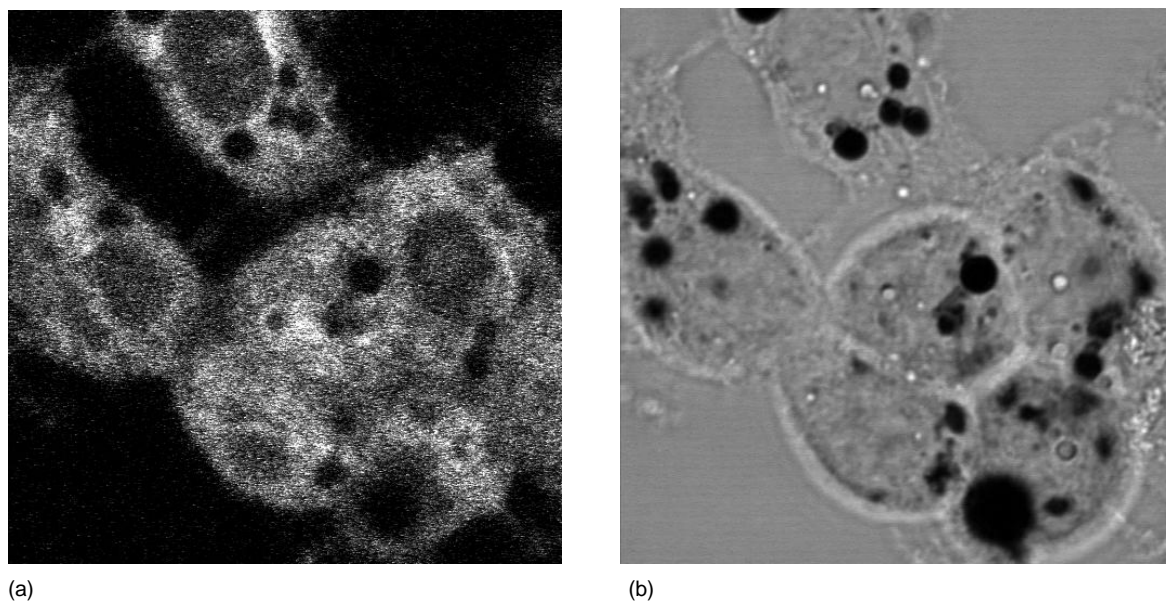


**Figure 34**      *Neutral Red (2 h, 0.02 %) in HepG2 cells:*  
(a) *Diffuse cytoplasmic fluorescence exempting lysosomes,*  
(b) *Deeply stained lysosomes in transmission image.*

### **3.10.3      Monitoring PDT in ALPc-Incubated Cells**

Upon irradiation (here: 676 nm, 100 mW/cm<sup>2</sup>, 20 s, i.e. 2 J/cm<sup>2</sup>), the pattern of ALPc-fluorescence changes distinctly to a diffuse cytosolic distribution with dark 'holes', probably vacuoles, as soon as 5 min after PDT (*Figure 35.c-d*).



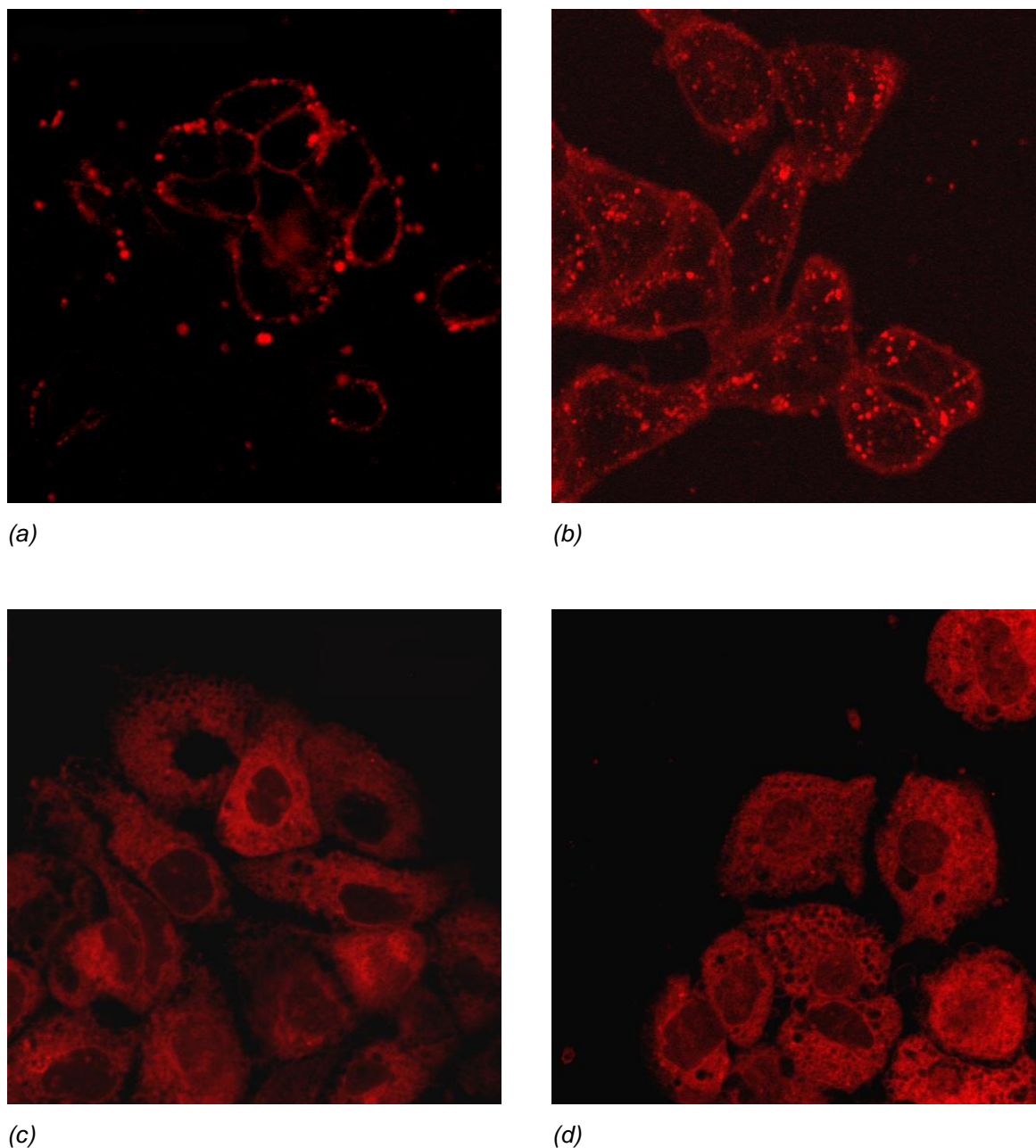
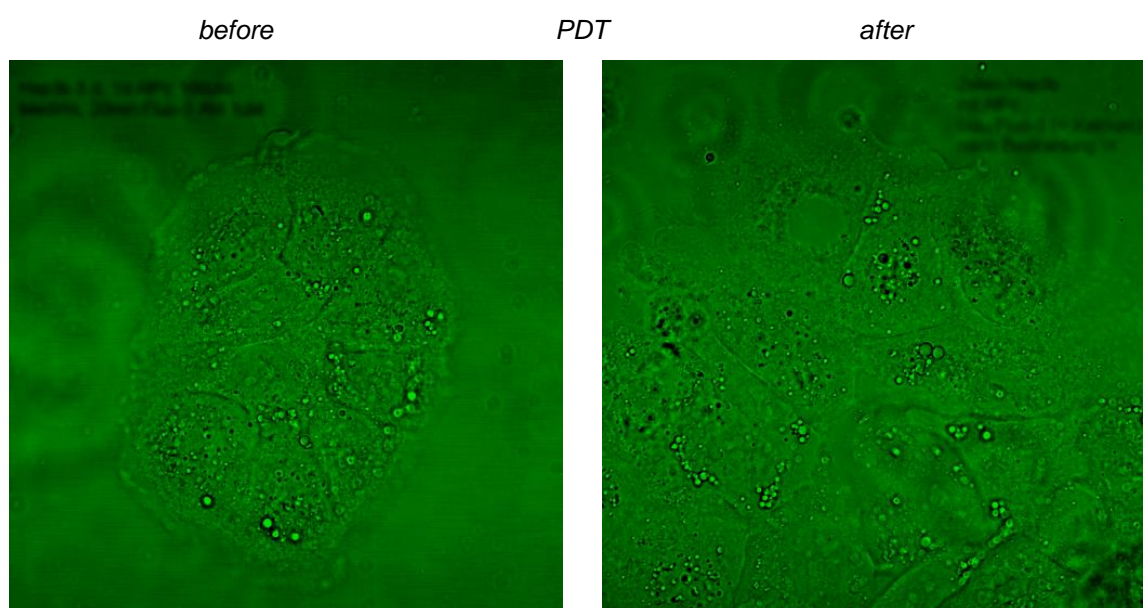


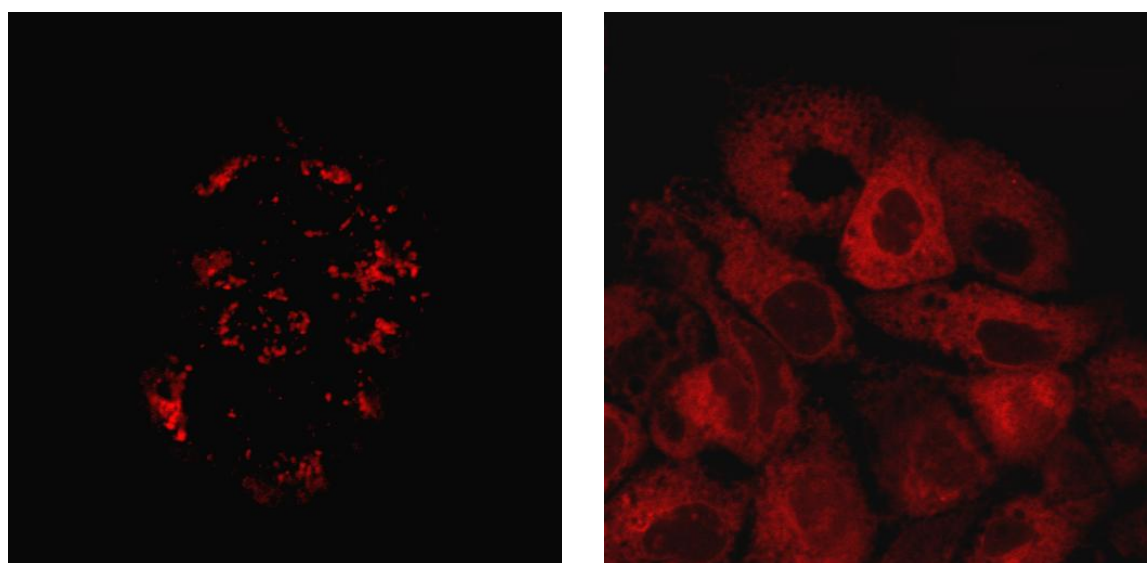
*Figure 35 Comparison of aluminum phthalocyanine fluorescence pattern before (a,b) and after (c,d) PDT. The images (a) and (b) are the same as in Figure 31 (a) and (c).*

Mitochondrial fluorescence (*Figure 36.d*) seems to become somehow more diffuse in the same time but the changes are much less dramatic than for the photosensitizer itself, again an indication for lysosomal damage being an early effect of AlPc-PDT.





(a) Hep3b cells, 3.d after seeding



(b) 24h AIPc 100 $\mu$ M

Figure 36.a/b Comparison of fluorescence pattern before (left) and after (right) PDT.

(a) Hep3b cells, 3 d after seeding.

(b) aluminum phthalocyanine (AIPc) 100  $\mu$ M, 24 h

cf Figure 36.b/c for pattern of lysosomal and mitochondrial tracker.

PDT = photodynamic therapy.

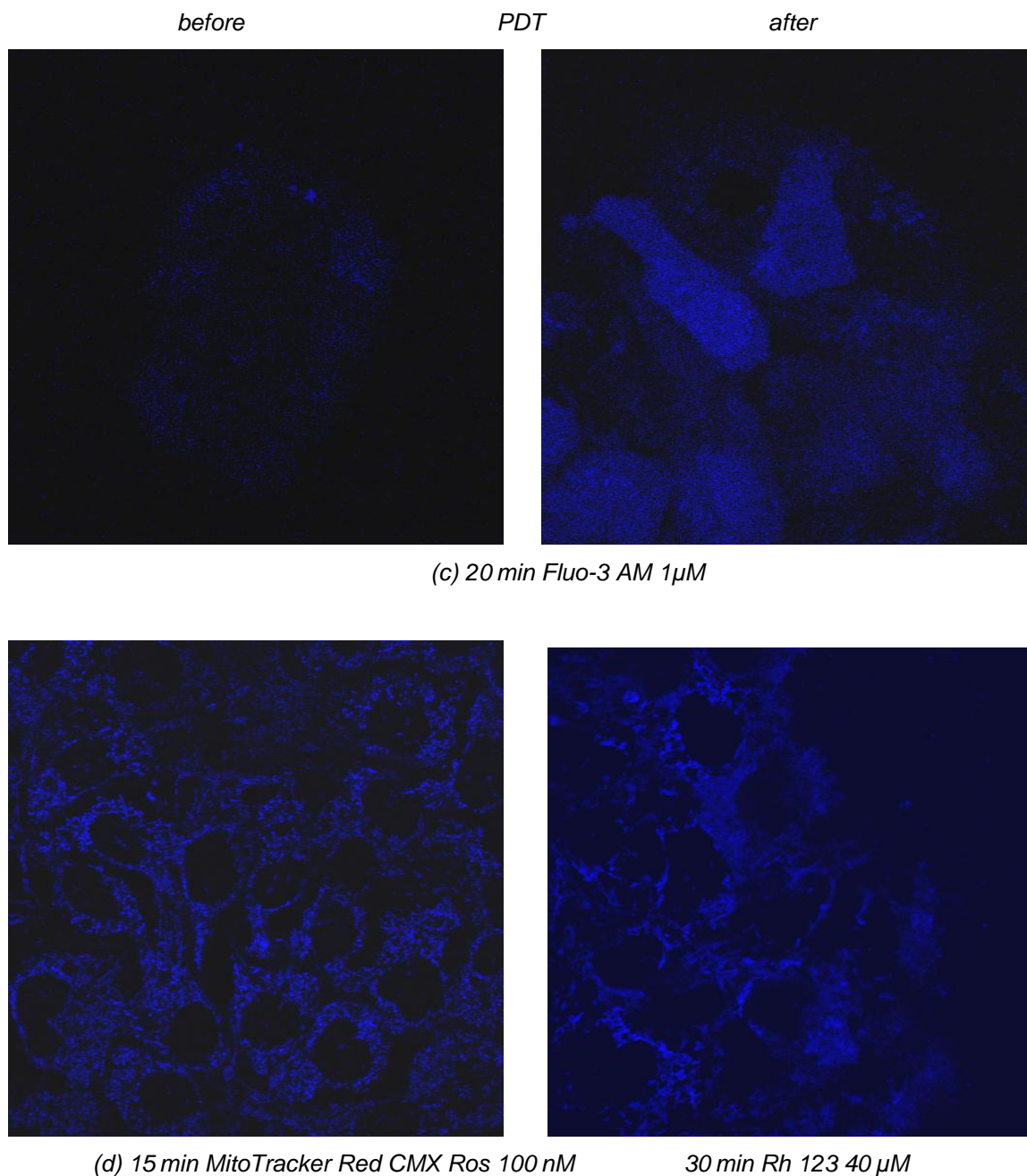


Figure 36.c/d Comparison of fluorescence pattern before (left) and after (right) PDT.

(c) calcium indicator Fluo-3 AM 1  $\mu$ M, 20 min

(d) MitoTracker (100 nM, 15 min) respectively Rh 123 (40  $\mu$ M, 30 min)

cf. Figure 36.b for pattern of AIPc. PDT = photodynamic therapy.

Fluorescence of the calcium indicator Fluo-3 seems to increase upon PDT (Figure 36.c), but other experiments showed that this indicator was very sensitive to incubation conditions and probably cell physiology too. Long incubation times and/or high concentrations lead to a granular fluorescence pattern (Figure 37) that

colocalizes partly with LysoTracker. It can be assumed that after a long incubation, Fluo-3 reaches intracellular compartments with high calcium content. Finally, imaging of Fluo-3 by LSM is impaired by rapid bleaching of the fluorochrome.

To further investigate the possibilities of Fluo-3 calcium monitoring under PDT conditions will therefore be object of future studies.

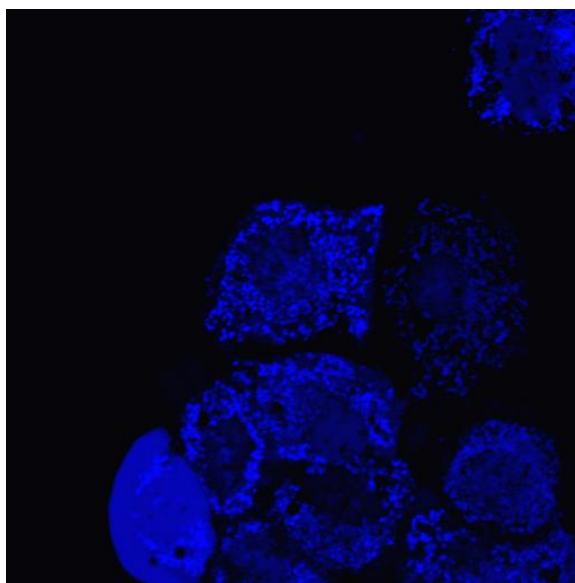


*Figure 37* Fluorescence pattern of calcium indicator Fluo-3 after incubation at high concentration. Hep3b cells, 30 min Fluo-3 5  $\mu$ M.

The post-PDT changes in AIPc fluorescence pattern (*Figure 35* and *Figure 36.b*) correlate very well with the findings in electron microscopy (cf. *Figure 24*), both showing cytoplasmic vacuoles as result of PDT. Moreover, the fluorescence image after PDT is somewhat the negative of the one before PDT: The strongly fluorescent dots (possibly lysosomes) in faintly stained cytosol become unstained vacuoles in a diffusely fluorescent cytosol. The nuclei, where obviously AIPc does not accede to, are in any case not involved in the process.

## 4 Discussion

Cells submitted to photodynamic therapy may die for different reasons. The mode of dying does (1) affect *in vivo* secondary reactions of the organism towards the applied treatment; and (2) might offer a target for exogenous interference. It is therefore of undeniable interest to know by which death pathway the cells will proceed, and how this can eventually be influenced.

PDT has been reported to cause necrotic or apoptotic cell death or else to involve autophagy. While necrosis leads to leakage of cell content into the environment, which can provoke inflammation reactions *in vivo*, apoptosis does usually keep the cell membrane intact. It can start from different points. Roughly, an upstream signal induces further reactions in the cells, inducing the caspase cascade that usually ends in the active caspase 3. The latter cleaves, among others, PARP and provokes degradation of DNA into pieces that appear of regular length in gel electrophoresis, leading to a characteristic pattern known as "laddering" of the DNA. This is a late sign of apoptosis. Early signs of apoptosis depend on the pathway pursued:

The so-called intrinsic or mitochondrial pathway affects the mitochondria at an early stage. Starting with loss of the mitochondrial membrane potential and the permeability transition, this pathway proceeds via release of cytochrome c from the mitochondrial intermembrane space to the cytosol, and formation of the apoptosome, to the activation of caspase 9 that in turn activates caspase 3.

The extrinsic pathway involves transmembrane receptors that, via binding of 'death signal ligands' like CD 95 or TNF, form a death domain in the interior of the cell that further activates cytosolic initiator caspases 8 and 10 and later caspase 3. Eventually, yet another apoptotic pathway comprises calcium release from the endoplasmic reticulum and activation of caspase 12. All of these have been observed upon PDT (Almeida et al. 2004).

As has been mentioned in the introduction, besides the 'classical' distinction between apoptosis and necrosis, further research has in the mean time revealed other forms of cell death (Sperandio et al. 2000), the features of which have some commonalities with either apoptosis or necrosis, while quite distinct with regard to

other important features. Inhibition or expression of single proteins can switch the pathway followed by cell.

Photosensitizers are capable of generating reactive oxygen species (ROS) upon activation by light. These substances then react with surrounding molecules, depending on the localization of the photosensitizer, or in other words, on its hydrophilicity. Hydrophilic photosensitizers tend to accumulate in the cytosol or the mitochondria, while one would expect to find hydrophobic photosensitizers preferentially in membranous compartments.

Here, we investigated in the context of ALPcS4-PDT on carcinoma cells, reactions pertaining to the mitochondrial pathway (cytochrome c release, MTT Test) as well as lysosomal damage (Neutral Red Assay). With regard to caspase activation, caspase inhibitors were assayed, while potential antioxidants respectively radical scavengers could have given a hint on the involvement of reactive oxygen species or other radicals.

Localization of the photosensitizer and morphology changes during treatments were observed with microscopic techniques to complement with the above experiments.

Three different hepatocarcinoma cell lines, initially issued from three patients with hepatoma, were compared. These cells have been reported to differ in their expression of p53 (cf. Material & Methods) and bcl-2, two proteins susceptible of interfering in apoptotic pathways.

PDT has been reported to cause up-regulation of p53 expression but, on the other hand, the cell death upon PDT-treatment does not seem to depend on p53 (Almeida et al. 2004); in particular, even cancer cells that might be resistant to DNA-damaging agents such as radiation or chemotherapy due to mutation or absence of p53 have been reported to undergo apoptosis upon PDT (Harrod-Kim 2006).

Concerning bcl-2, the photodamage of which is provoked by some photosensitizers and promotes apoptosis (Miller et al. 2007), while there is no report about the bcl-2 *gene*, authors have, as shown in the by far not exhaustive Table 8, quite some different opinions about the level of bcl-2 *expression* in HCCs.

*Table 8      Some references reporting on the protein bcl-2 status of hepatocellular carcinoma cells. (n.e. = not expressing)*

Reference		Hep3b	HepG2	HuH7
Takehara 2001		n.e.	n.e.	n.e.
Takeda 2001				n.e.
Mazzocca 2003			increased expression may be induced	
Huang 1998		lacking	expressing	lacking
Takahashi 1999			no constitutive expression	
Seki 1999				40-70% of cells expressing
Lamboley 2000		high levels expressed		
Luo 1999			n.e.	

A reason for these rather diverging findings may be the different conditions in which the cells are being held. As obviously only protein expression has been investigated, nothing is said about the presence, absence or mutation of the corresponding gene. Moreover, the different assertions concerning the protein expression seem to suggest that the genetic information is intact, while conditions in which the cells are kept lead to varying protein constitution.

Takahashi (Takahashi et al. 1999) showed that another cell line usually expressing bcl-2 underwent apoptosis when the expression was prevented, while HepG2, lacking the bcl-2 protein according to their findings, obviously does not need it for survival. The authors assume that other proteins may have taken over its function.

Another comment should be dedicated to the procedure used for surveying mitochondrial cytochrome c release. As has been described previously, the first step is rupturing the cells and separating mitochondrial and cytosolic fractions. Then, the respective fractions are probed separately for the presence of cytochrome c by Western blotting and detection with specific antibodies. Results

obtained are essentially qualitative (presence or absence of cytochrome c in a fraction) or semi-quantitative (comparison of the relative sizes of the autoradiography dots when the gel has been charged with equal amounts of protein).

Misinterpretation can result if, while processing the cells, organelles are disrupted and mitochondrial proteins leak into the cytosol. To discern such artifacts from apoptotic cytochrome c release, the kit used includes probing of COX 4, a protein that remains in the mitochondria following apoptosis but not if mitochondria are mechanically damaged. Unfortunately, we had to abandon this concept because, for reasons that remain unknown, we failed to detect COX 4 in our HCCs (although it was found in our L929 cells). We did not investigate further this problem, considering that in the literature, although cytochrome c release has been detected using the same principle, the necessity for such a control is not reported.

To recapitulate the obtained results, first it should be noted that the cell lines used did mostly not differ significantly in their behavior to any tested procedure, although, as described, they differ in the expression of several apoptosis relevant proteins. (Single experiments with differing results have been described in the preceding chapter.) According to Takahashi (Takahashi et al. 1999), cells might replace the function of a missing protein (like bcl-2 in HepG2 cells) by others. This suggests that comparing the three hepatoma cell lines on the basis of just a few apoptosis related proteins might be rather futile, particularly if their protein endowment is subject to variations as those mentioned above for bcl-2.

The photosensitizer of interest, AIPcS<sub>4</sub>, is rapidly taken up by the cells, probably by an active concentration process as highly fluorescent granules can be observed at the cell edges as soon as two minutes after starting the incubation. After prolonged incubation, the cytosol seems to be penetrated with increasing concentrations too. The granules show a cytoplasmic distribution pattern similar to lysosomal markers while being quite distinct from the fluorescent pattern obtained with mitochondrial markers.

In parallel with increasing uptake of AIPcS<sub>4</sub> (because of higher applied concentration or prolonged incubation time) PDT efficiency increases. While higher concentrations yield higher cell killing until almost 100 %, at a given AIPcS<sub>4</sub>

concentration PDT efficiency reaches a maximum after about five hours of incubation to remain constant or even decrease slightly afterwards.

He (He et al. 1998) suggested that such compartment might be due to an intracellular redistribution of the photosensitizer over time. Indeed, in different experiments, we observed various distributions of AIPcS<sub>4</sub> fluorescence (granular versus diffuse), which do not depend solely on the duration of incubation with the photosensitizer. We suspect the phase of cell growth to play a role, because the distribution seems to be towards the more diffuse pattern in older culture plates. When addition of AIPcS<sub>4</sub> is done early after seeding, the AIPcS<sub>4</sub>-fluorescence is granular, similar to a lysosomal staining (Figure 31.a-b), while a diffuse cytoplasmic pattern is overlaid when time between seeding and AIPcS<sub>4</sub>-addition is longer (Figure 31.c).

Following PDT, the AIPcS<sub>4</sub> fluorescence pattern did not show such remarkable differences from one experiment to another (Figure 35.c-d).

Laser scanning microscopy could possibly assess this phenomenon more in detail by studying whole cells under different conditions of cell culture and incubation times. While it is possible to scan the cells in vertical direction (z-stack) to get information about the whole cell volume, here we restrained most imaging to the vertical level of the best transmission image, which means loss of maybe relevant information.

It should be noted, that the level of the photosensitizer's accumulation in a cellular compartment does not necessarily mean that this compartment is at the origin of the major toxic effect of PDT. Thus it could be for instance, that PDT damage starts from cytosolic AIPcS<sub>4</sub> while the highest concentration of the photosensitizer is found in lysosomes.

PDT induced cell killing in a range of AIPcS<sub>4</sub> concentrations and irradiation doses that were not toxic either alone, which is the typical prerequisite for this treatment / therapy.

The efficiency of response could be modulated over a range of cell survival from 100 to 10 % by modifying AIPcS<sub>4</sub> concentration and/or irradiation dose. Because in



the domain of low cell killing, small changes in AIPcS<sub>4</sub> concentration or in irradiation dose are susceptible of inducing significant changes in survival response, reproducible results are potentially difficult to obtain. Therefore the experiments were carried out under conditions where only about 20% of the cells survived. In some cases, two couples of AIPcS<sub>4</sub> concentration / irradiation dose were used for comparison.

Under these conditions the following results were obtained:

PDT promotes a very early mitochondrial cytochrome c release.

Caspase inhibitor D-boc-fmk can protect a small percentage of cells from being killed, while z-VAD-fmk does not.

Comparison of the two viability assays (NR and MTT) in their response after PDT seems to indicate early damage of lysosomes followed only later by impairment of the mitochondrial enzyme necessary for the MTT Test. The latter occurs about at least an hour later than the observed cytochrome c release, thus confirming the findings of Waterhouse (Waterhouse et al. 2001], that mitochondrial cytochrome c release does not by itself suffice to destroy mitochondrial functions.

Optical microscopy, besides indicating an accumulation of AIPcS<sub>4</sub> in the lysosomes, and to a lower extent, in the cytosol (but not in the mitochondria), showed an early modification of intracellular AIPcS<sub>4</sub> distribution following PDT, that could be explained with the formation of vacuoles starting from lysosomes filled with AIPcS<sub>4</sub>. These were observed in electron microscopy too. Mitochondrial morphology and their cytoplasmic distribution do not seem to be affected immediately in fluorescence microscopy, although in electron microscopy mitochondria appear swollen. Morphology of the cells after PDT was not typical for apoptosis (e.g. no blebbing).

To summarize, no clear evidence for apoptosis was obtained in the experiments conducted herein. If the cells die by necrosis, it is on the other hand not surprising that all three cell lines investigated behave in the same way.

Mitochondrial cytochrome c release has been described as occurring after sublethal cell damage (Waterhouse et al. 2001, Oleinick et al. 2002] or during

necrotic cell death too (Green et al. 1998, Samali et al. 1999], meaning that these findings are not contradictory.

Lysosomes seem to be very early targets of AIPcS<sub>4</sub>-PDT as indicated by the very early reduction of NR uptake as well as cell morphology in optical and electron microscopy featuring large vacuoles depleted of photosensitizer.

Prior to PDT, these organelles seem to be the primary accumulation site of AIPcS<sub>4</sub> together with a more diffuse cytosolic distribution.

As already explained, PDT conditions were quite drastic; less severe treatments might be necessary to allow the cells to die by a programmed cell death. The little protection conveyed to the cells by boc-D-fmk might be a measure of the fraction of cells undergoing apoptosis.

For investigations of cell death mechanisms under milder strains, PDT efficiency would have to be constantly assessed in parallel to assure steady experimental conditions.

Throughout the experiments performed, we suspected some influence of cell cycle status on the results. Synchronizing the cell cycle prior treatment might be a way to ensure all cells in a probe are submitted to PDT under the same cell-inherent conditions.

As has been stated, the described PDT effects occur very early, e.g. vacuole formation is observed by electron microscopy as soon as 15min after irradiation. This means that mechanistic studies and the corresponding securing of the cells needed for probing (e.g. for the cytochrome c fractionation kit) have to be conducted in the range of minutes following irradiation. On the other hand, this finding too is in favor of a necrotic cell death mode, as apoptotic processes have been reported to take in the range of hours to be completed.

It seems reasonable to conclude that in hepatocellular carcinoma cells, AIPcS<sub>4</sub> accumulates in lysosomes from where it is released upon PDT in a destroying process occurring in minutes. Under the conditions used herein, following this treatment, the cells die by a necrotic process, although accompanied by

mitochondrial cytochrome c release, a condition that might well be modulated by less stringent irradiation doses.

Thus, this work served to describe some effects of photodynamic therapy with tetrasulfonated aluminum phthalocyanine in hepatocellular carcinoma cell culture and showed the feasibility of some techniques as well as their limits in the context of this PDT-model.

Further experiments should characterize the cells with respect to their proteins relevant for certain cell death pathways, and then aim at modulating PDT conditions and investigating very early processes under different conditions of incubation and irradiation. Control and inhibition of specific caspases as well as monitoring of cell organelle function can help elucidate further the processes encountered. Typically, the laser scanning microscope equipped with a cell incubation device should be a valuable tool for online monitoring of PDT and possibly selecting cells presenting specific morphological or fluorescence pattern changes for further (e.g. molecular) probing. With the availability of fluorescent proteins that can be expressed by the cells, there is still much scope left. Moreover, (scanning) electron microscopy studies could be developed further with the help of specific markers.

On the long term, the applicability of photodynamic therapy will perhaps depend less on the mode of cell death the targeted cell finally undergoes but on the possibility to engender reproducible and controllable effects. Therefore the underlying mechanisms are still worth further investigation.

## 5 Summary

The object of the present work was photodynamic treatment (PDT) of three different human hepatocellular carcinoma cell lines with the photosensitizer tetrasulfonated aluminum phthalocyanine (AlPcS<sub>4</sub>).

Two different commercially available forms of AlPcS<sub>4</sub> were compared. Dark as well as photo-toxicity of the photosensitizer were assayed as function of concentration, irradiation dose (radiant exposure) and irradiance. Influence of duration of cell growth and incubation time with the photosensitizer was evaluated.

To assess cellular mechanisms involved in the observed cell death, response of neutral red and MTT ( 3-(4,5-Di-methylthiazol-2-yl)-2,5-diphenyl-tetrazolium Bromide ) assay were investigated, as well as the influence of caspase inhibitors and various anti-oxidants respectively radical scavengers. As potential indicator of apoptosis cytochrome c release from mitochondria was monitored.

Furthermore, possibilities to acquire information about photosensitizer uptake and reactions taking place in PDT with the help of laser scanning microscopy and specific fluorochromes as well as with other microscopic techniques were studied.

PDT with AlPcS<sub>4</sub> led to dying of hepatocellular carcinoma cells *in vitro* that was concentration and dose dependent but independent of the form of AlPcS<sub>4</sub> used or of the cell line considered. AlPcS<sub>4</sub> was shown to be readily taken up by the cells and accumulated in a lysosome like intracellular pattern, while upon irradiation AlPcS<sub>4</sub>-depleted vacuoles are formed. Lysosomal as well as mitochondrial damage was demonstrated in different techniques although the sequence of the observed events was not precisely established. One broad-spectrum caspase inhibitor seemed to provide a little protection, while no effect could be assigned to the anti-oxidants or radical scavengers tested.

It was concluded that AlPcS<sub>4</sub>-PDT on hepatocellular carcinoma cells probably induces necrotic cell death, although there is some evidence that apoptotic or other forms of organized cell death could account for a part of the treatment's effects, the ratio between both being possibly a target to modulation by varying experimental conditions.

Because major effects of PDT occur in minutes following irradiation, further experiments should aim at elucidating these effects with rapid techniques. Laser scanning microscopy, which can monitor appropriate indicators even during irradiation, may be a valuable tool in this context.

## 6 Literature

1. Alexiades-Armenakas M: Laser-Mediated Photodynamic Therapy. *Clin. Dermatol.* **24**: 16-25 (2006)
2. Ali SM, Chee SK, Yuen GY, Olivo M: Photodynamic Therapy Induced Fas-Mediated Apoptosis in Human Carcinoma Cells. *Int. J. Molec. Med.* **9**: 257-270 (2002)
3. Allen CM, Langlois R, Sharman WM, LaMadeleine C, van Lier JE: Photodynamic Properties of Amphiphilic Derivatives of Aluminum Tetrasulfophthalocyanine. *Photochem. Photobiol.* **76**: 208-216 (2002)
4. Allison R, Moghissi K, Downie G, Dixon K: Photodynamic Therapy (PDT) for Lung Cancer. *Photodiagnosis Photodyn. Ther.* **8**: 231-239 (2011)
5. Almeida RD, Manadas BJ, Carvalho AP, Duarte CB: Intracellular Signaling Mechanisms in Photodynamic Therapy. *Biochim. Biophys. Acta* **1704**: 59-86 (2004)
6. Ball DJ, Mayhew S, Vernon DI, Griffin M, Brown SB: Decreased Efficiency of Trypsinization of Cells Following Photodynamic Therapy: Evaluation of a Role for Tissue Transglutaminase. *Photochem. Photobiol.* **73**: 47-53 (2001)
7. Beil M, Micoulet A, von Wichert G, Paschke S, Walther P, Bishr Omary M, Van Veldhoven PP, Gern U, Wolff-Hieber E, Eggermann J, Waltenberger J, Adler G, Spatz J, Seufferlein T: Sphingosylphosphorylcholine Regulates Keratin Network Architecture and Visco-Elastic Properties of Human Cancer Cells. *Nature Cell Biol.* **5**: 803-811 (2003)
8. Bown SG, Rogowska AZ, Whitelaw DE, Lees WR, Lovat LB, Ripley P, Jones L, Wyld P, Gillams A, Hatfield AW: Photodynamic Therapy for Cancer of the Pancreas. *Gut* **50**: 549-557 (2002)

9. Brasseur N, Ouellet R, LaMadeleine C, van Lier JE: Water-Soluble Aluminium Phthalocyanine-Polymer Conjugates for PDT: Photodynamic Activities and Pharmacokinetics in Tumour-Bearing Mice. *Brit. J. Cancer* **80**: 1533-1541 (1999)
10. Brown SB, Brown EA, I W: The Present and Future Role of Photodynamic Therapy in Cancer Treatment. *Lancet Oncol.* **5**: 497-508 (2004)
11. Buytaert E, Dewaele M, Agostinis P: Molecular Effectors of Multiple Cell Death Pathways Initiated by Photodynamic Therapy. *Biochim. Biophys. Acta* **1776**: 86-107 (2007)
12. Calzavara-Pinton PG, Venturini M, Sala R: A Comprehensive Overview of Photodynamic Therapy in the Treatment of Superficial Fungal Infections of the Skin. *J. Photochem. Photobiol. B* **78**: 1-6 (2005)
13. Castano AP, Mroz P, Hamblin MR: Photodynamic Therapy and Anti-Tumour Immunity. *Nat. Rev. Cancer* **6**: 535-45 (2006).
14. Chauvier D, Ankri S, Charriaut-Marlangue C, Casimir R, Jacotot E: Broad-Spectrum Caspase Inhibitors: From Myth to Reality? *Cell Death and Differentiation* **14**: 387-391 (2007)
15. Chen B, Pogue BW, Luna JM, Hardman RL, Hoopes PJ, Hasan T: Tumor Vascular Permeabilization by Vascular-Targeting Photosensitization: Effects, Mechanism, and Therapeutic Implications. *Clin. Cancer Res.* **12**: 917-923 (2006)
16. Darwent JR, McCubbin I, Phillips D: Excited Singlet and Triplet State Electron-Transfer Reactions of Aluminium(III) Sulphonated Phthalocyanine. *J. Chem. Soc. Faraday Trans. 2*, **78**: 347-357 (1982)
17. Derycke ASL, Kamuhabwa A, Gijssens A, Roskams T, De Vos D, Kasran A, Huwyler J, Missiaen L, De Witte PAM: Transferrin-Conjugated Liposome Targeting of Photosensitizer ALPcS<sub>4</sub> to Rat Bladder Carcinoma Cells. *J. Nat. Cancer Inst.* **96**: 1620-1630 (2004)

18. Deutsches Medizin-Netz.de:  
<http://www.medizin-netz.de/therapien/krebstherapie-unter-verwendung-von-licht-farbstoffe-fuer-die-photodynamische-therapie/> (27.07.2012)
19. D'Mello SR, Aglieco F, Roberts MR, Borodezt K, Haycock JW: A DEVD-Inhibited Caspase Other than CPP32 Is Involved in the Commitment of Cerebellar Granule Neurons to Apoptosis Induced by K<sup>+</sup> Deprivation. *J. Neurochem.* **70**: 1809-18 (1998)
20. Du KL, Both S, Friedberg JS, Rengan R, Hahn SM, Cengel KA: Extrapleural Pneumonectomy, Photodynamic Therapy and Intensity Modulated Radiation Therapy for the Treatment of Malignant Pleural Mesothelioma. *Cancer Biol. Ther.* **10**: 425-9 (2010).
21. Dutta S, Ray D, Kolli B, Chang K: Photodynamic Sensitization of *Leishmania amazonensis* in both Extracellular and Intracellular Stages with Aluminum Phthalocyanine Chloride for Photolysis *in vitro*. *Antimicrob. Agents Chemother.* **49**: 4474-4484 (2005)
22. Edinak NJ, Rueck AC, Steiner RW, Genze F, Loschenov VB: Laser-Induced Fluorescence Spectroscopy of AlPc4 and liposomal ZnPc in a Rat Bladder Tumor Model and Correlation with PDT Efficiency. *Proc. SPIE* **2924**, 266 (1996)
23. Ekert PG, Silke J, Vaux DL: Caspase Inhibitors. *Cell Death and Differentiation* **6**, 1081-1086 (1999)
24. EMD Millipore Chemicals:  
[http://www.merckmillipore.com/DE/en/product/caspase-inhibitor-i-cas-187389-52-2-calbiochem,EMD\\_BIO-627610](http://www.merckmillipore.com/DE/en/product/caspase-inhibitor-i-cas-187389-52-2-calbiochem,EMD_BIO-627610) and  
[http://www.emdmillipore.com/US/en/product/caspase-inhibitor-iii-cas-634911-80-1-calbiochem,EMD\\_BIO-218745](http://www.emdmillipore.com/US/en/product/caspase-inhibitor-iii-cas-634911-80-1-calbiochem,EMD_BIO-218745) (10.12.2015)
25. Fan B, Andrén-Sandberg A: Photodynamic Therapy for Pancreatic Cancer. *Pancreas* **34**: 385-389 (2007)
26. Farmer E: <http://commons.wikimedia.org/wiki/File%3AApoptosis.png> (29.07.2012; public domain)



27. Filonenko EV, Sokolov VV, Chissov VI, Lukyanets EA, Vorozhtsov GN: Photodynamic Therapy of Early Esophageal Cancer. *Photodiagnosis Photodyn. Ther.* **5**: 187-190 (2008)
28. Gollnick SO, Vaughan L, Henderson BW: Generation of Effective Antitumor Vaccines Using Photodynamic Therapy. *Cancer Res.* **62**: 1604-1608 (2002)
29. Green DR, Reed JC: Mitochondria and Apoptosis. *Science* **281**: 1309-1312 (1998)
30. Harrod-Kim P: Tumor Ablation with Photodynamic Therapy: Introduction to Mechanism and Clinical Applications: *J. Vasc. Interv. Radiol.* **17**: 1441-1448 (2006)
31. He J, Horng MF, Deahl JT, Oleinick NL, Evans HH: Variation in Photodynamic Efficacy during the Cellular Uptake of Two Phthalocyanine Photosensitizers. *Photochem. Photobiol.* **67**: 720-728 (1998)
32. Hopper C: Photodynamic Therapy: A Clinical Reality in the Treatment of Cancer. *Lancet Oncol.* **1**: 212-219 (2000)
33. Huang YL, Chou CK: Bcl-2 Blocks Apoptotic Signal of Transforming Growth Factor-beta in Human Hepatoma Cells. *J. Biomed. Sci.* **5**: 185-91 (1998)
34. Huang Z, Xu H, Meyers AD, Musani AI, Wang L, Tagg R, Barqawi AB, Chen YK.: Photodynamic Therapy for Treatment of Solid Tumors – Potential and Technical Challenges. *Technol. Cancer Res. Treat.* **7**: 309-320 (2008)
35. Hug H, Strand S, Grambihler A, Galle J, Hack V, Stremmel W, Krammer PH, Galle PR: Reactive Oxygen Intermediates Are Involved in the Induction of CD95 Ligand mRNA Expression by Cytostatic Drugs in Hepatoma Cells. *J. Biol. Chem.* **272**: 28191-28193 (1997)
36. Hug H: Programmierter Zelltod – Bedeutung der Apoptose für zukünftige Therapien. *Deutsche Apotheker Zeitung* **138**: 614-619 (1998)

37. Hug H, Los M, Hirt W, Debatin K-M: Rhodamine 110-Linked Amino Acids and Peptides as Substrates to Measure Caspase Activity upon Apoptosis Induction in Intact Cells. *Biochemistry* **38**: 13906-13911 (1999)
38. Jia X, Jia L: Nanoparticles Improve Biological Functions of Phthalocyanine Photosensitizers Used for Photodynamic Therapy. *Current Drug Metabolism* **13**, 1119-1122 (2012)
39. Jori G, Fabris C, Soncin M, Ferro S, Coppelotti O, Dei D, Fantetti L, Chiti G, Roncucci G: Photodynamic Therapy in the Treatment of Microbial Infections: Basic Principles and Perspective Applications. *Lasers in Surg. Med.* **38**: 468-481 (2006)
40. Juzenas P, Juzeniene A, Rotomskis R, Moan J: Spectroscopic Evidence of Monomeric Aluminium Phthalocyanine Tetrasulfonate in Aqueous Solutions. *J. Photochem. Photobiol. B* **75**: 107-110 (2004)
41. Juzeniene A, Peng Q, Moan J: Milestones in the Development of Photodynamic Therapy and Fluorescence Diagnosis. *Photochem. Photobiol. Sci.* **6**: 1234-1245 (2007)
42. Ke MR, Yeung SL, Fong WP, Ng DK, Lo PC: A Phthalocyanine-Peptide Conjugate with High *in vitro* Photodynamic Activity and Enhanced *in vivo* Tumor-Retention Property. *Chemistry* **18**: 4225-4233 (2012)
43. Kessel D, Arroyo AS: Apoptotic and Autophagic Responses to Bcl-Inhibition and Photodamage. *Photochem. Photobiol. Sci.* **6**: 1290-1295 (2007)
44. Kinzler I, Haseroth E, Hauser C, Rück A: Role of Mitochondria in Cell Death Induced by Photofrin-PDT and Ursodeoxycholic Acid by Means of SLIM. *Photochem. Photobiol. Sci.* **6**: 1332-40 (2007).
45. Kress M, Meier T, Steiner R, Dolp F, Erdmann R, Ortmann U, Rück A: Time-Resolved Microspectrofluorometry and Fluorescence Lifetime Imaging of Photosensitizers Using Picosecond Pulsed Diode Lasers in Laser Scanning Microscopes. *J. Biomed. Opt.* **8**: 26-32 (2003)

46. Kujundzic M, Vogl TJ, Stimac D, Rustemovic N, His RA, Roh M, Katicić M, Cuenca R, Lustig RA, Wang S: A Phase II Safety and Effect on Time to Tumor Progression Study of Intratumoral Light Infusion Technology Using Talporfin Sodium in Patients with Metastatic Colorectal Cancer. *J. Surg. Oncol.* **96**: 518-524 (2007)
47. Lamboley C, Bringuier AF, Feldmann G: Apoptotic Behaviour of Hepatic and Extra-Hepatic Tumor Cell Lines Differs after Fas Stimulation. *Cell Mol. Biol.* **46**: 13-28 (2000)
48. Luo D, Cheng SC, Xie Y: Expression of Bcl-2 Family Proteins during Chemotherapeutic Agents-Induced Apoptosis in the Hepatoblastoma HepG2 Cell Line. *Br. J. Biomed. Sci.* **56**: 114-122 (1999)
49. Malik E, Meyhöfer-Malik A, Berg C, Böhm W, Kunzi-Rapp K, Diedrich K, Rück A: Fluorescence diagnosis of endometriosis on the chorioallantoic membrane using 5-aminolaevulinic acid. *Hum. Reprod.* **15**: 584-8 (2000)
50. Marcus SL, McIntyre WR: Photodynamic Therapy Systems and Applications. *Expert Opin. Emerg. Drugs* **7**: 321-334 (2002)
51. Marmur ES, Schmults CD, Goldberg DJ: A Review of Laser and Photodynamic Therapy for the Treatment of Non-melanoma Skin Cancer. *Dermatol. Surg.* **30(2.2)**: 264-271 (2004)
52. Mazzocca A, Giusti S, Hamilton AD, Sebti SM, Pantaleo P, Carloni V: Growth Inhibition by the Farnesyltransferase Inhibitor FTI-277 Involves Bcl-2 Expression and Defective Association with Raf-1 in Liver Cancer Cell Lines. *Mol. Pharmacol.* **63**: 159-166 (2003)
53. Miller JD, Baron ED, Scull H, Hsia A, Berlin JC, McCormick T, Colussi V, Kenney ME, Cooper KD, Oleinick NL: Photodynamic Therapy with the Phthalocyanine Photosensitizer Pc 4: The Case Experience with Preclinical Mechanistic and Early Clinical-translational Studies. *Toxicology and Applied Pharmacology* **224**: 290-299 (2007)

54. Molecular Probes Handbook:  
*<http://www.lifetechnologies.com/de/de/home/references/molecular-probes-the-handbook.html>* (14.10.2013)
55. Moghissi K: Role of Bronchoscopic Photodynamic Therapy in Lung Cancer Management. *Curr. Opin. Pulm. Med.* **10**: 256-260 (2004)
56. Moor AC, Lagerberg JW, Tijssen K, Foley S, Truscott TG, Kochevar IE, Brand A, Dubbelman TM, VanSteveninck J: *In vitro* Fluence Rate Effects in Photodynamic Reactions with AlPcS4 as Sensitizer. *Photochem. Photobiol.* **66**: 860-865 (1997)
57. Nagata JY, Hioka N, Kimura E, Batistela VR, Terada RS, Graciano AX, Baesso ML, Hayacibara MF: Antibacterial Photodynamic Therapy for Dental Caries: Evaluation of the Photosensitizers Used and Light Source Properties. *Photodiagnosis Photodyn. Ther.* **9**: 122-131 (2012)
58. Nakabayashi H, Taketa K, Miyano K, Yamane T, Sato J: Growth of Human Hepatoma Cell Lines with Differentiated Functions in Chemically Defined Medium. *Cancer Res.* **42**: 3858-3863 (1982)
59. Nowis D, Makowski M, Stoklosa T, Legat M, Issat T, Golab J: Direct Tumor Damage Mechanisms of Photodynamic Therapy. *Acta Biochim. Pol.* **52**: 339-352 (2005)
60. Norum OJ, Gaustad JV, Angell-Petersen E, Rofstad EK, Peng Q, Giercksky KE, Berg K: Photochemical Internalization of Bleomycin is Superior to Photodynamic Therapy Due to the Therapeutic Effect in the Tumor Periphery. *Photochem. Photobiol.* **85**: 740-749 (2009)
61. Oleinick NL, Morris RL, Belichenko I. The Role of Apoptosis in Response to Photodynamic Therapy: What, where, why, and how. *Photochem. Photobiol. Sci.* **1**: 1-21 (2002).
62. Orth K, Beck G, Genze F, Rück A: Methylene Blue Mediated Photodynamic Therapy in Experimental Colorectal Tumors in Mice. *J. Photochem. Photobiol. B* **57**: 186-92 (2000)

63. Pfaffel-Schubart G, Rück A, Scalfi-Happ C: Modulation of Cellular  $\text{Ca}^{2+}$  Signaling during Hypericin-Induced Photodynamic Therapy (PDT). *Med. Laser Appl.* **21**: 61-66 (2006)
64. Phthalocyanines in Sigma-Aldrich Product Directory:  
<http://www.sigmaaldrich.com/materials-science/material-science-products.html?TablePage=19353678> (08.12.2015)
65. Pushpan SK, Venkatraman S, Anand VG, Sankar J, Parmesvaran D, Ganesan S, Chandrashekar TK: Porphyrins in Photodynamic Therapy – A Search for Ideal Photosensitizers. *Curr. Med. Chem. Anti-Canc. Agents* **2**: 187-207 (2002)
66. Rück A, Heckelsmiller K, Kaufmann R, Grossman N, Haseroth E, Akgün N: Light-Induced Apoptosis Involves a Defined Sequence of Cytoplasmic and Nuclear Calcium Release in ALPcS4-Photosensitized Rat Bladder RR 1022 Epithelial Cells. *Photochem. Photobiol.* **72**: 210-6 (2000)
67. Samali A, Nordgren H, Zhivotovsky B, Peterson E, Orrenius S: A Comparative Study of Apoptosis and Necrosis in HepG2 Cells: Oxidant-Induced Caspase Inactivation Leads to Necrosis. *Biochem. Biophys. Res. Commun.* **255**: 6-11 (1999)
68. Saraste M: Oxidative Phosphorylation at the *fin du siècle*. *Science* **283**: 1488-1493 (1999) (Reprinted with permission from AAAS)
69. Schmitt F, Juillerat-Jeanneret L: Drug Targeting Strategies for Photodynamic Therapy. *Anticancer Agents Med. Chem.* **12**: 500-525 (2012)
70. Seki S, Kitada T, Sakaguchi H, Kawada N, Iwai S, Kadoya H, Nakatani K: Expression of Fas and Bcl-2 Proteins and Induction of Apoptosis in Human Hepatocellular Carcinoma Cell Lines. *Med. Electron. Microsc.* **32**: 199-203 (1999)
71. Sheppard CJR, Shotton DM: Confocal Laser Scanning Microscopy. Microscopy Handbook Series 38. Bios Scientific Publisher, Springer, New York, pp. 36 ff (1997)

72. Simone CB 2nd, Friedberg JS, Glatstein E, Stevenson JP, Sterman DH, Hahn SM, Cengel KA: Photodynamic Therapy for the Treatment of Non-small Cell Lung Cancer. *J. Thorac. Dis.* **4**: 63-75 (2011)
73. Singh MK, Pal H, Bhasikuttan AC, Sapre AV: Dual Solvatochromism of Neutral Red. *Photochem. Photobiol.* **68**: 32-38 (1998)
74. Singh G, Espiritu M, Shen XY, Hanlon JG, Rainbow AJ: *In vitro* Induction of PDT Resistance in HT29, HT1376 and SK-N-MC Cells by Various Photosensitizers. *Photochem. Photobiol.* **73**: 651-656 (2001)
75. Sokolov VV, Chissov VI, Yakubovskya RI, Aristarkhova EI, Filonenko EV, Belous TA, Vorozhtsov GN, Zharkova NN, Smirnov VV, Zhitkova MB: Photodynamic Therapy (PDT) of Malignant Tumors by Photosensitizer Photosens: Results of 45 Clinical Cases. *Proc. SPIE* **2625**: 281-287 (1996)
76. Soergel P, Löning M, Staboulidou I, Schippert C, Hillemanns P: Photodynamic Diagnosis and Therapy in Gynecology. *J. Environ. Pathol. Toxicol. Oncol.* **27**: 307-320 (2008).
77. Sperandio S, de Belle I, Bredesen DE: An Alternative, Nonapoptotic Form of Programmed Cell Death. *Proc. Natl. Acad. Sci. USA* **20**: 14376-14381 (2000)
78. Stepp H: Photodynamische Therapie: Lichtblitze gegen Tumoren. *Im Fokus Onkologie* **9**: 46-52 (2003)
79. Tacelosky DM, Creecy AE, Shanmugavelandy SS, Smith JP, Claxton DF, Adair JH, Kester M, Barth BM: Calcium Phosphosilicate Nanoparticles for Imaging and Photodynamic Therapy of Cancer. *Discov. Med.* **13**: 275-285 (2012)
80. Takahashi M, Saito H, Okuyama T, Miyashita T, Kosuga M, Sumisa F, Yamada M, Ebinuma H, Ishii H: Overexpression of Bcl-2 Protects Human Hepatoma Cells from Fas-Antibody-Mediated Apoptosis. *J. Hepatol.* **31**: 315-322 (1999)

81. Takeda Y, Nakao K, Nakata K, Kawakami A, Ida H, Ichikawa T, Shigeno M, Kajiya Y, Hamasaki K, Kato Y, Eguchi K: Geranylgeraniol, an Intermediate Product in Mevalonate Pathway, Induces Apoptotic Cell Death in Human Hepatoma Cells: Death Receptor-Independent Activation of Caspase-8 with Down-Regulation of Bcl-xL Expression. *Jpn. J. Cancer Res.* **92**: 918-925 (2001)
82. Takehara T, Liu X, Fujimoto J, Friedman SL, Takahashi H: Expression and Role of Bcl-xL in Human Hepatocellular Carcinomas. *Hepatology* **34**: 55-61 (2001)
83. Terada S, Kumagai T, Yamamoto N, Ogawa A, Ishimura J, Fujita T, Suzuki E, Miki M: Generation of a Novel Apoptosis-Resistant Hepatoma Cell Line. *J. Biosci. Bioeng.* **95**: 146-51 (2003)
84. Triesscheijn M, Baas P, Schellens JHM, Stewart FA: Photodynamic Therapy in Oncology. *The Oncologist* **11**: 1034-1044 (2006)
85. Trushina OI, Novikova EG, Sokolov VV, Filonenko EV, Chissov VI, Vorozhtsov GN: Photodynamic Therapy of Virus-Associated Precancer and Early Stages Cancer of *Cervix uteri*. *Photodiagnosis Photodyn. Ther.* **5**: 256-259 (2008)
86. Upile T, Jerjes WK, Sterenborg HJ, Wong BJ, El-Naggar AK, Ilgner JF, Sandison A, Witjes MJ, Biel MA, van Veen R, et al., Bigio I, Yodh AG, Hopper C: At the Frontiers of Surgery: Review. *Head Neck Oncol.* **3**: 7 (2011)
87. van Dongen GA, Visser GW, Vrouenraets MB: Photosensitizer-Antibody Conjugates for Detection and Therapy of Cancer. *Adv. Drug Deliv. Rev.* **56**:31-52 (2004)
88. van Duijnhoven FH, Aalbers RIJM, Rovers JP, Terpstra OT, Kuppen PJK: The Immunological Consequences of Photodynamic Treatment of Cancer, a Literature Review. *Immunobiol.* **207**: 105-113 (2003)
89. van Duijnhoven FH, Rovers JP, Engelmann K, Krajina Z, Purkiss SF, Zoetmulder FA, Vogl TJ, Terpstra OT: Photodynamic Therapy with 5,10,15,20-Tetrakis(m-Hydroxyphenyl)-Bacteriochlorin for Colorectal Liver Metastases Is Safe and Feasible: Results from a Phase I Study. *Ann. Surg. Oncol.* **12**: 808-816 (2005)

90. Verteporfin Roundtable Participants: Guidelines for Using Verteporfin (Visudyne) in Photodynamic Therapy for Choroidal Neovascularization Due to Age-Related Macular Degeneration and Other Causes: Update. *Retina* **25**: 119-34 (2005)
91. Vogl TJ, Eichler K, Mack MG, Zangos S, Herzog C, Thalhammer A, Engelmann K: Interstitial Photodynamic Laser Therapy in Interventional Oncology. *Eur. Radiol.* **14**: 1063-73 (2004)
92. Vrouwenraets MB, Visser GW, Stigter M, Oppelaar H, Snow GB, van Dongen GA: Targeting of Aluminum (III) Phthalocyanine Tetrasulfonate by Use of Internalizing Monoclonal Antibodies: Improved Efficacy in Photodynamic Therapy. *Cancer Res.* **61**: 1970-1975 (2001).
93. Wainwright M: Methylene Blue Derivatives – Suitable Photoantimicrobials for Blood Product Disinfection? *Int. J. Antimicrob. Agents* **16**: 381-394 (2000)
94. Waksman R, McEwan PE, Moore TI, Pakala R, Kolodgie FD, Hellings DG, Seabron RC, Rychnovsky SJ, Vasek J, Scott RW, Virmani R: PhotoPoint Photodynamic Therapy Promotes Stabilization of Atherosclerotic Plaques and Inhibits Plaque Progression. *J. Am. Coll. Cardiol.* **16**: 1024-32 (2008)
95. Waterhouse NJ, Goldstein JC, von Ahsen O, Schuler M, Newmeyer DD, Green DR: Cytochrome c Maintains Mitochondrial Transmembrane Potential and ATP Generation after Outer Mitochondrial Membrane Permeabilization during the Apoptotic Process. *J. Cell Biol.* **153**: 319-328 (2001)
96. Wilson BC, Patterson MS: The Physics, Biophysics and Technology of Photodynamic Therapy. *Phys. Med. Biol.* **53**: R61-R109 (2008)
97. Yavari N, Andersson-Engels S, Segersten U, Malmstrom PU: An Overview on Preclinical and Clinical Experiences with Photodynamic Therapy for Bladder Cancer. *Can J Urol.* **18**: 5778-5786 (2011)
98. Zeiss product information for LSM 510 meta (reprinted with permission from Carl Zeiss GmbH)



# *Acknowledgement*

*The presented work was conducted at the Institute for Lasertechnologies in Medicine and Metrology at the University of Ulm.*

*It is my great pleasure to acknowledge the valuable help that my colleagues have continuously offered me during all that time.*

*First, I would like to thank Professor R. Steiner for having accepted me as doctoral student and for the interest and support he has always given to my work.*

*My gratitude is also due to Professor T. Syrovets, Professor T. Seufferlein and Professor R. Hibst, who kindly accepted the tasks of reviewer and auditors of this thesis.*

*I am very thankful to my supervisor, Dr. Angelika Rück, for her support over many years.*

*Dilek Dayanakli, Carmen Hauser, Frank Dolp, Dr. Claudia Scalfi-Happ and Dr. Ingrid Kinzler - many thanks to you for having made this time most enjoyable, for having been available for help and advice in every circumstance, and especially to Dr. Scalfi-Happ for proof-reading the thesis.*

*Certainly, this list would not be complete without mentioning Felicitas Genze with whom I started my work at the Institute, spending hours over chicken eggs and microscope slides.*

*I also wish to thank very much Elke Wolff-Hieber from the Department of Internal Medicine I for preparing and probing the samples for electron microscopy.*

*As I look back to many years of work at the Laser Institute, I appreciate the spirit of cooperation and interdisciplinarity it bears; and thus, I would like to give a grateful thought to all those who contributed to it. The page would not suffice to mention all the people, who, besides creating the pleasant working atmosphere, helped me with practical or ideal contributions.*

*This work was supported by a grant of the Interdisciplinary Center for Clinical Research (iZKF) of the University of Ulm.*

*The Graduate College "Diagnostic and Therapeutic Methods in Molecular Medicine", besides providing many possibilities for enlarging my scientific as well as my general knowledge, has given me financial support for attending several international congresses.*

*I dedicate this work to my friendship with Nermin Akgün.*

# Curriculum vitae

## Persönliche Daten

Name, Vorname                      Haseroth, Elke  
Geburtsort, Geburtsdatum      Genf / Schweiz, 03. Oktober 1968

## Schul- und Hochschulbildung (mit Abschlüssen)

1974 - 1977                      Ecole primaire du Lignon / Genf  
1977 - 1987                      Deutsche Schule Genf (Allgemeine Hochschulreife)  
1987 - 1993                      Universität Genf: (Bio-)Chemie, Analytische Umweltchemie (Dipl.chem.)  
1995 - 2001                      Universitäten Genf / Ulm: Studium der Humanmedizin (Approbation)  
2001 - 2003                      Universität Ulm: Promotionsbegleitendes Studium am GRK 460

## Berufliche Tätigkeiten

1993 - 1995    Wissenschaftlicher Mitarbeiter, Analytische Chemie, Universität Genf  
2001 - 2003    Wissenschaftlicher Mitarbeiter, ILM, Stipendium des iZkF, Universität Ulm  
2003 - 2005    Arzt im Praktikum/Assistenzarzt, Innere Medizin I, Universitätsklinik Ulm  
2005 - 2009    Assistenzarzt, Chirurgie, Oberschwabenkliniken, Isny/Leutkirch und Ravensburg  
2010 - 2012    Assistenzarzt, Chirurgie, Paracelsus Krankenhaus Ruit  
2012 -         Assistenzarzt, Chirurgie, Kreiskrankenhaus Ehingen

## Sonstiges

1999                      Kurs 'Laser in der Medizin', ILM, Ulm  
2002                      Kurs 'Sicherheit in der Gentechnik', Universität Ulm  
04 - 06/2005        'Kursus für Tropenmedizin', Bernhard-Nocht-Institut, Hamburg  
03 - 06/2000        Volontariat am Marie Adelaide Leprazentrum, Karachi, Pakistan  
2009                      Fachkunde Röntgendiagnostik

GRK 460 - Graduiertenkolleg "Molekularbiologische Methoden in der Medizin", Universität Ulm

iZkF - Interdisziplinäres Zentrum für Klinische Forschung, Universität Ulm

ILM - Institut für Lasertechnologien in der Medizin und Meßtechnik an der Universität Ulm